TECHNISCHE UNIVERSITÄT MÜNCHEN

Fakultät für Medizin

Institut für Diabetes und Adipositas
(Helmholtz Zentrum München)

Modulation of hepatic glucocorticoid action by the bHLH factor E47

Marie Charlotte Hemmer

Vollständiger Abdruck der von der Fakultät für Medizin der Technischen Universität München zur Erlangung des akademischen Grades eines

Doktors der Naturwissenschaften

genehmigten Dissertation.

Vorsitzender: Prof. Dr. Percy A. Knolle

Prüfer der Dissertation:

1. Prof. Dr. Matthias Tschöp
2. Prof. Dr. Wolfgang Wurst

Die Dissertation wurde am 09.08.2018 bei der Technischen Universität München eingereicht und durch die Fakultät für Medizin am 17.04.2019 angenommen.

Acknowledgements

First and foremost, I wish to thank Prof. Dr. Matthias Tschöp for accepting the role as my first PhD supervisor and for providing an excellent research environment at the Institute of Diabetes and Obesity. I appreciated the critical assessment of my project, which greatly advanced the progress of my PhD thesis.

I also like to thank my second supervisor, Prof. Dr. Wolfgang Wurst, for the valuable and encouraging project feedback along the way.

My gratitude specifically goes to my direct supervisor Prof. Dr. Nina Henriette Uhlenhaut for giving me the unequalled chance to work on this project in her group. I greatly appreciated your scientific input, continuous encouragement and trust in my abilities, which have made the last years an incredibly fun and exciting experience! You not only guided me to shape my overall professional skills but also served as a great inspiration and role model for a young female scientist like me.

In addition, I would like to thank the Deutsche Forschungsgemeinschaft (DFG). The project (U275/1-1) was funded as part of the Emmy Noether program for independent junior research groups, which was awarded to Prof. Dr. Uhlenhaut.

My Mol Endo team - Franzi, Fabiana, Ken, Michaël, Laura, Céline, Omar, Ashfaq, Afzal, Katerina, Kostas, Kristina, Teresa, Cinzia, Sonja and Sybille. Thank you for your encouragement and help and your fantastic technical support!

The list of colleagues and friends who have shaped the last years is a long one. Your emotional support was greatly appreciated.

Und dann sind da Mama und Papa - ich bin die, die ich bin, wegen euch. Danke, dass ich immer weiß, wo zuhause ist.

Index of Contents

Abstract

Glucocorticoids (GCs) are used as powerful drugs in the treatment of various inflammatory and autoimmune disorders. However, their long-term effectiveness is associated with severe side effects including hyperglycemia, hyperlipidemia and obesity, which are hallmarks of the "Metabolic Syndrome".

GCs are steroid hormones and bind the glucocorticoid receptor (GR). GR acts as a ligand-activated transcription factor and binds to DNA sequences known as *glucocorticoid response elements*. GR can activate or repress genes but the exact mechanism has not been fully explained. The metabolic side effects of steroid treatment are thought to be caused by the transcriptional activation of metabolic GR target genes. Performing ChIP-Sequencing in mouse livers, an E-Box motif bound by the bHLH transcription factor E47 was identified. Co-occupancy of GR and E47 at promoters and enhancers of metabolic genes suggested a functional role for the factor in liver metabolism. Using mouse genetics*, E47* mutant mice were shown to be protected from hyperglycemia and hepatic steatosis *in vivo* in response to GCs. This protective phenotype was caused by the impaired up-regulation of glucose and lipid genes necessary to exert GR's full impact on hepatic metabolism.

ChIP-MS was performed in wildtype and *E47* mutant livers and revealed the Mediator complex and FoxO1 to be among the pool of GR-associated factors. In *E47* mutant livers, GR was less efficiently bound to chromatin. Subsequently, recruitment of important coregulators such as Mediator to metabolic promoters and enhancers was diminished. In addition, human GR-regulated sequences revealed the E47 motif to be specifically associated with transcriptional activation by GR. This suggests a conserved function for E47 in the regulation of certain human gene programs by GCs.

The data presented here illustrates that crosstalk of GR and E47 is needed for adequate assembly of the transcriptional machinery and to regulate GR target gene expression. Targeting E47 might provide a new approach to separate the beneficial effects of GC treatment from the harmful metabolic side effects.

Zusammenfassung

Glucocorticoide (GCs) gehören zu den am häufigsten verschriebenen Arzneimitteln für die Behandlung von entzündlichen Erkrankungen, z.B. Allergien und Autoimmunerkrankungen. Die Therapie ist jedoch mit Nebenwirkungen verbunden, welche häufig den Stoffwechsel betreffen. Hierzu gehören Hyperglykämie, Hyperlipidämie und Fettleibigkeit, die alle Kennzeichen des "metabolischen Syndroms" sind.

GCs sind Steroidhormone und dienen als Liganden für den Glucocorticoid-Rezeptor (GR). Dieser bindet DNA-Sequenzen, die als *glucocorticoid response elements* bekannt sind. Bis heute sind die Mechanismen der Genaktivierung und Genrepression durch GR nicht vollständig entschlüsselt. ChIP-Sequencing in Mäuselebern identifizierte das E-Box Motiv des bHLH Transkriptionsfaktors E47. Das gemeinsame Binden von GR und E47 an metabolische Promotoren und Enhancern deutete darauf hin, dass E47 an der Modulation GR-Zielgenen beteiligt ist. *In vivo* Experimente zeigten, dass bei *E47* Knockout Mäuse die charakteristisch auftretende Hyperglykämie und Fettleber nach GC-Behandlung weniger stark ausgeprägt war. Dies war auf die fehlende Hochregulation von Glukose-und Lipid-Genen in der Leber zurückzuführen. Ein Hepatozyten-spezifischer *E47* Knockout bestätigte die Ergebnisse und implizierte somit die Leber als das Zielgewebe für das Zusammenspiel von E47 und GR. Um das GR-Interaktom in Wildtyp- und mutanten Lebern zu untersuchen, wurde ChIP-MS durchgeführt. Komponenten des Mediator-Komplexes und FoxO1 wurden als GR-assoziierte Transkriptionsfaktoren in der Leber identifiziert. Mutante Lebern wiesen jedoch eine reduzierte Bindung von GR, FoxO1 und Mediator an metabolische Gene auf. Darüberhinaus war das Vorhandensein des E47 Motivs in einem zellbasierten Luciferase Reporter Screen mit humanen GR-regulierten Sequenzen spezifisch mit der Transkriptionsaktivierung durch GR verbunden.

Zusammenfassend identifizierten die Daten E47 als einen neuen Co-Regulator von GR in der Leber, welcher für die Hochregulierung von GR-Zielgenen in der Leber benötigt wird. In der Medizin könnte E47 daher einen neuen Ansatz bilden, um die metabolischen Nebenwirkungen von den wichtigen anti-inflammatorischen Effekten zu trennen, um so eine sichere Behandlung durch Steroide zu ermöglichen.

Abbreviations

°C	degree celsius
µ	micro- (10)
ACTH	adrenocorticotrophic hormone
ANOVA	analysis of variance
BCA	bicinchoninic acid
bHLH	basic Helix-Loop-Helix
bp	base pair
BSA	bovine serum albumin
cDNA	complementary DNA
Cort	corticosterone
CRH	corticotrophin-releasing hormone
CT	threshold cycle
DAPI	4',6-diamidino-2-phenylindole
Dex	dexamethasone
DNA	deoxyribonucleic acid
DMEM	dulbecco's modified eagle's Medium
DTT	dithiothreitol
ECL	enzymatic chemiluminescence
EDTA	ethylenediaminetetraacetic acid
e.g.	exempli gratia
Elisa	enzyme-linked immunosorbent assay
FBS	fetal bovine serum
GC	glucocorticoid
GEO	gene expression omnibus
GFP	green fluorescent protein h hours
GO	gene ontology
GR	glucocorticoid receptor
GRE	glucocorticoid response elements
H&E	hematoxylin and eosin
HFD	high fat diet
HPA	hypothalamo-pituitary-adrenocortical
HRP	horseradish peroxidase
IHC	immunohistochemistry
IgH	immunoglobulin H
IgG	immunoglobulin G

IP	immunoprecipitation
LB	Luria-Bertani medium
M	molar concentration
min	minute
$MgCl_2$	magnesium chloride
mRNA	messenger RNA
NaCL	natrium chloride
NaOH	natrium hydroxide
OptiMEM	reduced serum media modification of Eagle's Minimum Essential Media
PBS	phosphate buffered saline
PCR	polymerase chain reaction
PFA	paraformaldehyde
pH	minus the decimal logarithm of the hydrogen ion activity in a solution
POMC	pro-opiomelanocortin
qPCR	quantitative PCR
RT-PCR	reverse transcriptase polymerase chain reaction
RNA	ribonucleic acid
rpm	revolutions per minute
SCN	suprachiasmatic nucleus
Sem	standard error of the mean
SDS	sodium dodecyl sulfate
SDS-PAGE	sodium dodecyl sulfate poly- acrylamide gel electrophoresis
Stdev	standard deviation
TBS-T	tris buffered saline with Tween 20
TF	transcription factor

All gene names are indicated in *italics*. All proteins are written in regular font. Compounds and chemical elements are abbreviated according to common chemical nomenclature.

Index of Figures

Index of Tables

1. Introduction

1.1 Glucocorticoid signaling in health and disease

Glucocorticoids (GCs) were first discovered for their anti-inflammatory potential, when Philip Showalter Hench and colleagues administered 17-hydroxy-11-dehydrocorticosterone (at the time called “compound E”) to patients suffering from rheumatoid arthritis (Hench et al., 1949). Treatment with the compound, today known as cortisone, powerfully suppressed inflammation in all subjects and alleviated the symptoms of rheumatoid arthritis. This resulted in the Nobel Prize in Physiology or Medicine for Philip Showalter Hench, Edward Kendall and Tadeus Reichstein for the discovery of adrenal cortex hormones in 1950 (Burns, 2016).

1.1.1 HPA axis and the physiological role of glucocorticoids

Glucocorticoids are 21-carbon steroid hormones that regulate a large number of physiological actions throughout the body. By acting on nearly every organ, GCs respond to normal diurnal changes and situations of acute or chronic stress in order to maintain energy homeostasis (Sapolsky et al., 2000). The increased demand for systemic glucose to fuel brain and peripheral tissue is met by enhanced circulating GCs. In metabolic tissues, this is executed through increased gluconeogenesis in liver and by inhibiting insulin secretion from ß-cells (Patel et al., 2014). Besides their potent effects in immune cells permitting their use as anti-inflammatory drugs (see 1.1.2), the actions of GCs influence, among others, the nervous system, the cardiovascular and reproductive system, the respiratory system and neonatal growth (Sapolsky et al., 2000).

Due to their broad physiologic impact on multiple organ systems, the process of adrenal GC synthesis and secretion needs to be tightly regulated (**Fig. 1**). As a major neuroendocrine circuit, the hypothalamic-pituitary-adrenal (HPA axis) is the focal point of signal integration for the secretion of GCs. Upon neurochemical signals, corticotrophin-releasing hormone (CRH) is secreted from the hypothalamus, which in turn acts on the anterior pituitary to activate pro-opiomelanocortin (POMC) gene transcription to synthesize and secrete the POMC-encoded adrenocorticotropic hormone (ACTH) (Herman et al., 2016). ACTH then acts on the zona fasciculata of the adrenal cortex to produce adrenal GCs. Cortisol is the major active GC in humans and is synthesized *de novo* from cholesterol (Sprague et al., 1950). Cholesterol is first transported from cellular stores to the outer mitochondrial membrane and converted to the steroid precursor pregnenolone. This is followed by successive enzymatic modifications in a process called steroidogenesis and cortisol is subsequently released into the blood

stream to act on peripheral target tissues (Chung et al., 2011, Herman et al., 2016). In a classical negative feedback loop, GCs suppress the HPA axis. By inhibiting CRH gene expression at the level of the hypothalamus and inhibiting secretion of ACTH from the anterior pituitary, GCs essentially restrict their own production (Herman et al., 2016) (**Fig. 1**).

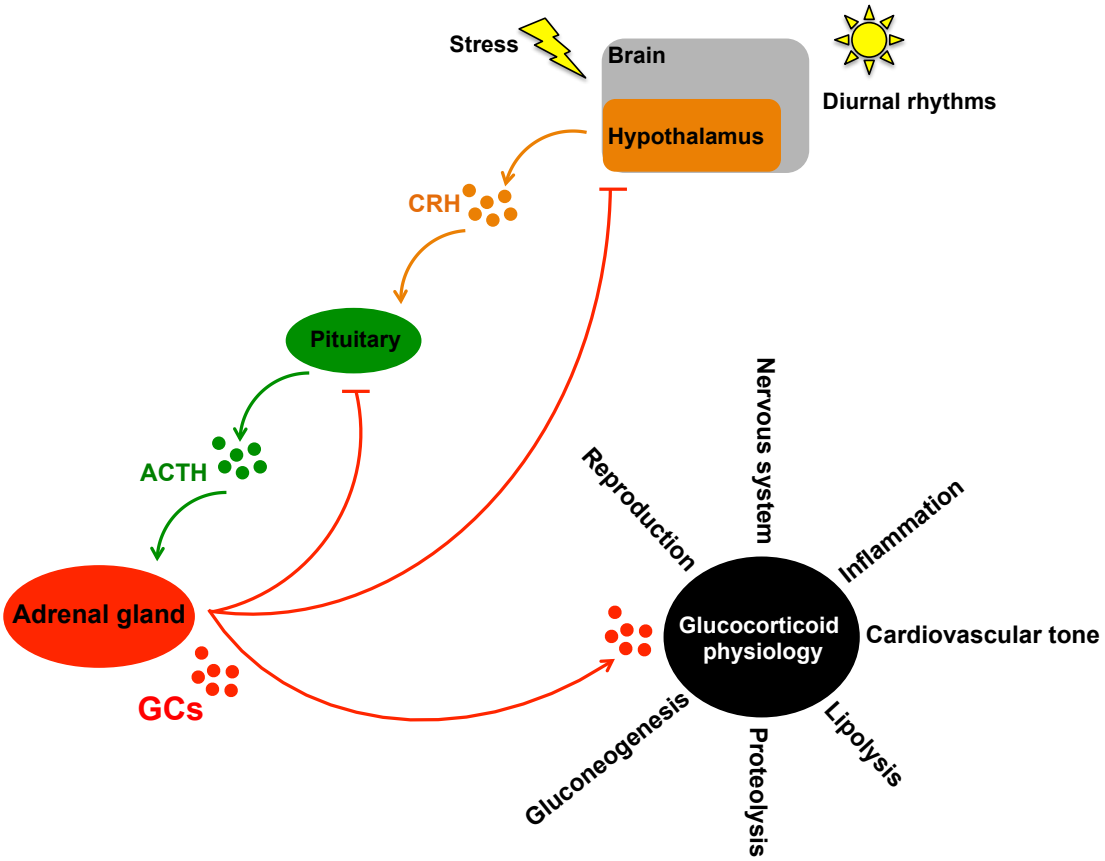

Figure 1: Schematic representation of the HPA axis.
Stress and diurnal rhythms activate the hypothalamus to produce and secrete the corticotrophin-releasing hormone (CRH). CRH then acts on the anterior pituitary and induces the secretion of adrenocorticotropic hormone (ACTH), which in turn signals the adrenal cortex to produce cortisol from cholesterol. Via a classical negative feedback loop, cortisol suppresses secretion of CRH and ACTH and regulates its own production. GCs have widespread physiological functions in the body. Picture modified from (Garabedian et al., 2017).

In basal conditions, secretion of adrenal GCs changes with a robust circadian and pulsatile rhythm, which is characterized by circulating levels peaking at the onset of activity and throughout (daytime for diurnal animals and nighttime for nocturnal animals) (Herman et al., 2016, Chung et al., 2011, Spiga et al., 2014) (**Fig. 1**). In addition, the HPA axis plays an important role for the body's response to outside factors or "stressors" challenging homeostasis (Herman et al., 2016). During acute or prolonged stress activation of the HPA axis, synthesis and secretion of GCs from the adrenal cortex is induced in order to meet temporary increased energy demands and readjust homeostasis (Herman et al., 2016).

1.1.2 Clinical value of glucocorticoid therapy

The discovery that sufficient amounts of synthetically derived GCs such as dexamethasone and prednisolone could be produced, spearheaded the evolution of the different GC treatment regimes. Estimates for prescription of oral GCs range between 1.2% of the adult US population (Overman et al., 2013). In this regard, GCs represent the most widely prescribed and effective medication for inflammatory and immune diseases worldwide. These range from short-term applications for skin rashes or seasonal allergies to long-term treatment of rheumatoid arthritis and asthma (Desmet and De Bosscher, 2017). The clinical success of GCs stems from their potential to effectively suppress inflammation in a variety of immune cells, depending on the disease model and the inflammatory stimulus. Macrophages represent the main target for the anti-inflammatory action of GCs, specifically in the case of septic shock and contact allergies (Kleiman et al., 2012, Tuckermann et al., 2007). As part of their potent immunosuppressive function, GCs can activate many anti-inflammatory genes. However, their dominant action lies in actively suppressing pro-inflammatory and immune genes. These include cytokines, chemokines, inflammatory enzymes and receptors as well as adhesion molecules important for cell migration to sites of inflammation. These genes are activated by pro-inflammatory transcription factors such as NF-κB and AP-1, which are attenuated by the action of GCs (Barnes, 1998, Beck et al., 2009a, Greulich et al., 2016). GCs are also prescribed after transplantation to prevent organ rejection and present an important part of chemotherapy regimes in the treatment of several hematological cancers, e.g. multiple myeloma, leukemia and lymphoma (Herold et al., 2006). This stems from their ability to induce apoptosis in many lymphoid cells, including thymocytes, monocytes and eosinophils, which complement their anti-inflammatory action (Necela and Cidlowski, 2004).

1.1.3 Side effects of glucocorticoid use

The initial enthusiasm for GCs in the 1950s and following years was quickly dampened when more and more side effects were reported. Rising circulating GC levels are the body's anticipatory response to meet an increased energy demand in situations of stress (Sacta et al., 2016). Since this stress response is only intended to be short to readjust the energy balance, exogenous administration of GCs will ultimately become maladaptive. Due to the systemic and pleiotropic effects of GCs, arising complications are in most cases so severe that they lead to cessation of treatment. Side effects depend on the choice of GC, duration and dosage of treatment and mode of application. However, systemic use usually results in more severe side effects than topical use (Schacke et al., 2002).

In dermatology, GCs present the most widely used therapy for cutaneous conditions. When used topically, long-term application of hydrocortisone can induce skin atrophy as well as steroid acne and delay effective wound healing (Schacke et al., 2002). There are several side effects of GC treatment concerning the musculoskeletal system. By increasing protein breakdown and inhibiting protein synthesis, GCs directly affect muscle protein content and induce skeletal muscle atrophy (Rose and Herzig, 2013) (Patel et al., 2014, Schacke et al., 2002). One of the most devastating side effects of long-term GC treatment is the development of osteoporosis. Throughout adult life, bone tissue is constantly replaced and remodeled by osteoclasts mediating bone resorption and osteoblasts mediating bone formation (Schacke et al., 2002). By suppressing osteoblast proliferation and increasing bone resorption, bone formation is affected and an overall loss of bone mineral density is induced (Frenkel et al., 2015). Long-term GC can have effects on the central nervous system by stimulating „steroid psychoses“ in previously stable patients or aggravate existing psychiatric problems including anxiety and depression (Schacke et al., 2002) (**Fig. 2**). Termination of GC treatment, on the other hand, can adversely affect the HPA axis itself. Due to the negative feedback response of GCs on the production and secretion of CRH and ACTH, atrophy of the adrenal cortex and secondary adrenal insufficiency are consequences, once exogenous GCs are withdrawn (Schacke et al., 2002).

The physiological role of GCs lies in stimulating hepatic gluconeogenesis to provide energy for the brain and peripheral tissue under conditions of stress or nutrient deficiency. A persistent elevation of GCs therefore entails severe disturbances of glucose and lipid metabolism. Long-term GC treatment is an associated risk factor for developing hyperglycemia and insulin resistance in peripheral tissue. This state is called “steroid diabetes” and frequently allows a deteriorating condition in diabetic patients (Schacke et al., 2002, van Raalte and Diamant, 2014). Treatment with GCs is linked to increased adiposity due to promoting pre-adipocyte differentiation (Geer et al., 2014, Vegiopoulos and Herzig, 2007). The resulting weight gain and development of an obese phenotype is one of the features of prolonged GC treatment. On the other hand, GCs enhance lipolysis and *de novo* lipogenesis in peripheral adipose tissue. Elevated levels of circulating free fatty acids promote an overall state of dyslipidemia (Geer et al., 2014). GC treatment is also associated with intracellular lipid accumulation in the liver. The development of hepatic steatosis is due to the induction of genes involved in lipogenesis and triglyceride synthesis (Vegiopoulos and Herzig, 2007, Patel et al., 2014). Moreover, mobilized free fatty acids from increased lipolysis in adipocytes are taken up the liver and are incorporated and stored into triglycerides in lipid droplets (Wang et al., 2012). A persistent state of dyslipidemia has also been identified as one the main adverse effect on the cardiovascular system. Prolonged GC treatment

frequently leads to the development of hypertension in patients. Mechanisms by which GCs induce hypertension may include an increase in contractility of cardiac smooth muscle cells as well as an increase in extracellular volume (Schacke et al., 2002, Walker, 2007) (**Fig. 2**).

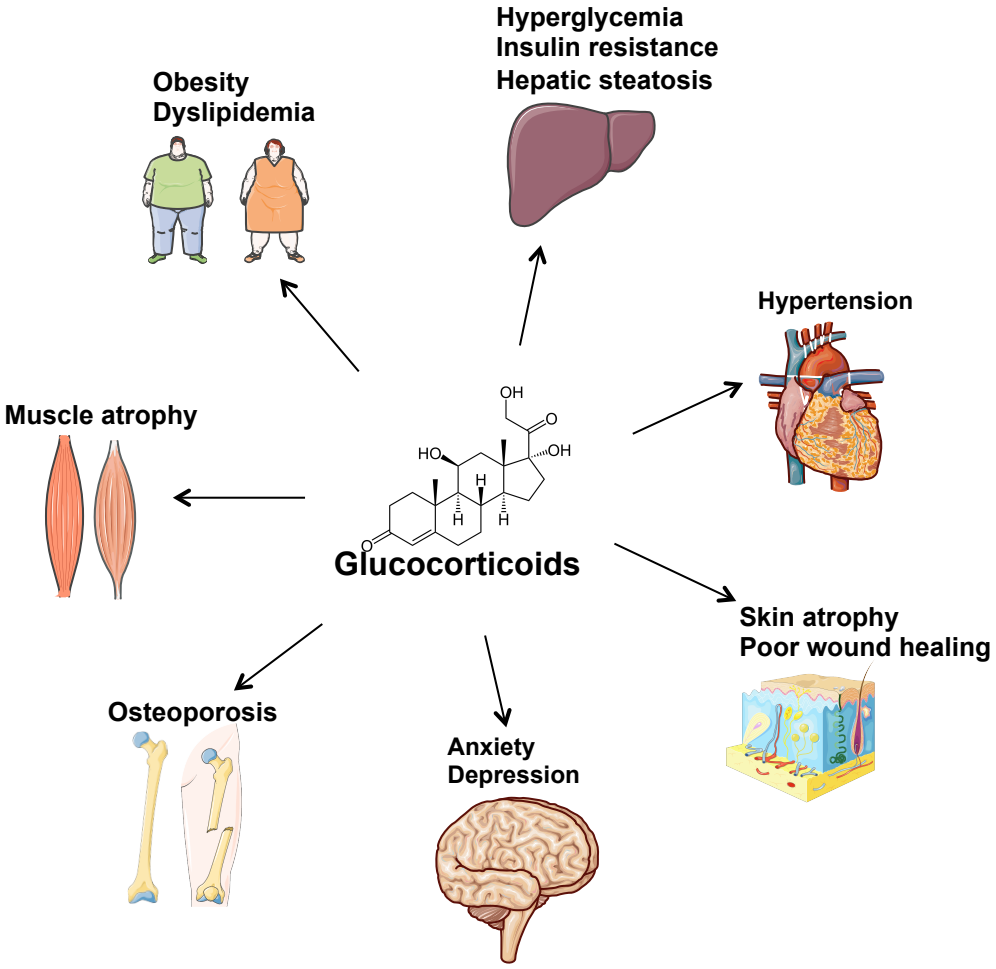

Figure 2: Side effects of glucocorticoid therapy.
The long-term use of GCs for the treatment of chronic inflammatory diseases leads to burdening side effects due to GCs' pleiotropic physiological effects in the body. Specifically in the case of long-term treatment and prescription of higher doses early cessation of treatment is often inevitable. Picture modified from <https://endo.wustl.edu/harris-lab/>, viewed May 2018. Individual cartoons taken from Servier Medical Art, licensed under a Creative Common Attribution 3.0 Generic License, <http://smart.servier.com/>.

Many of the complications of GC excess are typical components of the Metabolic Syndrome, which presents as an array of associated metabolic disorders, including hyperglycemia, insulin resistance, obesity, dyslipidemia and hypertension. Mounting clinical evidence suggests a strong correlation between elevated GC activity and the development of the Metabolic Syndrome. In insulin-resistant patients, circulating cortisol levels are elevated, which is seen as an underlying cause of chronic hyperglycemia and systemic dyslipidemia (Rose and Herzig, 2013, Wang, 2005). This link is also exemplified in Cushing's disease, an

endogenous overproduction of GCs. Here, tumors in the pituitary or ACTH-producing tumors result in a prolonged hypersecretion of GCs and sustained high levels of circulating GCs in the blood (Shibli-Rahhal et al., 2006). Patients suffering from Cushing's disease present with central obesity, muscle wasting, hypertension, hyperglycemia, insulin resistance and the development of hepatic steatosis; an array of symptoms fatal if left untreated (Shibli-Rahhal et al., 2006).

How glucocorticoids regulate systemic energy metabolism is still not fully understood. The challenge lies in the separation of the beneficial anti-inflammatory effects from the adverse side effects to eventually develop safer steroid drugs for the clinic.

1.2 Cellular mechanisms of glucocorticoid receptor signaling

Glucocorticoids bind to the Glucocorticoid Receptor (GR) and serve as small molecule ligands. GR belongs to a superfamily of ligand-activated transcription factors, the Nuclear Hormone Receptor family (NR) (**Fig. 3**). This superfamily comprises the classic steroid receptors including GR, the estrogen receptor (ER), the mineralocorticoid receptor (MR), the androgen receptor (AR) and the progesterone receptor (PR). GR and ER represent the founding members of the NR family since their complete cDNAs were the first to be isolated in the 1980s (Hollenberg et al., 1985, Green et al., 1986, Evans and Mangelsdorf, 2014).

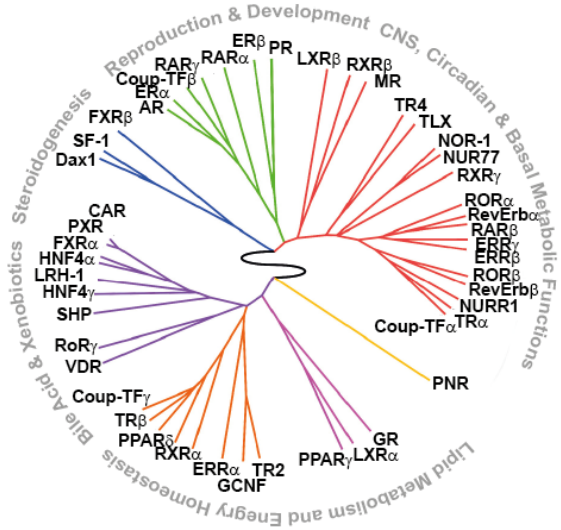

Figure 3: The superfamily of nuclear hormone receptors.
Nuclear hormone receptors were clustered according to tissue distribution revealing the link to physiological pathways, e.g. reproduction, development, lipid and energy homeostasis. Picture modified from (Bookout et al., 2006).

Among the other important members are the peroxisome proliferator activated receptors (PPARs), the liver X receptors (LXRs) and the thyroid hormone receptor (TR). Together, NRs

regulate key physiological processes, e.g. reproduction, metabolism, homeostasis, inflammation and development (Mangelsdorf et al., 1995, Evans, 1988, Evans and Mangelsdorf, 2014).

1.2.1 The glucocorticoid receptor protein

The human GR is encoded by the *Nr3c1* gene located on chromosome 5q31–32 and comprises 9 exons (Oakley and Cidlowski, 2011). GR is a modular protein, which is characteristic of the nuclear receptor family. It contains a N-terminal transactivation domain (NTD), a central DNA-binding domain (DBD), and a C-terminal ligand-binding domain (LBD) **(Fig. 4).** Exon 2 encodes most of the NTD, exons 3 and 4 encode the DBD, and exons 5–9 encode the hinge region (H) and LBD (Oakley and Cidlowski, 2011). The DBD and LBD domains are separated by a flexible region termed the hinge region (H). The DBD contains 2 zinc finger motifs necessary for recognition and binding of target DNA sequences. The first zinc finger region contains amino acids, which contact specific bases and confer specificity to DNA binding. The second zinc finger region contains a stretch of amino acids, the D loop, which enables homodimerization of GR (Kumar and Thompson, 2005, Dahlman-Wright et al., 1991).

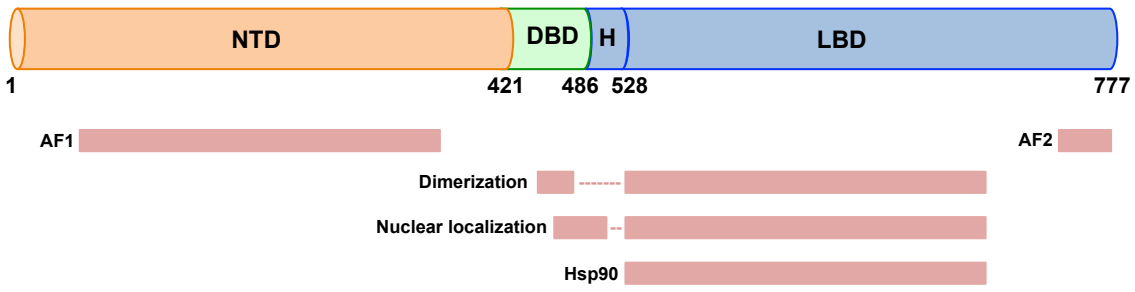

Figure 4: Schematic representation of the glucocorticoid receptor structure.
The glucocorticoid receptor is composed of 3 domains: the N-terminal transactivation domain (NTD), the central DNA-binding domain (DBD), the hinge region (H) and the C-terminal ligand-binding domain (LBD). Regions involved in transcriptional activation (AF1 and AF2), dimerization, nuclear localization, and chaperone Hsp90 binding are indicated in red. Numbers depict amino acids for human GR. Picture modified from (Oakley and Cidlowski, 2013).

The NTD harbors a strong transcriptional activation function domain (AF1) important for interaction with multiple coregulators and components of the basal transcription machinery. A hydrophobic pocket required for ligand binding is located in the LBD. The LBD also houses a second, albeit small, activation function domain (AF2), which interacts with certain co-activators and co-repressors in a ligand-dependent manner (Kumar and Thompson, 2005).

Two nuclear localization signal sequences located at the junction of DBD/hinge region and within the LBD ensure efficient transport into the nucleus (Kumar and Thompson, 2005, Oakley and Cidlowski, 2011). The traditional view that a single glucocorticoid receptor protein exists has been challenged in recent years with the discovery that alternative splicing and translation give rise to different receptor isoforms. The two most well known isoforms are termed GRα and GRβ and differ at the C termini. GRβ lacks the LBD domain and therefore cannot bind to glucocorticoids. It constitutively resides in the nucleus and was shown to function as a dominant-negative inhibitor of GRα (Oakley and Cidlowski, 2011).

1.2.2 Gene regulation by GR: Activation versus Repression

In the absence of ligands, GR primarily resides in the cytoplasm in a transcriptionally inactive state as part of a multiprotein complex that includes various chaperone proteins and immunophilins. Key components of this complex are the heat shock proteins 90 and 70 (Pratt and Toft, 1997). GCs diffuse through the cell membrane and are bound at the LBD domain of GR. This leads to a conformational change of GR resulting in the disassembly of the multiprotein complex. The nuclear translocation signals are exposed and enable nuclear translocation of the activated GR. Ligand-activated GR has two mechanisms of action: upregulation of genes (activation) versus downregulation of genes (repression) (Sundahl et al., 2015, Beck et al., 2009a, Vandevyver et al., 2013). However, the underlying mechanisms leading to activation versus repression are still unknown.

Ligand-activated GR is known to interact directly with regulatory DNA sequences. These DNA sequences are located in promoters and enhancers of GR target genes, termed glucocorticoid response elements (GRE). The consensus GRE sequence is classically defined as inverted repeats (5‘-nGnACAnnnTGTnCn-3‘) comprising two 6-bp half sites and a 3-nucleotide spacer (Lim et al., 2015, Starick et al., 2015, Greulich et al., 2016, Oakley and Cidlowski, 2011). GR can influence gene expression directly by binding as a homodimer to GREs (Dahlman-Wright et al., 1990), by interaction with other DNA-bound transcription factors or via “composite elements”. They present as a combination of GREs and other transcription factor motifs in close proximity (Glass and Saijo, 2010, Langlais et al., 2012) (**Fig. 5**). For GR-mediated repression, several additional mechanisms have been postulated. Suppression of pro-inflammatory stimuli is generally attributed to the inhibition of both AP-1 and NF-κB family members by GR (Beck et al., 2009a, Glass and Saijo, 2010). Repressive scenarios also include binding of monomeric GR to other DNA-bound TFs, termed “tethering”, as opposed to the direct and sequence-specific DNA interaction of homodimeric GR (Vandevyver et al., 2013, Beck et al., 2009a). The competition for binding sites

overlapping with other transcription factors or the sequestration of important cofactors are among the other potential mechanisms previously described (Beck et al., 2009a, Sundahl et al., 2015, Vandevyver et al., 2013). In addition, the existence of a so-called negative GRE (nGRE) has been proposed to mediate transcriptional repression by direct DNA binding (Surjit et al., 2011, Beck et al., 2009a, Morrison and Eisman, 1993).

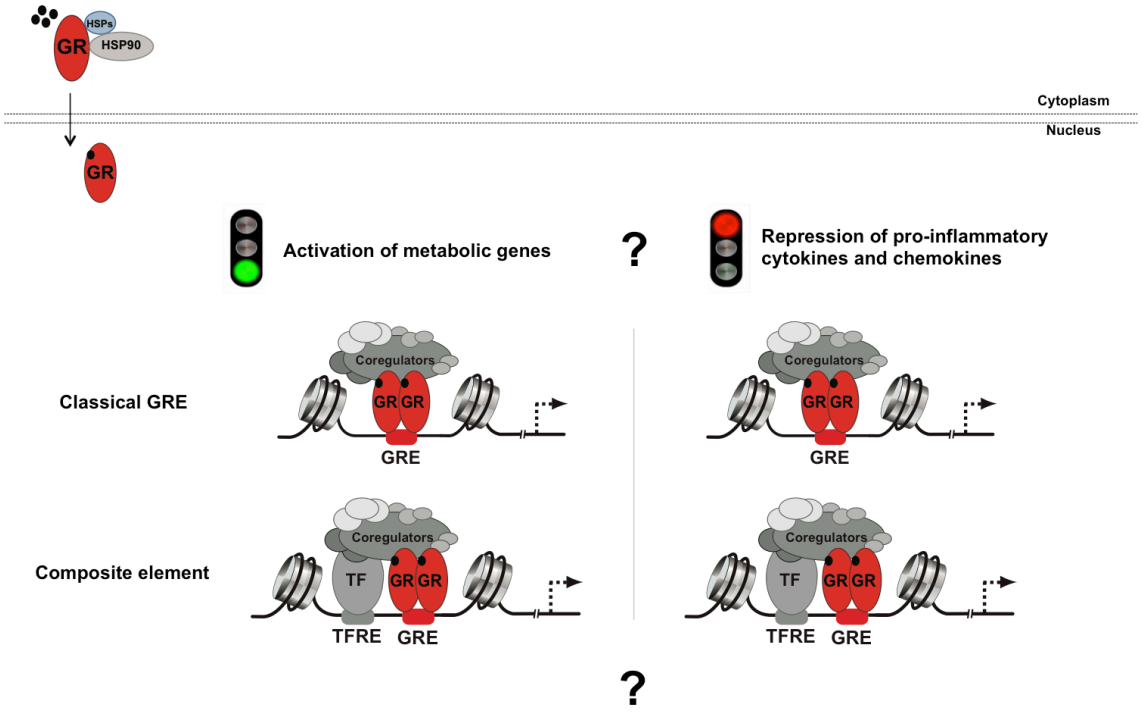

Figure 5: GR can activate and repress genes via binding to DNA response elements.
Ligand-activated GR translocates into the nucleus where it positively or negatively regulates target genes. GR activates gene transcription by binding as a homodimer to *glucocorticoid response elements* in promoters and enhancers of target genes or via composite elements together with other transcription factors (TFRE= transcription factor response element). How GR distinguishes between gene activation versus gene repression is not known, but regulatory polarity might be determined by yet unknown factors interacting with GR at promoters or enhancers of target genes.

GR does not act in isolation but interacts with a repertoire of different transcription factors to assemble multiprotein complexes at promoters and enhancers of target genes. GRE-bound GR undergoes conformational changes and recruits coregulators and chromatin-remodeling complexes, e.g. histone-modifying enzymes. Recruitment of distinct coregulators ultimately enables chromatin remodeling and histone modifications and directly affects the assembly of the basic transcriptional machinery and the activity of the RNA polymerase II (Greulich et al., 2016, Vandevyver et al., 2013).

The therapeutic benefits of GC treatment are mainly explained via the repression of inflammatory genes, whereas the detrimental side effects are mostly ascribed to the dimer-

mediated activation of metabolic genes (Beck et al., 2009a, Sundahl et al., 2015, Vandevyver et al., 2013). Since the intrinsic factors governing the positive versus negative transcriptional outcome by GR are still unclear, a more complex manner of GR-mediated gene regulation has been suggested. Regulatory polarity might rather depend on cellular environment, chromatin context, epigenetic regulators and the presence of other yet unknown interacting transcription factors (Greulich et al., 2016).

1.3 Genomic GR action

By binding to its genomic response elements, GR plays a central role in the regulation of gene expression. GR action is highly cell-type specific. While GR is widely expressed, the GR cistromes from different cell types show very little overlap in binding patterns (Grontved et al., 2013) (**Fig. 6**). A cistrome is defined as the sum of all binding sites of a transcription factor in a given cell type, which is represented by the ChIP-Seq data set. This emphasizes a tissue and context-specific gene regulation and suggests parameters outside the recognition sequence to be of importance.

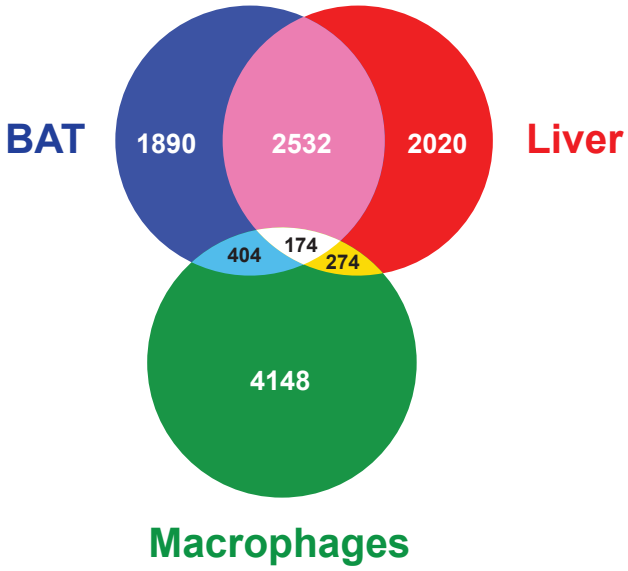

Figure 6: GR cistromes differ between cell types.
GR ChIP-Seq data from Dex-treated liver, macrophages and brown adipose tissue (BAT) were compared. The top 5000 peaks of each data set according to peak strength were used for comparison. The limited overlap in GR binding events (cistromes) demonstrates tissue-specificity. ChIP data from macrophages taken from (Uhlenhaut et al., 2013). Data can be accessed from NCBI GEO (accession number: GSE31796). ChIP data from liver and BAT is unpublished.

1.3.1 Direct GR signaling in liver and macrophages

Tight regulation of distinct sets of target genes ensures proper control over two of GR's signature functions: inducing gluconeogenesis in liver and suppressing inflammatory processes in immune cells. In liver, GR directly controls expression of the two main regulatory and rate-limiting enzymes in hepatic gluconeogenesis: *phosphoenolpyruvate*

carboxykinase 1 (*Pck1*) and *glucose-6-phosphatase* (*G6pc*). Promoters of both genes harbor functional GREs. These have been extensively characterized over the past 20 years and serve as paradigms of GR-controlled transcriptional activation (Imai et al., 1990, Vander Kooi et al., 2005). In agreement with this, in liver-specific *GR* knockout mice the transcriptional activation of *Pck1* and *G6pc* is diminished in response to prolonged fasting (Opherk et al., 2004). In hepatic lipid metabolism, on the other hand, GR directly regulates the *hairy and enhancer of split-1* (*Hes1*) gene. GR represses *Hes1* expression by recruiting histone decacetylases to its promoter (Lemke et al., 2008). In liver-specific GR knockout mice, *Hes1* expression is derepressed and hepatic steatosis is ameliorated in a fatty liver mouse model (Lemke et al., 2008). Similarly, loss of hepatic *Hes1* results in abnormal GR-mediated target gene regulation (Revollo et al., 2013).

Macrophages represent the major targets for GR in the resolution of inflammatory processes. Here, the expression of anti-inflammatory genes, e.g. glucocorticoid-induced leucine zipper (*Tsc22d3*/ *Gilz*), dual specificity phosphatase/MAP kinase phosphatase 1 (*Dusp1*) or kruppel-like factors 2 and 9 (*Klf2*, *Klf9*) is effectively induced by GR. GR's crucial anti-inflammatory function, however, is executed through the repression of inflammatory genes. These include classic inflammatory cytokines such as interleukin 6 (*Il6*), interleukin 1 alpha/beta (*Il1a/b*) and other inflammatory mediators such as inducible nitric oxide synthase 2 (*Nos2*), the matrix metalloproteases 12 and 13 (*Mmp12/13*) and tumor necrosis factor (*Tnf*) (Uhlenhaut et al., 2013, Kleiman et al., 2012).

1.3.2 Role of the neighboring chromatin: endowing cell-specificity

Motif enrichment analysis of ChIP-Sequencing data sets from GR in mouse livers identified several footprints of transcription factors to be significantly enriched together with GREs (Lim et al., 2015, Grontved et al., 2013, Phuc Le et al., 2005). These include CCAAT/enhancer binding protein (c/EBP), hepatic nuclear factor 4 alpha (Hnf4α), Hnf6 and the Forkhead factor family (Fox) (**Fig. 7A**). c/EBP was shown to be indispensable for GR to access and bind DNA in mouse livers, since disruption of c/EBP function interferes with recruitment and DNA binding of GR (Grontved et al., 2013). On the other hand, Hnf4α, Hnf6 and members of the FoxA family all hold important roles in liver development, which supports their role as lineage-determining pioneering factors (**Fig. 7B**). Hnf4α is essential for mammalian hepatocyte differentiation and maintenance of hepatic gene expression (Li et al., 2000, Hayhurst et al., 2001). Hnf6 controls the early migration of hepatoblasts and is responsible for the coordinated time-specific gene expression during liver development (Margagliotti et al., 2007, Beaudry et al., 2006). FoxA2 was previously shown to establish competency by

opening up closed chromatin in liver-specific genes. By occupying the albumin enhancer during hepatic differentiation from the gut endoderm, FoxA2 keeps the enhancer transcriptionally silent but accessible for binding of additional factors and subsequent gene activation (Gualdi et al., 1996). The crucial role of FoxA1 and FoxA2 in the onset of hepatogenesis is furthermore supported by knockout mouse models for both factors, which fail to develop a liver bud (Lee et al., 2005). Footprints of transcription factors Hnf6 and FoxA were also identified as most closely enriched to GREs in different cell lines (Lim et al., 2015, Starick et al., 2015). Apart from their crucial role in liver development, c/EBP (Park et al., 1993), Hnf4α (Hall et al., 1995), FoxA2 (Wang et al., 1996) and FoxO1 (Hall et al., 2000) all have accessory functions in enabling efficient recruitment of GR to the *Pck1* locus and facilitate its full induction (Chakravarty et al., 2005).

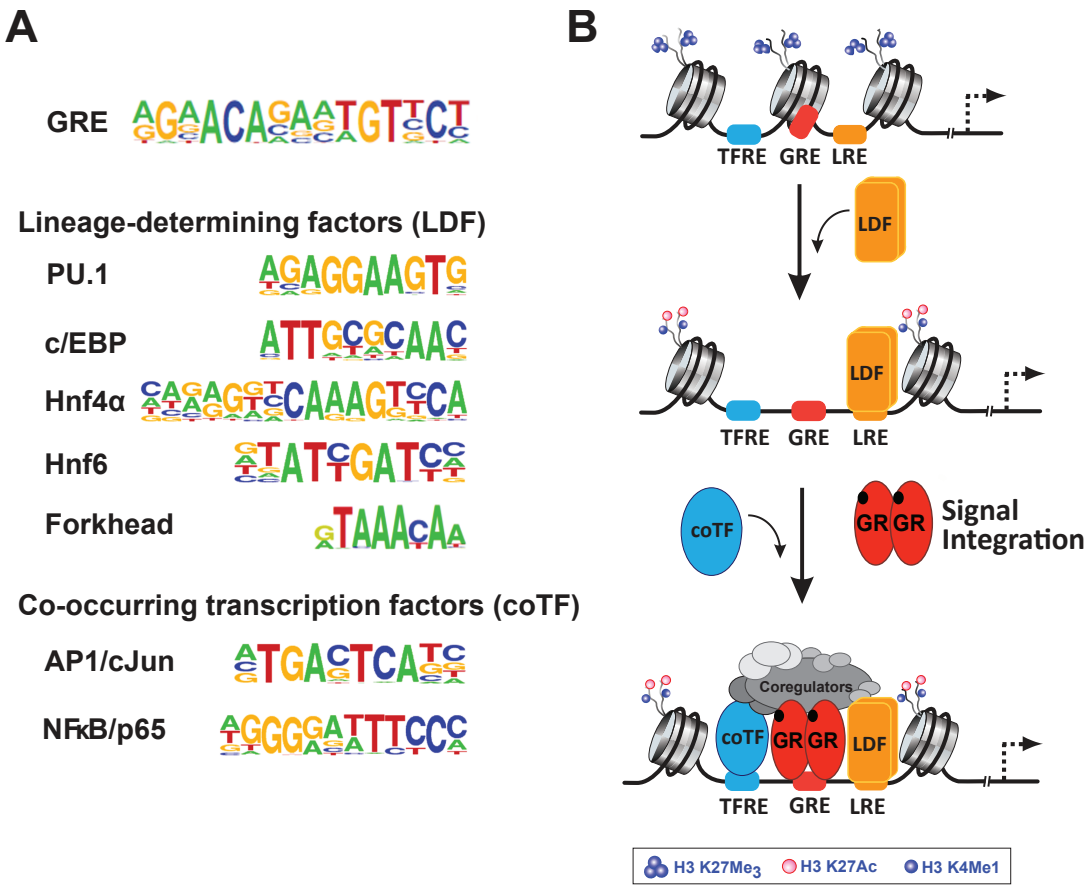

Figure 7: Mechanism of cell-type specific gene regulation by GR.
(A) Transcription factor binding motifs enriched together with with GREs in ChIP-Seq data in liver and macrophages are classified into lineage-determining factors (LDF) or co-occurring transcription factors (coTF). **(B)** LDFs bind to their motif in compacted chromatin and recruit histone demethylases/methylases and histone acetyltransferases to open chromatin and establish a cell-type specific enhancer landscape. Repressed chromatin is marked by tri-methylated H3K27, which is acetylated in open chromatin (H3K27ac). Active enhancers are marked by both acetyled H3K27 and monomethylated H3K4me1. GR can access open chromatin and bind to GRES upon signal integration. Together with other transcription factors binding their respective motif (TFRE) GR regulates target genes in a locus-specific manner. Picture modified from (Greulich et al., 2016).

In macrophages, binding site motifs of PU.1 (also known as Spleen focus forming virus (SFFV) Proviral Integration oncogene), c/EBP, the NF-kB subunit p65 and the AP-1 subunits c-Jun were identified and present possible binding partners of GR (Lim et al., 2015, Uhlenhaut et al., 2013) (**Fig. 7A**). PU.1 and c/EBP are indispensable for the development of the myeloid lineage (Heinz et al., 2010, Iwasaki et al., 2005). By "priming" for the myeloid lineage they establish the enhancer landscape specific to monocytes (Heinz et al., 2010, Jin et al., 2011). Suppression of inflammatory stimuli by GR is linked to the presence of co-occurring transcription factor binding motifs for the NF-kB subunit p65 and the AP-1 subunit c-Jun. Studies in HeLa cells identified direct protein-protein interactions of GR with p65 and c-Jun (Ogawa et al., 2005, Diamond et al., 1990) and AP-1 was shown to be necessary for recruitment of GR to a subset of AP-1/GR composite elements in 3134 cells (Biddie et al., 2011). This argues for a concurrent binding of all three factors at enhancers and a role of GR in inhibiting the downstream action of NF-kB and AP-1 in the resolution of inflammatory processes.

In addition to incorporating sequence data into predicting genomic transcription factor binding sites, the epigenetic landscape of a given cell represents one of the major contributors of cell-type-specific responses. The majority of hormone-induced GR binding events occur at pre-existing accessible chromatin, with far less in *de novo* remodeled chromatin (Grontved et al., 2013, John et al., 2011, Biddie et al., 2011). Chromatin bound by transcription factors is associated with specific histone modifications at promoters or enhancers. Whereas active promoters are enriched for trimethylated H3K4 (H3K4me3) and acetylated H3K9 (H3K9ac), active enhancers show acetylation at H3K27 (H3K27ac) and monomethylation of H3K4 (H3K4me1) (Heintzman et al., 2007). Metabolic genes, e.g. *Pck1* and *G6pc* or inflammatory cytokines, e.g. *Il6* and *Il1a* change their expression depending on the cell type. GR binds the enhancer and promoter regions of *Pck1* and *G6pc* in liver (Grontved et al., 2013), but not in activated macrophages. In activated macrophages, the receptor binds the enhancers of *Il6* and *Il1a* (Uhlenhaut et al., 2013), but not in hepatocytes (**Fig. 8**). This differential binding is accompanied by changes in the epigenetic signature of the bound loci. Enhancers for *Pck1* and *G6pc* are acetylated at H3K27 and monomethylated at H3K4 in hepatocytes (Yue et al., 2014), but not in activated macrophages (Ostuni et al., 2013). In macrophages, the *Il6* enhancer shows the same pattern of histone marks, but not in hepatocytes (**Fig. 8**). Since nearly a third of all GR-bound sites in hepatocytes and macrophages are enriched for H3K27ac and H3K4me1 (Grontved et al., 2013, Uhlenhaut et al., 2013, Ostuni et al., 2013, Yue et al., 2014), this highlights the requirement for open chromatin for GR to efficiently bind its target genes in liver and macrophages.

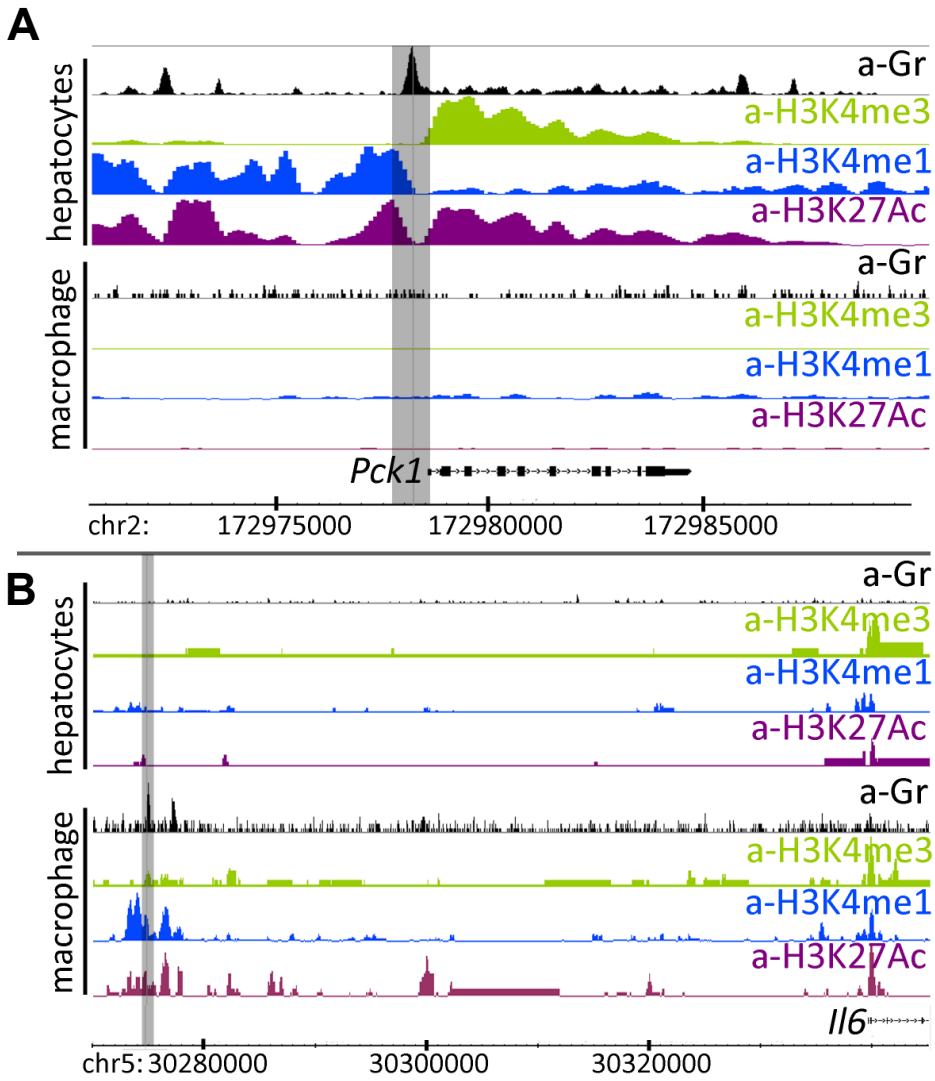

Figure 8: GR binds accessible chromatin in hepatocytes and macrophages.
ChIP-Seq tracks for GR, H3K4me3, H3K4me1 and H3K27ac are shown in hepatocytes and LPS-activated macrophages. **(A)** In hepatocytes, GR binds the *Pck1* promoter. Chromatin surrounding harbors the double mark of H3K4me1/H3K27ac for active enhancers and the additional H3K4 trimethylation mark (H3K4me3), indicating the proximity to the *Pck1* promoter. In macrophages, this locus is not bound by GR and is void of any enhancer/promoter-specific histone marks. **(B)** In macrophages, the *Il6* enhancer is bound by GR and harbors the double H3K4me1/H3K27ac histone mark for active enhancers. In hepatocytes this chromatin is not accessible for GR binding and is lacking these histone marks. Picture taken from (Greulich et al., 2016).

The past years have shown that GR depends on the presence of lineage-determining pioneering factors to generate chromatin accessibility for binding to enhancers and promoters and to create cell-type specific hormone responses (Granner et al., 2015, Miranda et al., 2013). Deciphering the factors, which determine GR's functionality as a transcriptional regulator at cell-type specific sites, will shed light on how the anti-inflammatory versus metabolic actions are defined.

1.4 The E protein family of basic helix-loop-helix transcription factors

To gain insight into tissue-specific crosstalk involved in the transcriptional activation of metabolic programs in response to GCs, ChIP-Sequencing and motif analysis for GR in mouse livers was performed. In addition to motifs for Hnf4α, Hnf6 and Fox, an E-Box was found as specifically enriched near GREs in hepatic promoters and enhancers. This particular E-Box was predicted to be bound by the basic helix-loop-helix (bHLH) transcription factor E47.

The basic helix-loop-helix (bHLH) proteins constitute a large superfamily of transcriptional regulators regulating many critical developmental processes including cell proliferation, cell differentiation and lineage determination. More specifically, they were identified to be key regulators of neurogenesis, myogenesis, hematopoeisis, and heart and pancreas development (Massari and Murre, 2000, Skinner et al., 2010, Jones, 2004). As dimeric transcriptional regulators, bHLH proteins commonly bind a consensus DNA sequence (CANNTG) called the E-Box.

1.4.1 The E-Box: function and physiological relevance

The E-box was originally discovered as part of a *cis*-acting DNA control element in the immunoglobulin heavy chain (IgH), known as the IgH intronic enhancer, and important for gene transcription (Ephrussi et al., 1985). These sites were present in both the heavy chain and light chain enhancers and shared a motif, which consisted of the core hexanucleotide sequence CANNTG (Ephrussi et al., 1985). After additional sites were discovered in B-cell specific promoter and enhancer elements it was subsequently named Ephrussi-box (E-Box) (Ephrussi et al., 1985, Massari and Murre, 2000, Staudt and Lenardo, 1991).

In the following years, more and more E-Box sites were also identified in promoters and enhancers of genes governing muscle-, pancreas-, and neuron development. These findings quickly established their important role in mediating tissue-specific gene transcription. In myogenesis, the upstream enhancer of the muscle creatine kinase gene contains two E-Box elements, which are bound by MyoD for full muscle-specific enhancer activity (Lassar et al., 1989) whereas multiple E-box regulatory sites have been identified in the insulin gene to drive pancreatic-cell-specific gene expression in a cooperative and tissue-restricted manner (Naya et al., 1995). Finally, E-Box elements constitute an essential part of the transcription-translation feedback loop comprising the circadian clock (Munoz et al., 2002). Hao et al. initially showed that transcription from the *period* gene of Drosophila happens in a circadian

manner driven by an enhancer found 69 bp upstream of the transcriptional start site (Hao et al., 1997). An E-Box element within this enhancer drives high levels of mRNA expression of the *period* gene (Hao et al., 1997). It was later discovered that circadian E-Boxes share the feature of recruiting the two master transcription factors BMAL1/CLOCK. These bind to them and drive rhythmic gene expression under circadian control (Partch et al., 2014, Munoz et al., 2002). Despite its brevity of merely 6 nucleotides and broad tissue distribution, the E-Box influences a large number of genes and is an integral part of tissue-specific gene expression.

1.4.2 Structure and classification of bHLH proteins

In 1989, Murre et al. reported two transcription factors E12 and E47, which arise from alternative splicing from E2A, to bind the original E-Box in the immunoglobulin kappa gene enhancer (Murre et al., 1989a, Sun and Baltimore, 1991, Henthorn et al., 1990). The E-Box site was critical for DNA binding of both factors and constituted a shared region of homology with MyoD, the myogenic differentiation factor, the Myc family of transcription factors, the *Daughterless* protein and the *achaete-scute* gene complex of *Drosophila* (Massari and Murre, 2000, Murre et al., 1989a). Analysis of the shared homology sequence revealed two alpha amphipathic helices (H) separated by hydrophobic residues frequently found in loops (L) and a number of conserved basic amino acid residues attached to one helix (basic region) (**Fig. 9**).

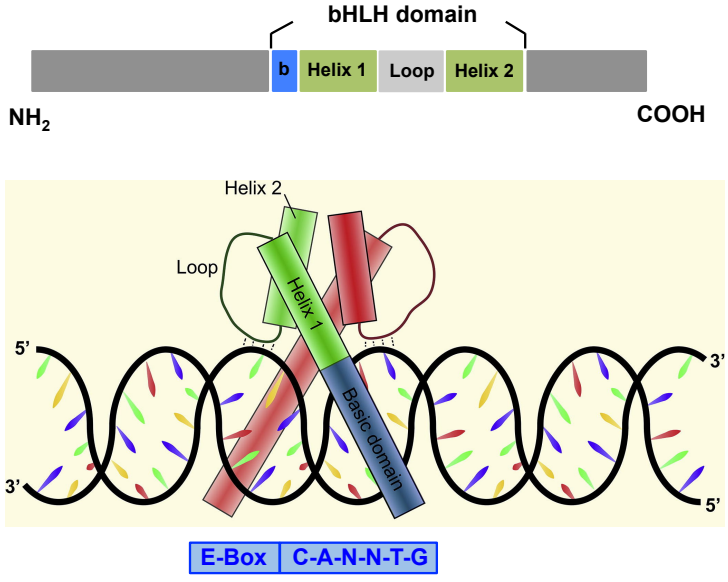

Figure 9: Structure of a bHLH transcription factor.
bHLH transcription factors are comprised of two alpha amphipathic helices (helix 1 and 2) and are separated by a hydrophobic loop. A string of conserved basic amino acid residues (**b**) mediates DNA binding. bHLH factors can homo-or heterodimerize facilitated by the two helices and the basic domain recognizes and binds E-Box sequences in the DNA. Picture modified from (Dennis et al., 2018).

Whereas the HLH part of the domain allows for dimerization with other HLH proteins, the basic region facilitates DNA binding. This motif was named basic helix-loop-helix (bHLH) motif and was recognized as the cognate recognition site for bHLH proteins (Murre et al., 1989a, Massari and Murre, 2000, Murre et al., 1994). Using electrophoretic mobility shift assays, Murre et al. could show that different HLH proteins are able to bind to DNA as heterodimers with other HLH members and in some cases form weak homodimers (Murre et al., 1989b). A classification scheme was established and consists of seven classes based on a number of structural and functional criteria, e.g. dimerization profile, tissue distribution and DNA binding properties (Murre et al., 1994, Massari and Murre, 2000). In the following, E12 and E47 were classified as the first bHLH factors and named E proteins for binding the original Ephrussi-box (Murre et al., 1989a). **Table 1** shows an overview of the different classes of bHLH proteins and describes their structural properties.

Table 1: Classification of bHLH proteins.

Classes	Members	Description/special features
I	E2A (E47, E12), Heb, E2-2, *Daugtherless*	E-proteins; bind classical E-Box
II	MyoD, NeuroD/Beta2, MASH, *Twist, Achaete, Scute*	preferentially heterodimerize with E proteins
III	Myc, TFE3, SREBP1	Leucine zipper adjacent to HLH domain mediates dimerization
IV	Mad, Max	Leucine zipper adjacent to HLH domain mediates dimerization
V	ID proteins (1-4)	lack basic region and cannot bind to DNA, preferentially bind to E proteins
VI	HES, H*airy*, *Enhancer of split*	proline residue in basic region; CACG(C/A)G or the N-Box CACNAG; low affinity for E-Boxes
VII	Arnt, AHR, Hif1a, Clock, *Period*	Pas domain adjacent to HLH domain mediates dimerization; ACGTG or GCGTG

For *Drosophila*, proteins are italicized. Classes according to (Murre et al., 1994). Table modified from (Jones, 2004).

1.4.3 E2A and the E proteins

The family of E proteins comprises E2A (E12 and E47), E2-2, HEB and *Drosophila's Daughterless* and their binding is restricted to the E-Box site (Murre et al., 1989b). By homodimerization, E proteins function as transcriptional activators. Heterodimers with class II bHLH proteins can function both as activators or repressors depending on the co-activators or co-repressors recruited (Kee, 2009). Homodimers preferentially bind the E-Box sequence

CACCTG. Heterodimers between E proteins and class II bHLH factors can bind both canonical and non-canonical E-box sites (Murre et al., 1989b, Kee, 2009, Massari and Murre, 2000)(**Fig. 10**). Since E proteins are ubiquitously expressed, tissue-specific gene expression is facilitated through heterodimerization with the more tissue-restricted class II bHLH factors (Wang and Baker, 2015). E proteins can also bind to class V bHLH proteins (**Table 1**). Members from this group, the ID proteins, lack a basic region required for contact with the DNA. Heterodimers between E proteins and ID proteins are therefore unable to bind DNA (Massari and Murre, 2000, Kee, 2009).

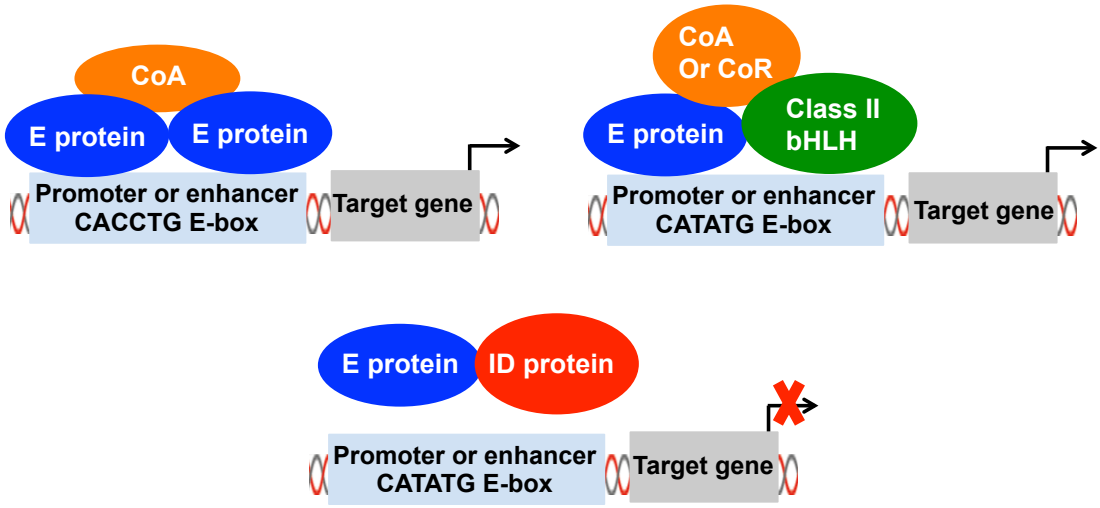

Figure 10: E proteins have different transcriptional modalities.
E proteins bind as homodimers to E-boxes in target genes and recruit co-activators (CoA) (left). Heterodimers between E proteins and class II bHLH activate or repress gene expression depending on whether co-activators (CoA) or co-repressors are recruited (middle). Heterodimers between E proteins and ID proteins fail to bind DNA and do not activate gene transcription (right). Picture modified from (Kee, 2009).

Consistent with its known role in activating expression of genes specific to the B and T-cell lineages, E2A preferentially functions as a transcriptional activator. The two encoded splice variants E47 and E12 only differ in their basic DNA binding region (Sun and Baltimore, 1991, Murre et al., 1989b). *E2A* null mutant mice display a high rate of postnatal lethality (Zhuang et al., 1994). Heterozygous mice survive but fail to generate committed B cell progenitors (pro-B cells) and display a partial block at the earliest stage of T-lineage development (Bain et al., 1997a, Zhuang et al., 1994, Bain et al., 1994). The full arrest of B cells occurs early and E47 and E12 each have distinct roles in B lymphopoiesis (Bain et al., 1997b, Beck et al., 2009b). Both *E47* and *E12* null mice are viable and do not display any developmental growth defects (Beck et al., 2009b). They synergistically promote B lymphocyte maturation whereby deletion of *E47* in mice results in a complete block in early B cell development (prepro-B cells) but not in *E12* mutant mice (Beck et al., 2009b). At a later stage, a gradient of both

factors is needed for proper pre-B and immature B cells (Beck et al., 2009b). In hematopoiesis, ID2 and ID3 act as dominant regulators of dosage and activity of E47 and E12 thereby controlling lymphoid development (Lazorchak et al., 2005, Engel and Murre, 2001, Murre, 2005).

In vitro studies have demonstrated that E47 is involved in regulating cell-type specific pathways in differentiation and development. E47 was shown to interact with the class II bHLH proteins MyoD and plays an important role in muscle differentiation (Lassar et al., 1991, Murre et al., 1989b). Moreover, E47 can heterodimerize with NeuroD/Beta2, another class II bHLH factor. NeuroD/Beta2 is a key regulator of pancreatic islet development and the insulin gene in β cells (Naya et al., 1997, Naya et al., 1995). *NeuroD/Beta2* null mice display a reduced number of insulin-producing cells, fail to develop mature islets and die shortly after birth due to severe hypoglycemia (Naya et al., 1997). In transient transfection assays, a heterodimer between NeuroD/Beta2 and E47 can bind the insulin E-Box sequence and tissue-specifically activate the insulin enhancer. This implicates the NeuroD/Beta2:E47 heterodimer as a part of the transcriptional complex which cooperatively activates the insulin gene (Naya et al., 1995). Moreover, E47 and its negative regulator ID3 have both been implicated as novel regulators of the adiponectin promoter mediated by the class III bHLH factor Srebp-1c (Doran et al., 2008). E47 and ID3 were shown to affect transcription of the adiponectin promoter, an adipocyte-derived cytokine, in a dose-dependent manner. In the undifferentiated state, binding of E47 is not detected since high levels of ID3 reduce its availability. Decreasing levels of ID3 in differentiating adipocytes correlate with rising adiponectin expression since E47 is now able to cooperate together with Srebp-1c and induce adiponectin expression (Doran et al., 2008, Rahmouni and Sigmund, 2008). Interestingly, knockout mouse models link some of the four ID proteins to the regulation of energy metabolism (Wang and Baker, 2015). Deletion studies of ID proteins alone or in combination result in phenotypical changes ranging from aberrant glucose and lipid metabolism, impaired adipocyte differentiation, cardiac defects to an elevated risk of atherosclerosis (Wang and Baker, 2015).

The E-protein E47 is well known for its crucial involvement in the differentiation of B- and T-cell lineages. Although the factor is expressed in many tissues, a role in liver metabolism has not been studied before this thesis.

2. Scope of the thesis

The past years have revealed that tissue-specific gene regulation by GR depends on a large repertoire of interacting factors to generate accessibility to chromatin and influence gene expression. ChIP-Seq for GR in mouse livers identified the binding motif for the bHLH factor E47 to be specifically enriched near GREs.

The underlying hypothesis for this PhD thesis was that co-occupancy of GR and E47 might play a role for the transcription of a subset of genes and that E47 could modulate GR-dependent gene activation in hepatic lipid and glucose metabolism. Three specific aims are detailed as follows:

1. Define the genome-wide binding profile of GR and E2A

ChIP-Sequencing was performed to define genome-wide binding profiles for GR and E2A in liver. Gene ontology annotations of co-bound loci revealed functional pathways cooperatively affected by both factors.

2. Characterize global and tissue-specific E47 knockout mouse models and the response to GC treatment and diet-induced obesity

E47 plays a critical role in B cell development but has so far not been implicated in liver metabolism. Global and tissue-specific *E47* mutant mice were metabolically phenotyped in response to GC treatment. How loss of E47 affects the response to different biological settings of excess GC levels presented a main objective of this thesis.

3. Mechanistically define the interaction between GR and E47

It still remains elusive how GR differentiates between activation and repression depending on cellular context and tissue type. By binding together with GR at promoter and enhancer sites in liver, E47 possibly affects the assembly of transcriptional complexes needed to activate gene transcription. Deciphering the mode of crosstalk between E47 and GR will shed light on how GR tissue-specifically impacts gene regulation.

In light of metabolic side effects upon GC treatment, mostly linking to gene activation, identifying the tissue-specific interactome of GR is of high significance. Elucidating the crosstalk between GR and E47 as a potential tissue-specific interaction partner might provide valuable insight into separating the beneficial from the harmful side effects and ultimately lead to the development of safer drugs.

3. Material and Methods

3.1 Chemicals, commercial kits, antibodies and primers

Table 2: List of chemicals and reagents.

Chemicals and reagents	Company/provider
Agarose	VWR Chemicals
Bovine serum albumin	Sigma Aldrich
Bradford	Carl Roth GmbH
Charcoal-stripped FBS	Life Technologies GmbH
Chelex	Sigma Aldrich
Complete Mini protease inhibitor	Roche Applied Science
Corticosterone	Sigma Aldrich
D-(+)-Glucose solution	Sigma Aldrich
Dapi	Sigma Aldrich
Dexamethasone	Sigma Aldrich
DMEM (high glucose) cell culture medium	Sigma Aldrich
DMEM (phenol red-free) cell culture medium	Life Technologies GmbH
dNTP	Thermo Fisher Scientific GmbH
Dynabeads M-280 sheep anti-rabbit IgG-10	Life Technologies GmbH
Dithiothreitol	Serva Electrophoresis GmbH
EDTA	G-Biosciences
Eosin Y	Sigma Aldrich
Eukitt quick hardening mounting medium	Sigma Aldrich
Ethanol	AppliChem GmbH
Fetal bovine serum	Sigma Aldrich
Ficoll paque	Life Technologies GmbH
Formaldehyde (w/v)	Thermo Fisher Scientific GmbH
Fugene HD transfection reagent	Promega
Glycerol	Carl Roth GmbH
Glycine	Sigma Aldrich
GoTaq Green DNA Polymerase	Promega
Hematoxylin Gill no.3	Sigma Aldrich
HEPES buffer	Carl Roth GmbH
Igepal (NP-40)	Sigma Aldrich
Isopropyl alcohol	Merck Millipore
Lipopolysaccharide from E.coli	Sigma Aldrich
Macrophage-SFM medium	Thermo Fisher Scientific GmbH
Magnesium chloride	Carl Roth GmbH
Methanol	Sigma Aldrich
Milk powder	Carl Roth GmbH
Igepal (NP-40)	Sigma Aldrich
Oil Red O	Sigma Aldrich
Opti-MEM reduced serum medium	Life Technologies GmbH
Paraformaldehyde	Sigma Aldrich

Penicilin/Streptomycin	Sigma Aldrich
Phosphate-buffered saline (PBS)	Thermo Fisher Scientific GmbH
Phosphatase inhibitor	Thermo Fisher Scientific GmbH
Physiological saline (0.9%)	B-Braun group
Potassium chloride	Carl Roth GmbH
Potassium hydroxide	Carl Roth GmbH
Power SYBR Green Master mix	Thermo Fisher Scientific GmbH
Protein G-coupled Dynabeads	Life Technologies GmbH
Proteinase K	Sigma Aldrich
Rnase A (Dnase-free)	AppliChem GmbH
Roti-Mount Aqua mounting medium	Carl Roth GmbH
RPMI cell culture medium	Sigma Aldrich
Sepharose A/G beads	Biomol GmbH
Sodium chloride	Sigma Aldrich
Sodium dodecyl sulfate (20%)	Sigma Aldrich
Sodium pyruvate	Sigma Aldrich
Sucrose	Carl Roth GmbH
Triton-X	AppliChem GmbH
Trypsin (0.25%) EDTA	Sigma Aldrich
Tween-20	AppliChem GmbH
Xylene	AppliChem GmbH

Table 3: List of commercial kits.

Kits	Company/provider
Ambion DNase Treatment and Removal Kit	Life Technologies GmbH
Corticosterone Enzyme Immunoassay Kit	Arbor assay
DNA Maxi Plasmid kit	Qiagen
Dual-Glo Luciferase kit	Promega
High Sensitivity DNA Kit	Agilent Technologies
LabAssay Triglycerides Colorimetric Assay	Wako Chemicals
MinElute PCR Purification Kit	Qiagen
QIAquick Gel Extraction Kit	Qiagen
QuantiTect Reverse Transcription Kit	Qiagen
QUBIT dsDNA HS kit	Thermo Fisher Scientific GmbH
RNeasy Extraction Mini Kit	Qiagen
RNA 6000Nano Reagents	Agilent Technologies
KAPA Hyperprep Kit	Kapa Biosystems
KAPA Library Quantification Kit	Kapa Biosystems

Table 4: List of primary and secondary antibodies.

List of antibodies	Reference	Provider
anti-rabbit E2A	sc-349X	Santa Cruz Biotechnology
anti-mouse E2A	sc-133075	Santa Cruz Biotechnology
anti-Foxo1a	ab39670	Abcam

anti-rabbit GR	24050-1-AP	Proteintech
anti-rabbit GR	12041	Cell Signalling Technology
anti-mouse GR	sc-393232	Santa Cruz Biotechnology
anti-rabbit IgG	2729	Cell Signalling Technology
anti-rabbit Med1	A300-793A	Bethyl Laboratories
anti-Snrp70	ab83306	Abcam
anti-rabbit Alexa 488 IgG	A-21206	Life Technologies GmbH
anti-mouse HRP-conjugates IgG2a	115035206	Dianova
anti-rabbit HRP-conjuagted IgG	sc-2317	Santa Cruz Biotechnology

Table 5: Primer sequences for qRT-PCR.

Abbreviation	Forward primer (5'-3')	Reverse primer (3'-5')
Acacb	CCTTTGGCAACAAGCAAGGTA	AGTCGTACACATAGGTGGTCC
Apoa4	CGTGGACCTGCAAGATCAGA	TCTGCATGCGCTGGATGTAT
Ccl2	TTAAAAACCTGGATCGGAACCAA	GCATTAGCTTCAGATTTACGGGT
Cyp2a22	GTCACTCGCCTCTGCAAAAC	TGTACACTGGGCTTGGGAAC
Cyp2c39	GAGGAAGCATTCCAATGGTAGAA	TGTGAAGCGCCTAATCTCTTTC
Dhcr7	AGCTTCAGGCAGGCACTTAG	TGCTGGGATTTCGAAGCCAT
Dhcr24	CTGAAGACAAACCGGGAGGG	AAGATGGGGTTGTTGCCGAA
E12	TGCAGGATGAGCAGTTTGGT	GAGGCCTTTAAGGAGCTCGG
E47	TTATCCGACTTGAGGTGCAG	CTGGAGGAGAAGGACCTGAG
Fasn	TGGATTACCCAAGCGGTCTG	AGTGTTCGTTCCTCGGAGTG
Gck	AACGACCCCTGCTTATCCTC	CTTCTGCATCCGGCTCATCA
Gilz	ACCACCTGATGTACGCTGTG	TCTGCTCCTTTAGGACCTCCA
G6pc	CGACTCGCTATCTCCAAGTG	GTTGAACCAGTCTCCGACC
Il6	TAGTCCTTCCTACCCCAATTTCC	TTGGTCCTTAGCCACTCCTTC
Igfbp1	TCGTGACCACTGAGCAACTG	AGTTAGGAACTCGGGCATCG
Pck1	CTGCATAACGGTCTGGACTTC	CAGCAAACTCCCGTACTCC
Per1	ACCAGGTCATTAAGTGTGTGC	CTCTCCCGGTCTTGCTTCA
Pparα	AGAGCCCCATCTGTCCTCTC	ACTGGTAGTCTGCAAAACCA
Srebp-1c	GGAGCCATGGATTGCACATT	GGCCCGGGAAGTCACTGT
U36b4	AGATTCGGGATATGCTGTTGGC	TCGGGTCCTAGACCAGTGTTC

Table 6: Primer sequences for ChIP qPCR.

Abbreviation	Forward primer (5'-3')	Reverse primer (3'-5')
Acacb	CAGGCAGCGAGCATTTCCTA	TCTGATGCCCTTGTGCCTAC
Apoa4	TCACTGGGGTGGAAAGAGGA	CCTGAACAGAACTGAGGCCC
Cyp2a22	AAGGCCATCATGTACCTGGC	TGGCATGGATCTACAAAGGCT
Cyp2c39	GGGTTACTCAACGATGCTCAA	TTGTGATCAGGCATCACTGGC
Dhcr7	CCTGCGTAGCTTGGTTTCCTA	CAGAAGCTGGGCTATGACGG
Dhcr24	CTGGATGCCCTGTGAGTTCTA	ACAGGCATTCGCAAACATACT
Gpam	ACACACAAGGAGGAGTGCAG	CACGGTTGCCCAATGAGTTA
Hmgcr	GGCCGCCAATAAGGAAGGAT	GGAGACCGTTCGTGACGTAG
Hmgcs1	TGGTCGGAGAACCTCTCACT	CGAGAACAAGCCTGCCAATG

Igfbp1	CAGCACTTTCCACCGTTGAC	GCAGCTCCAGAGTTAGGCAA
Pck1	CAGGGCTGTCCTCCCTTCTA	CTGTTGACCGAGGGTGTGTT
nCtrl	GCTGGCAGAATAGCATCCG	TGATGAAGCACTCGTTGAGGC

Acacb (Acetyl-Coenzyme A carboxylase beta), *Apoa4* (Apolipoprotein A4), *Ccl2* (C-C motif chemokine ligand 2), *Cyp2a22* (cytochrome P450, family 2, subfamily a, polypeptide 22), *Cyp2c39* (cytochrome P450, family 2, subfamily c, polypeptide 39), *Dhcr7* (7-dehydrocholesterol reductase), *Dhcr24* (24-dehydrocholesterol reductase), *E12* (transcription factor 3, splice variant E12), *E47* (transcription factor 3, splice variant E47), *Gck* (glucokinase), *Fasn* (fatty acid synthase), *Gilz* (TSC22 domain family, member 3), *G6pc* (glucose-6-phosphatase catalytic subunit), *Il6* (interleukin 6), *Igfbp1* (insulin like growth factor binding protein 1), *Pck1* (phosphoenolpyruvate carboxykinase 1), *Per1* (period circadian clock 1), *Pparα* (peroxisome proliferator activated receptor alpha), *Srebp-1c* (sterol regulatory element binding transcription factor 1), *U36b4* (large ribosomal protein)

3.2 Animal experiments

3.2.1 Transgenic mouse lines

All animal procedures were approved by the relevant authorities - regional animal welfare committee of the state of Bavaria (2532-158-2014) and Berlin (LAGeSo Berlin, Reg 0103/11) - in accordance with Max Delbrück Zentrum and Helmholtz Zentrum München – Deutsches Forschungszentrum für Gesundheit und Umwelt (HMGU) guidelines for the care and use of animals.

E47 knockout (*E47-/-*) and E47 floxed alleles ($E47^{flx/flx}$) were bred on a C57BL/6 background. Both lines were generated by Kristina Schachtrup (Beck et al., 2009b) and kindly provided to us. For *E47-/-* mice, wildtype littermates served as controls. E47 floxed mice were crossed with hepatocyte-specific Albumin (Alb)-Cre mice obtained from JAX (B6.Cg-Tg(Alb-cre)21Mgn/J) to generate *Albumin-Cre x* $E47^{flx/flx}$ mice; from here on specified as $E47^{\Delta LKO}$. Albumin-Cre negative floxed littermates served as controls.

3.2.2 Housing and diets

Mice were housed in a controlled SPF facility with a 12 hr dark/light cycle in groups of 4 animals per cage. The cages were individually ventilated and the room was kept at 23°C with constant humidity. They were fed ad libitum with regulator chow diet (Altromin GmbH) or a

high fat diet (HFD; 58% kcal fat, Research Diets D12331) for a minimum period of 12 weeks. For all experiments, 10-16 week old males were used.

3.2.3 Genotyping

For genotyping of *E47-/-* mice and *E47$^{\Delta LKO}$* mice, DNA was extracted from ear punches. Ear tissue was digested in lysis buffer (50 mM Tris-HCl at pH8, 100mM EDTA at pH8, 100 mM NaCl, 1% SDS) containing Proteinase K (Sigma-Aldrich) at 56°C overnight. For extraction of DNA, 2M NaCl (Sigma-Aldrich) was added to the sample followed by ethanol precipitation. 1 µl of this DNA was used as template for the genotyping PCR. The PCR reaction mix contained 12.5 µl GoTaq Green DNA polymerase master mix (Promega), 40 mM MgCl2 (Carl Roth GmbH), 0.2 µM of each primer and was filled up to 25 ul with H_2O. Table 7 describes the PCR reaction, which was used for all genotyping procedures. Primers were produced by Eurofins Genomics.

Table 7: Genotyping PCR reaction.

Step	Temperature (°C)	Duration	Cycles
Initiation	95	5 min	
Denaturation	95	1 min	
Primer annealing	56	1 min	**35x**
Elongation	72	1 min	
Final elongation	72	10 min	

For the *E47-/-* line, three primers were used in a single PCR reaction:

Primer 1: *ccagctgcacctcaagtcgg*
Primer 2: *ggagagagcagtgggagac*
Primer 3: *gccatgcagtttctaaagg*

PCR products were separated on a 2% agarose gel (VWR Chemicals). Wildtype mice revealed a PCR product of 200bp, homozygous mice (*E47-/-*) revealed a PCR product of 400 bp whereas heterozygous mice (*E47-/+*) showed both products.

For the *E47$^{\Delta LKO}$* line, two separate PCRs were performed. To genotype for the E47 gene locus, two primers were used:

Primer 1: *tgcagtgtggacaactgtgcc*
Primer 2: *acatgcagtttggtctgtgcg*

Wildtype mice revealed a PCR product of 700 bp. Mice homozygous revealed a band at 750 bp and mice heterozygous showed both products. A second PCR was performed for the Albumin-Cre recombinase with three primers:

Primer 1*: cctgccagccatggatataa*
Primer 2: *gttgtcctttgtgctgctga*
Primer 3: *gaagcagaagcttaggaagatgg*

In Cre-positive mice, a 500 bp PCR product was detected. In Cre-negative mice, PCR products of 750 bp, 500 bp and 400 bp were detected.

3.2.4 Supplementation of drinking water

Dexamethasone (#D2915, Sigma Aldrich) and corticosterone (#27840, Sigma Aldrich) were either dissolved in H_2O or EtOH and supplied in the drinking water of mice for 3 consecutive weeks at a final concentration of 10ug/mL (Dex) or 100 ug/ml (Cort). Mice received regular chow diet (Altromin GmbH) during the course of water supplementation. Once a week the water was changed to fresh water supplemented with either of the indicated compounds.

3.2.5 Glucose tolerance test

For a GTT, mice were fasted for 16 hrs overnight with free access to water. Glucose (20% D-glucose; Sigma Aldrich) was administered by intraperitoneal injection at 2g/kg (dissolved in sterile physiological saline) and the injection volume was calculated based on the body weight of each individual mouse. Blood glucose levels were sampled from the tail vein using a handheld glucometer (AccuCheck Aviva, Roche Diagnostics). Blood glucose was measured at 0 (basal level before injection) and at 15, 30, 60 and 90 mins after intraperitoneal injection.

3.2.6 Pyruvate tolerance test

For a PTT, mice were fasted for 5 hrs during the day. Sodium pyruvate (#5280, Sigma Aldrich) was administered by intraperitoneal injection at 2g/kg (dissolved in sterile physiological saline) and the injection volume was calculated based on the body weight of each individual mouse. Blood glucose levels were determined from the tail vein using a handheld glucometer (AccuCheck Aviva, Roche Diagnostics). Blood glucose was measured at 0 (basal level before injection) and at 15, 30, 60 and 90 mins after intraperitoneal injection.

3.2.7 Dexamethasone suppression test

For the dexamethasone suppression test, dexamethasone (#D2915, Sigma Aldrich) was dissolved in H_2O and administered by intraperitoneal injection at a final concentration of 1mg/kg. The injection volume was calculated based on the body weight of each individual mouse. Mice were sacrificed 6 hrs post injection and had free access to food and water during the course of the treatment.

3.2.8 Body fat composition using Echo-MRI

Body composition (fat and lean mass) was measured using quantitative nuclear magnetic resonance technology (EchoMRI, Houston, TX) before and after long-term Cort treatment to calculate changes in fat and lean mass gain. For the measurement, each mouse was placed in a tube inside the machine for approximately 30 seconds.

3.3 Molecular biology techniques

3.3.1 RNA isolation from tissue

For RNA isolation, tissue was harvested after euthanasia of mice via cervical dislocation, snap-frozen in liquid nitrogen and stored at -80°C. Total RNA from tissue was isolated using the RNeasy Mini kit (Qiagen) according to manufacturer's instructions.

3.3.2 cDNA synthesis

Total RNA from tissue was reverse-transcribed into cDNA (complementary DNA) with the QuantiTect Reverse Transcription Kit (Qiagen) according to manufacturer's instructions. The total amount of RNA used for reverse-transcription was 1ug.

3.3.3 Real-time quantitative polymerase chain reaction

Real-time quantitative polymerase chain reaction (RT-qPCR) was performed using Power SYBR Green Master Mix (Life Technologies GmbH) in a ViiA 7 Real-Time PCR System (Thermo Fischer Scientific GmbH). The qPCR reaction contained 5 ul SYBR Green Master Mix, 0.9 ul H_2O, 0.1 ul primer mix (1uM) and 4 ul of diluted cDNA. Samples were run on 384-well plates as technical triplicates. The relative expression levels of each gene were

normalized to the housekeeping gene *U36b4*. RT-qPCR primers were produced by Eurofins and are listed in **Table 5**.

3.3.4 Nuclear protein extraction from liver

Lysis of liver tissue was performed using a tissue lyser (Qiagen) with 5mm steel beads (Qiagen) in cold cell lysis buffer (10 mM Hepes-KOH at pH 7.9, 1.5 mM MgCl2, 10 mM KCl, 0.5 mM DTT, 0.15% NP40, 1uM Dexamethasone) containing complete mini protease inhibitors (Roche Applied Science) and phosphatase inhibitors (Thermo Fisher Scientific). Cytosolic and nuclear fractions were separated by centrifugation for 20 min at 2700g at 4°C and the nuclear fraction was washed once with PBS. Nuclear lysis was performed in nuclear lysis buffer (420 mM NaCl, 20 mM Hepes-KOH pat H 7.9, 2 mM MgCl2, 0.2 mM EDTA, 0.5 mM DTT, 0.1% NP40, 20% glycerol, 1uM Dexamethasone; complete protease and phosphatase inhibitors) and passed through a syringe for complete lysis. After incubation for 1 hr at 4°C with rotation, nuclear extracts were obtained by centrifugation at maximum speed for 45min. Protein content was determined using Bradford reagent (Bio Rad) according to manufacturer's instructions.

3.3.5 Co-immunoprecipitation

For each Co-immunoprecipiation (Co-IP), 300ug of nuclear extracts (see 3.3.4) were subjected to a pre-clearing by incubation with unblocked Dynabeads M-280 (Life Technologies GmbH) for 1 hr at 4°C with rotation. Pre-cleared nuclear extratcs were incubated in IP buffer (20mM Tris pH 8, 100mM KCl, 5mM $MgCl_2$, 0.2mM EDTA, 20% glycerol, complete protease inhibitors) with rabbit anti-GR (3ug; #24050-1-AP, Proteintech) and rabbit anti-IgG (3ug; #2729, Cell Signaling) for 2 hrs at 4°C with rotation before 1%-BSA blocked Dynabeads M-280 were added for overnight immunoprecipitation. The next day, the IP-coupled beads were washed 5 times - twice with wash buffer (20 mM Tris at pH 8, 500 mM KCl, 5 mM MgCl2, 0.2 mM EDTA, 20% glycerol) with addition of 1% Triton-X, twice without Triton-X and once with HEPES buffer (Carl Roth GmbH). Each wash step was performed for 5 min with rotation at 4°C. Proteins were eluted twice from washed beads using elution buffer (200mM DTT, 6x Laemmli loading buffer) at 37°C for 30 mins at 1000 rpm shaking before eluates were combined.

3.3.6 Western Blot analysis

Western blot of Co-IP samples (see 3.3.5) were boiled for 5 min at 95°C followed by separation on a 4-12% Bis-Tris gel (Invitrogen). After transfer to a PDVF membrane (Merck Millipore), membranes were blocked for 1 hr at room temperature in 5% milk/TBS-T (50 mM Tris-Cl, 150 mM NaCl, pH 7.6) supplemented with 1% Tween20 (AppliChem GmbH) and then incubated overnight at 4°C with mouse anti-GR antibody (1:1000; #sc-393232, Santa Cruz Biotechnology) and mouse anti-E2A antibody (1:500; #sc-133075, Santa Cruz). Incubation for 1 hr at room temperature with mouse HRP-conjugated anti-IgG2a secondary antibody (1:5000; #115035206, Dianova) was used to detect protein signal. Peroxidase activity was measured using HRP Western substrate (Merck Millipore) and visualized using high sensitive X-ray films (GE Healthcare) for chemiluminescence detection of proteins.

Western blot for nuclear localization of GR was performed using nuclear extracts from Dex-treated wildtype and *E47-/-* livers (see 3.3.4). For each sample, 8 ug of protein were loaded on a 4-12% Bis-Tris gel (Invitrogen) and Western blot was performed as described above. Overnight incubation of the membrane was performed using rabbit anti-GR antibody (1:2000; #12041, Cell Signaling technology). Incubation for 1 hr at room temperature with anti-rabbit HRP-conjuagted IgG secondary antibody (1:30.000; #sc-2317, Santa Cruz Biotechnology) was used to detect protein signal. Peroxidase activity was measured using HRP Western substrate (Merck Millipore) and visualized using X-ray films (CEA X-ray) for chemiluminescence detection of proteins.

3.4 Tissue assays

3.4.1 Elisa corticosterone measurement

Blood was harvested from the heart of euthanized mice and collected in EDTA-coated microvette tubes on ice. Plasma was obtained after centrifugation at 1500*g* for 15min. Plasma corticosterone levels were measured by an enzyme immunoassay kit (#K014-H1, Arbor assays) according to the manufacturers' instructions.

3.4.2 Triglyceride measurement in plasma and liver

Plasma was obtained as described in 3.4.1 Livers were harvested and 0.1g subsequently digested in EtOH / 30% potassium hydroxide (2:1, v/v) at 60°C. Digested samples were mixed with 1M MgCl2 at a ratio of 1.08:1 (volume of MgCl2:volume of sample) and incubated

on ice for 10 min followed by centrifugation for 30 min at max speed for separation. The supernatant containing extracted triglycerides was transferred to a new tube. Triglycerides were measured in liver and plasma samples by colorimetric assay (#290-63701, Wako Chemicals) according to the manufacturers' instructions.

3.4.3 Immunohistochemistry for GR

Livers were harvested and immediately fixed in 4% paraformaldehyde (Karatsoreos et al.) overnight at 4°C and cryoprotected in 30% sucrose. Livers were embedded in embedding media (Leica Biosystems) and sectioned on a cryostat (Leica Biosystems) at 6 µm. Antigen retrieval was performed on the sections in citrate-based buffer (pH 6) before blocking with PBS containing 0.1% Triton-X and 5% BSA for 1 hr. Incubation with rabbit anti-GR antibody (1:200; #12041, Cell Signaling) was done in blocking buffer at 4°C overnight followed by incubation with rabbit anti-IgG Alexa 488 antibody (1:250; #A-21206, Life Technologies GmbH) for 1 h at RT and final stain with DAPI. Stained slides were mounted in aqueous mounting medium (Carl Roth GmbH). A Zeiss AXIO Scope A1 microscope was used for image analysis at a magnification of 63x.

3.4.4 Oil red O staining

Liver tissue was harvested and immediately fixed in 4% PFA overnight at 4°C and cryoprotected in 30% sucrose. Sections of 6 µm were performed by cryostat (Leica Biosystems) and stained with Oil Red O solution (Sigma Aldrich) dissolved in isopropyl alcohol for 5 min followed by hematoxylin gill no.3 (#GHS332, Sigma Aldrich) staining for 15 sec and repeated washing with H_2O. Stained slides were mounted in aqueous mounting medium (Carl Roth GmbH). Brightfield microscopy was performed with a Keyence BZ-9000 microscope at a magnification of 20x.

3.4.5 Paraffin embedding of liver tissue

Livers were harvested and immediately fixed in 4% PFA overnight at 4°C. For dehydration, PFA-fixed liver tissue was first placed in 70% EtOH overnight at 4°C and then dehydrated in increasing percentages of EtOH for 1 hr each (80%-100%) followed by 3 washes in xylene (AppliChem GmbH). Dehydrated liver tissue was then placed in paraffin and kept in an oven at 65°C overnight before being embedded in paraffin and cut in 6µm sections in a microtome.

3.4.6 Hematoxylin and Eosin staining

For hematoxylin and eosin (H&E) stainings, liver tissue was embedded in paraffin as described in 3.3.8. Slides were first placed in xylene and then hydrated by passing through decreasing concentration of alcohol baths and water (100%, 96%, 70%). Staining with hematoxylin gill no.3 (#GHS332, Sigma Aldrich) and eosin Y (#HT110216, Sigma Aldrich) was each performed for 30 seconds followed by washing in tab water. Stained slides were dehydrated again in increasing concentrations of ethanol and cleared in xylene. Stained slides were mounted in non-aqueous mounting medium (Sigma Aldrich). Brightfield microscopy was performed with a Keyence BZ-9000 microscope at a magnification of 20x.

3.5 Cell culture experiments

3.5.1 Isolation of bone marrow-derived macrophages

For isolation of bone marrow, mice were euthanized and hind legs were surgically removed. Total bone marrow was harvested using a 25G needle and washed in RPMI medium (Sigma-Aldrich) with 2% FBS (Sigma-Aldrich). To lyse erythrocytes, ACK lysis buffer (151 mM NH4Cl, 10 mM KHCO3, 0.2 mM EDTA in H_2O) was added and the pellet was repeatedly washed with PBS. Next, Ficoll-paque (GE Healthcare) was added to obtain monocytes through gradient centrifugation. The middle fraction containing purified monocytes was carefully transferred to a cell culture plate. For differentiation of monocytes, differentiation medium (DMEM medium, 30% L929 supernatant, 20% FBS, 1% Pen/Strep) was added for 5 consecutive days. Differentiated macrophages were counted and seeded in Macrophage-SFM medium (Thermo Fisher Scientific GmbH) supplemented with 1% Pen/Strep. Macrophages were either treated with 1uM LPS for 3 hrs, 1uM dexamethasone overnight or with a combination of both treatments. Macrophages were harvested and total RNA was isolated using the RNeasy Mini kit (Qiagen) according to manufacturer's instructions.

3.5.2 Switchgear luciferase reporter screen

GR responsive human promoter/enhancer luciferase reporter constructs were obtained from Switchgear Genomics ("GR pathway"). The reporter constructs were transfected together with the expression vector for human GR - pcDNA3.1-human GR - and a CMX-LacZ plasmid expressing β-galactosidase (β-gal) for normalization of transfection efficiency. Each DNA-transfection reaction contained:

50 ng luciferase reporter construct
25 ng pcDNA3.1-human GR
25 ng CMX-lacZ

Luciferase activity was measured in CV-1 cells (African green monkey (*Cercopithecus aethiops*) and run in triplicates. CV-1 cells were transfected using Fugene reagent (Promega) according to manufacturer's protocol. The DNA-Fugene mix was prepared in 100ul Optimem reduced serum medium (Life Technologies GmbH). After 24 hrs, medium was changed to PhenolRed free DMEM (Life Technologies GmbH) containing 10% charcoal-stripped FBS (Life Technologies GmbH) and 1% Pen/Strep. Transfected cells were treated overnight with 100nM Dexamethasone, 100nM Cortisol or ethanol as control. To measure luciferase activity of transfected constructs and β-galactosidase (β-gal), a colorimetric assay was used as described in (Uhlenhaut et al., 2013). Relative luciferase activity was compared to vehicle and empty vector and clustered based on fold changes. Overrepresented motifs in up- and downregulated *cis*-regulatory sequences were identified using OTFBS based on TRANSFAC and aligned using T-Coffee; motif position weight matrices were generated using Weblogo.

3.5.3 Luciferase reporter assays

Reporter constructs from the Switchgear screen (3.5.2) were used for additional luciferase assays. Mutagenesis of the two predicted E47-binding sites for ATPB2 to TTGGCC from was performed by gene synthesis (Eurofins Genomics). CV-1 cells were seeded in high glucose DMEM cell culture (Sigma Aldrich) containing 10% FBS and 1% Pen/Strep in 96-well plates one day prior to transfection to reach a confluency of around 80%. Each DNA-transfection reaction contained:

50 ng luciferase reporter construct
25 ng pcDNA3.1-human GR and/or
pcDNA3.1-human E47 and/or
pCI human ID3
25 ng pRL-TK *Renilla*

Reporter constructs were co-transfected with the pRL-TK *Renilla* luciferase control vector (Promega) to normalize for transfection efficiency. To ensure equal uptake of DNA within an experiment, the empty vector (pcDNA3.1) was co-transfected whenever DNA content needed to be adjusted. All transfection reactions were run in triplicates. Transfection was

performed using Fugene reagent (Promega) according to manufacturer's protocol and the DNA-Fugene mix was prepared in 100ul Optimem reduced serum medium (Life Technologies GmbH). After 24 hrs, medium was changed to PhenolRed free DMEM (Life Technologies GmbH) containing 10% dialyzed FBS, 1% Pen/Strep and 1% sodium-pyruvate. Transfected cells were either treated with 1 µM Dexamethasone (#D4902, Sigma-Aldrich) or EtOH as control overnight. Luciferase activity was measured using the Dual-Glo luciferase kit (Promega) according to protocol. Luminescence signal was measured using a PHERAstar plate reader and normalized to renilla luminescence for each well.

3.6 Next generation sequencing techniques

3.6.1 ChIP-Sequencing

For pellet preparation, livers were harvested, snap-frozen in liquid nitrogen and stored at -80°C until use. For ChIP-Seq, 0.2g of frozen liver tissue was homogenized in lysis buffer (10mM Hepes-KOH, 10mM KCL, 5mM MgCl2, 0.5mM DTT) containing complete proteinase inhibitors (Roche Applied Science) using a TissueLyser (Qiagen) with 5 mm steel beads. Lysates were passed through a cell strainer and cross-linked in 1% formaldehyde for 15 min followed by quenching with 0.2M glycine solution for 5 min and final washing with PBS.

Pellets were resuspended three times with IP buffer (150 mM NaCl, 5 mM EDTA at ph 7.5, 5 mM Tris at pH 7.5, 1% Triton X-100, 0.5% NP40, complete mini protease inhibitors) and passed through a syringe (24G). The chromatin was sonicated in shearing buffer (50 mM Tris at pH8, 10 mM EDTA at pH8, 1% SDS, complete mini protease inhibitors) to a 0.1-1kb size using a bioruptor (Diagenode). Sonicated chromatin was centrifuged at 12.000 rpm at 4°C for 10 min. Chromatin immunoprecipitation (IP) was set up in dilution buffer (167 mM NaCl, 16.7 mM Tris at pH 8, 1.2 mM EDTA at pH 8, 1.1% Triton X-100, 0.01% SDS, complete mini protease inhibitors) overnight at 4°C with rotation. For each IP, 8 ug of the following antibodies were used: rabbit anti-GR antibody (8ug; #24050-1-AP, Proteintech), rabbit anti-E2A antibody (8ug; sc-349X, Santa Cruz Biotechnology) and rabbit anti-IgG antibody (8ug; #2729, Cell Signaling). Sheared chromatin was kept as input control at -20°C overnight. The next day, chromatin was cleared by centrifugation at 3500 rpm for 20 min at 4°C. 90% of each IP samples was incubated with 0.5%-blocked Dynabeads M-280 (Invitrogen) for 6 hrs at 4°C with rotation. Coupled Dynabeads M-280 were washed six times with wash buffer (150 mM NaCl, 5 mM EDTA at ph 7.5, 5 mM Tris at pH 7.5, 1% Triton X-100, 0.5% NP40) and once with TE-Buffer. Elution of IP samples from the beads was performed in elution buffer (105 mM NaHCo3, 1% SDS in H_2O) for 15 min at 1000 rpm at

room temperature. For crosslink reversal, 200mM NaCl was added to the ChIP-chromatin as well as the input control and incubated at 65°C overnight followed by treatment with 0.05 ug RNAse A (AppliChem GmbH) at 37°C for 30 mins and treatment with Proteinase K solution (0.05 ug Proteinase K, 10mM EDTA at pH 8, 40 mM Tris at pH 7.5) for 2 hrs at 45°C. ChIP-DNA and input were isolated with MinElute PCR Purification Kit (QIAGEN). DNA concentration was determined using QUBIT dsDNA HS kit (Thermo Fisher Scientific).

Libraries were prepared using the KAPA Hyperprep Kit (#KK8504, Kapa Biosystems). Illumina compatible adapters were synthesized by IDT (Integrated DNA Technologies) and used at a final concentration of 68nM. Size-selection (360-610bp) of adapter-ligated libraries was performed using 2% dye free gels (#CDF2010, Sage Science) in a Pippin Gel station (Sage Science). qPCR was used to estimate library concentrations with the KAPA Library Quantification Kit (#KK4873, Kapa Biosystems). Library quality was verified using the Agilent High Sensitivity DNA Kit (Agilent) in a 2100 Bioanalyzer (Agilent).

3.6.2 ChIP qPCR

Sonication of chromatin and immunoprecipitation was performed as described in 3.6.1. For each IP, 3 ug of the following antibodies were used: rabbit anti-GR antibody (3ug; #24050-1-AP, Proteintech), rabbit anti-Med1 (3ug; #A300-793A, Bethyl laboratories), rabbit anti-Foxo1a (#ab39670, Abcam), and rabbit anti-IgG antibody (3ug; #2729, Cell Signaling). Sheared chromatin was kept as input control and precipitated in 3 volumes of EtoH at -20°C overnight. The next day, chromatin was cleared by centrifugation at 12.000 rpm for 10 min at 4°C. 90% of each IP samples was incubated with 0.5% BSA-blocked Sepharose Protein A/G beads (Rockland Inc.) for 3 hrs at 4°C with rotation. Coupled Sepharose Protein A/G beads were washed four times with wash buffer (150 mM NaCl, 5 mM EDTA at ph 7.5, 5 mM Tris at pH 7.5, 1% Triton X-100, 0.5% NP40) by centrifugation at 500 rpm at 4°C. For isolation, 100 µl of 10% Chelex (Sigma Aldrich) was added to the washed sepharose beads and vortexed. After boiling for 10 min, proteinase K is added and the beads are incubated for 30 min at 55°C while shaking, followed by another round of boiling for 10 min. For elution, the bead suspension is centrifuged and the supernatant is collected twice after addition of another 100 µl water. Precipitated input was centrifuged at maximum speed for 10 min and the pellet was dried and processed the same way. The ChIP-DNA and input DNA was purified using the MinElute PCR purification kit according to manufacturer's instructions.

ChIP-DNA was diluted accordingly and served as template for quantitative PCR (qPCR) using Power SYBR Green Master Mix (Life Technologies) in a ViiA 7 Real-Time PCR System

(Thermo Fischer Scientific). Each sample was run in technical triplicates on a 384-well plate. Fold enrichment was calculated over IgG using the raw CT-values: (CT IP) - (CT IgG) = double delta CT (DDCT) = 2^{-DDCT}. This normalization method divides the ChIP signal by the mock-antibody signal, representing the ChIP signal as the fold increases relative to the background signal. Primers for ChIP qPCR are listed in **Table 6**.

3.6.3 ChIP coupled to mass spectrometry

ChIP coupled to mass spectrometry (ChIP-MS) was performed in livers of Dex-injected *E47*$^{\Delta LKO}$ and control littermates. ChIP was carried out as described in 3.6.1 with minor modifications. All IPs were done in three biological replicates. Chromatin was sonicated to an average size of 200bp. After overnight immunoprecipitation with rabbit anti-GR (5ug; #24050-1-AP, Proteintech) and rabbit anti-IgG (5ug; #2729, Cell Signaling), antibody-bait complexes were bound by protein G-coupled Dynabeads (Life Technologies) and washed three times with wash buffer A (50mM HEPES pH 7.5, 140mM NaCl, 1% Triton), once with wash buffer B (50mM HEPES pH 7.5, 500mM NaCl, 1% Triton) and twice with TBS. Precipitated proteins were eluted with an on-bead digest (Hein et al., 2015). Beads were incubated for 30min with elution buffer 1 (2M Urea, 50mM Tris-HCl (pH 7.5), 2mM DTT, 20µg/ml trypsin) followed by a second elution with elution buffer 2 (2M Urea, 50mM Tris-HCl (pH 7.5), 10mM Chloroacetamide) for 5min. Both eluates were combined and further incubated over night at room temperature. Tryptic peptide mixtures were acidified with 1% TFA and desalted with Stage Tips containing 3 layers of C18 reverse phase material and analyzed by mass spectrometry. Peptides were separated on 50-cm columns packed in-house with ReproSil-Pur C18-AQ 1.9µm resin (Dr. Maisch GmbH). Liquid chromatography was performed on an EASY-nLC 1000 ultra-high-pressure system coupled through a nanoelectrospray source to a Q-Exactive HF mass spectrometer (Thermo Fisher Scientific). Peptides were loaded in buffer A (0.1% formic acid) and separated applying a non-linear gradient of 5–60% buffer B (0.1% formic acid, 80% acetonitrile) at a flow rate of 250nl/min over 105min. Data acquisition switched between a full scan and 15data-dependent MS/MS scans. Multiple sequencing of peptides was minimized by excluding the selected peptide candidates for 25s. All other settings were set as previously described (Scheltema et al., 2014).

3.6.4 RNA-Sequencing

RNA-Sequencing (RNA-Seq) was performed in different tissues. For Cort-treated liver tissue and Dex-treated liver, skeletal muscle and white adipose tissue, RNA was extracted using

the QIAzol lysis reagent (Qiagen) according to the manufacturer's instructions. This protocol is optimized for lysis of tissue with higher fat content. For Dex-injected liver tissue, RNA was extracted using the RNeasy minikit (Qiagen) according to manufacturer's instructions. All samples for RNA-Sequencing were DNAse-treated using the Ambion DNase I kit (Thermo Fisher Scientific) according to manufacturer's instructions. The quality of the RNA was verified using an Agilent 2100 Bioanalyzer with RNA 6000Nano Reagents (Agilent Technologies). Library preparation and rRNA depletion was performed using the Illumina TruSeq stranded/unstranded mRNA Library Prep Kit v2 chemistry in an automated system (Agilent Bravo liquid handling platform) starting with 1µg total RNA for each sample.

3.7 NGS data analysis

ChIP-Sequencing

Libraries were subjected to NGS on an Illumina HiSeq4000. Reads were aligned to the mouse mm10 reference genome using BWA-MEM version 0.7.13 (Li and Durbin, 2010) and duplicates were removed using Picard Tools version 2.8.3 (http://picard.sourceforge.net/). Reads were filtered for uniquely mapped read pairs with samtools (Li et al., 2009) and downsampled to 18 mio (GR ChIP-Seq) or 22 mio (E2A ChIP-Seq) read pairs. To visualize the tracks, mapped reads were converted to bedGraph using HOMER version 4.9 (Heinz et al., 2010), filtered for called peak regions ±2kb and displayed on the UCSC genome browser. Peaks were called using MACS2 version 2.1.1.20160309 (FDR<0.05) (Zhang et al., 2008). Called peaks for GR and E2A were defined as overlapping if 50% of chromosomal peak position was intersecting. Gene Ontology analysis performed with GREAT (McLean et al., 2010). Motif enrichment and read distribution analyses around GR peaks were conducted with HOMER.

ChIP-MS

Raw mass spectrometry data were analyzed with MaxQuant version 1.5.3.54 and Perseus version 1.5.4.1 software packages. Peak lists were searched against the mouse UniprotFASTA database (2015_08 release) combined with 262 common contaminants by the integrated Andromeda search engine. False discovery rate was set to 1% for both peptides (minimum length of 7 amino acids) and proteins. 'Match between runs' (MBR) with a maximum time difference of 0.7min was enabled. Relative protein amounts were determined by the MaxLFQ algorithm with a minimum ratio count of two (Cox et al., 2014). Missing values were imputed from a normal distribution applying a width of 0.2 and a downshift of 1.8 standard deviations. Significant outliers were defined by permutation-controlled Student's t-

test (FDR<0.05, s0=1) comparing triplicate ChIP-MS samples for each antibody and biological condition.

RNA-Sequencing

Libraries were sequenced on the Illumina HiSeq2500 or HiSeq4000. Sequencing quality was assessed with FastQC (http://www.bioinformatics.babraham.ac.uk/ projects/fastqc/). Reads were mapped to the mouse genome mm10 (Ensembl build 38.91) and reads per gene were counted using STAR version 2.4.2a (Dobin et al., 2013). Gene count normalization and differential expression analysis was performed using DESeq2 (Love et al., 2014). For gene annotation, biomaRt was used (Durinck et al., 2009). Functional enrichment according to gene ontology was carried out using Gorilla (Eden et al., 2009).

3.8 NGS data deposition

Scripts for ChIP-Seq and RNA-Seq analyses are deposited at github (https://github.com/FranziG/E47KO-liver). RNA-Sequencing data, normalized count data and DESeq2 output can be accessed via NCBI's Gene Expression Omnibus using the accession numbers GSE111877, GSE108688. NGS data and annotated peak files can be accessed via the NCBI's Gene Expression Omnibus using the accession numbers GSE111526 and GSE108689. ChIP-MS data files can be accessed at ProteomeXchange with identifier “PXD010157".

3.9 Statistical analysis

All tests were performed using statistical tools in Graph Prism 6 (GraphPad Software, San Diego, CA USA). For difference between two groups, unpaired two-tailed Student’s t-test was performed. Differences between more than two groups were assessed by 2-way ANOVA followed by Bonferroni’s multiple comparison test. For glucose and pyruvate tolerance tests, the area under the curve was calculated from the individual glucose excursion curves. All results are given as mean ± SEM unless otherwise specified. A P-value <0.05 was considered significant.

3.10 Contributions from collaborations

ChIP-MS was performed with Dr. Michael Wierer in the lab of Prof. Dr. Matthias Mann (Max Planck Institute, Munich, Germany). The Switchgear GR reporter screen was performed in the lab of Prof. Dr. Ronald Evans (Salk Institute of Biological Science, La Jolla, USA).

4. Results

4.1 Genomic binding of GR and E2A

4.1.1 Genome-wide binding profiles of GR and E2A overlap in liver

The parameters defining chromatin-accessibility and tissue-specific gene regulation by GR are still largely unknown. ChIP-Sequencing (ChIP-Seq) for GR was performed in mouse livers, to identify novel factors influencing GR binding patterns. Wildtype livers were collected in the late afternoon. At this time-point, endogenous corticosterone levels begin to rise significantly. In response to prolonged periods of fasting during the day, GCs upregulate gluconeogenic gene programs in the liver (Opherk et al., 2004). ChIP-DNA was prepared and sequenced reads were aligned to the mouse mm10 reference genome (**Supplemental Table 1).** Bound regions (peaks) were called using MACS2 and identified 8794 peaks. Of these, 2753 peaks were reproducibly called between two biological replicates. As expected, GR binding was detected at known GR target promoters and enhancers, e.g. *Pck1*, *G6pc*, *Per1* and *Tat*.

Bioinformatic motif analysis was performed on the GR ChIP-sequenced DNA. Besides GRE as the top motif, other enriched consensus sites for transcription factors were identified, namely c/EBP, HNF4α, HNF6, FoxA and Stat5. These have previously been published to co-localize together with GR at hepatic *cis*-regulatory elements (Greulich et al., 2016, Lim et al., 2015) (**Fig 11**). Interestingly, a thorough look at motifs revealed the E-Box consensus motif CANNTG to be enriched near GR-bound sequences. This motif was predicted to recruit the transcription factor E47. The E-Box motif for E47 had also previously been found in GR-bound fragments of mouse livers (Phuc Le et al., 2005).

GR cistrome

Sequence	Motif	P-value
	GRE	1e-237
	HNF4α	1e-89
	C/EBP	1e-64
	HNF6	1e-50
	FOX	1e-41
	DR1 NR	1e-40
	STAT5	1e-17
	E-Box	1e-5

Figure 11: Hepatic cistrome for GR in wildtype liver.
De novo motif analysis of the hepatic GR cistrome in wildtype livers is shown. The top eight enriched transcription factor consensus sites in ChIP sequences are shown for each factor and are ordered according to their p-value.

Expression levels of the E proteins E2A (E47 and E12), Heb and E2-2 as well as the Inhibitor of binding proteins were assessed to validate whether E47 might play a role in hepatic gene regulation. Robust levels of *E2A* mRNA was detected in wildtype mouse livers throughout the day and night cycle. Both *Heb* and *E2-2* were detectable, while *E2-2* had very low levels (**Fig. 12**). In addition, expression levels of all four ID proteins were assessed with high levels of *Id2*, robust levels of *Id1* and *Id3* and low expression of *Id4* (**Fig. 12**). The fact that expression of all E protein and ID protein family members could be detected in liver, suggested a functional role for E47 in hepatocytes.

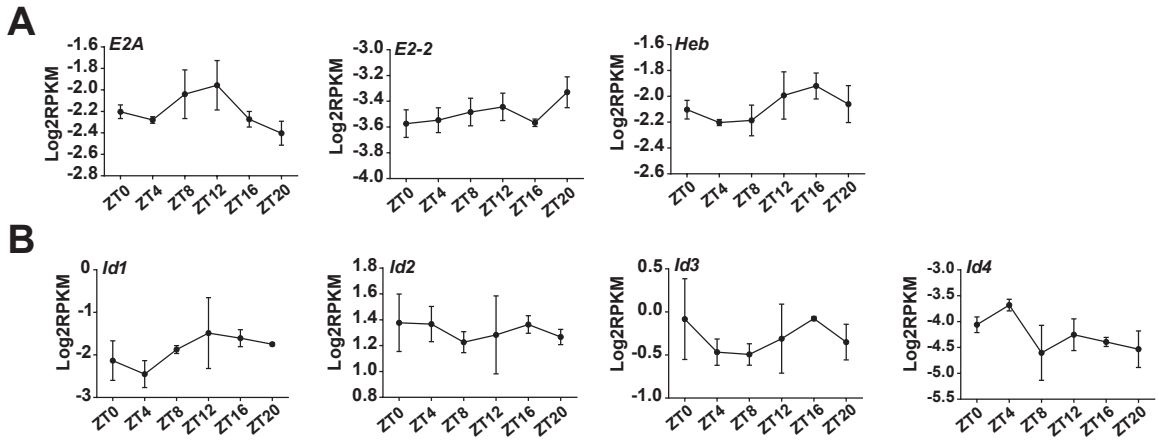

Figure 12: Expression profiles of E proteins and ID proteins in mouse liver around the clock.
A: RNA-Seq data from wildtypr livers at 6 time-points around the clock (ZT0= 7am; ZT12= 7pm). Expression of E proteins (**A:** *E2A, Heb, E2-2*) and ID Proteins (**B:** *Id1, Id2, Id3, Id4*) is displayed as mean Log2RPKM ±SEM, n= 4. Expression data from Quagliarini et al. (manuscript under revision).

4.1.2 GR and E2A converge on metabolic pathways

To test the hypothesis that E47 co-localizes to GR-bound hepatic enhancers, ChIP-Seq for E2A was performed in the same wildtype livers. ChIP-DNA was prepared and sequenced reads were aligned to the mouse mm10 reference genome (**Supplemental Table 1**). Bound regions (peaks) were called using MACS2 and 4783 peaks were identified. Of these 1123 peaks were reproducibly called between two biological replicates. Motif analysis of the E2A ChIP-sequenced DNA revealed the most prominent consensus binding sites to be shared between the two factors. Statistically overrepresented sites were c/EBP, HNF4α, FoxA, HNF6, AP-1, GRE and the nuclear receptor DR1 motif (**Fig. 13A**).

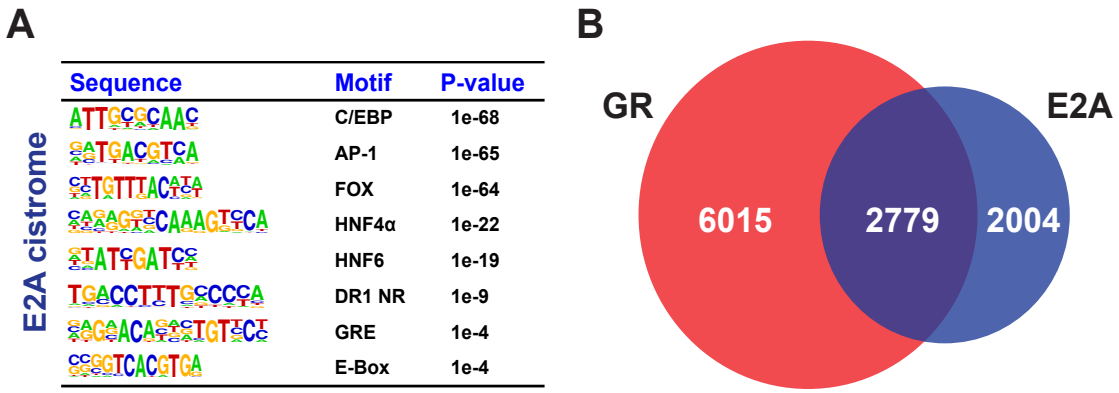

Figure 13: Overlapping binding of GR and E2A in liver converges on metabolic pathways.
A: *De novo* motif analysis of the hepatic E2A cistrome in wildtype livers. The top eight enriched transcription factor consensus sites in ChIP sequences are shown for each factor and are ordered by p-value. **B:** Area-proportional Venn diagram illustrates the overlap between the liver cistromes for GR and E2A. Numbers represent peaks identified in any of the two biological replicates.

Cistromes for GR and E2A were compared and revealed a partial overlap of 2779 peaks (**Fig. 13B).** This confirmed that GR and E47 share a large number of binding sites in liver. Examples for commonly bound hepatic loci included glucose genes such as *phosphoenolpyruvate carboxykinase 1* (*Pck1*), *insulin-like growth factor-binding protein 1* (*Igfbp1*) and *glucokinase* (*Gck*) or lipid genes such as *24-dehydrocholesterol reductase* (*Dhcr24*), *glycerol-3-phosphate acyltransferase (Gpam)* and *hydroxymethylglutaryl-CoA synthase (Hmgcs1)* (**Fig. 14**).

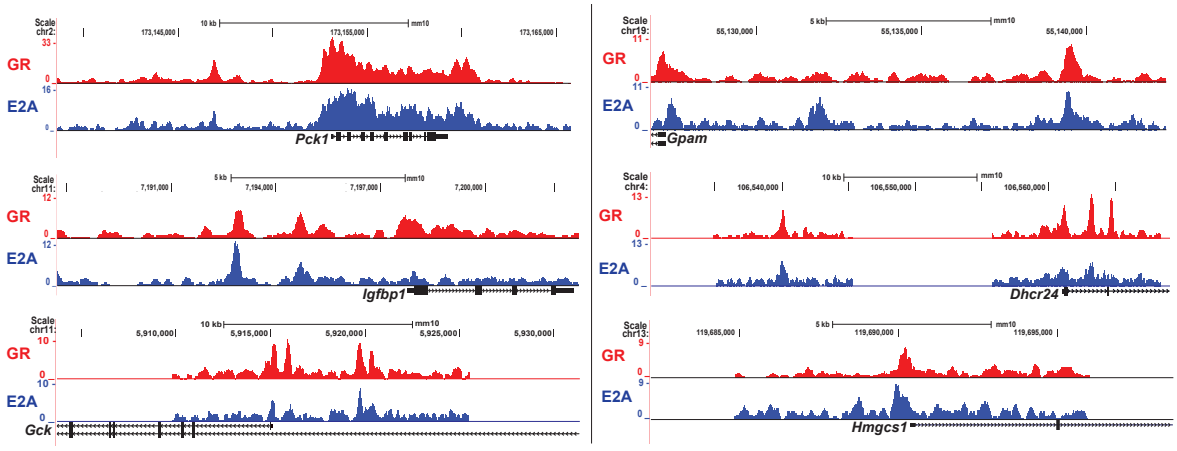

Figure 14: Co-occupancy of GR and E2A at metabolic promoters and enhancers.
Representative ChIP-Seq tracks display co-occupancy of GR and E2A at exemplary sites of glucose genes and lipid genes (left) in liver. ChIP peaks represent NGS read coverage aligned to the genome (**Supplemental Table 1&2**).

Interestingly, when functional annotation of these shared target genes was performed using GREAT pathway annotation tool, they linked to liver metabolism and metabolic disturbances (**Fig. 15**).

GO: Biological process	FDR Q-value
Carboxylic acid metabolic process	1.90e-39
Steroid metabolic process	7.04e-21
Fatty acid metabolic process	8.20e-17
Regulation of glucose metabolic process	1.30e-16
Regulation of lipid metabolic process	9.13e-15
Examples: *Gpam, Dhcr24, Gck, Foxo1, Apoc3, Irs1, Irs2, Elovl6*	

GO: Disease ontology	FDR Q-value
Lipid metabolic disease	1.44e-19
Fatty liver	1.10e-12
Familial hyperlipidemia	2.54e-12
Gestational diabetes	1.39e-9
Metabolic syndrome	6.97e-6
Examples: *Apoa4, Gck, Cd36, Serpina12, Apoc3, Hmgcr, Srebf2, Irs1*	

Figure 15: Functional pathway annotation of co-bound loci.
Functional annotation of shared GR-E2A target genes by GO analysis into pathways. Common ChIP peaks are annotated to the nearest coding gene and clustered into enriched pathways using GREAT pathway annotation tool.

Here, *cis*-regulatory elements bound by GR and E2A are annotated to the nearest coding genes (by linear proximity) and are then clustered into enriched pathways. For GR and E2A, co-bound genes classified into pathways linked to e.g. regulation of lipid and fatty acid metabolism as well as regulation of glucose metabolism. Furthermore, these genes were specifically associated with metabolic diseases such as diabetes and hepatic steatosis (**Fig. 15**). The link to glucose and lipid metabolism was specific to binding sites commonly shared with GR. On the other hand, pathway annotation of peaks specific for E2A clustered into pathways such as cellular amino acid processes and MAPK signaling pathways, whereas GR binding without E2A revealed its known link to lipid and carbohydrate metabolic processes (**Fig. 16A&B**).

The data presented here shows that E47 co-occupies a subset of GR-bound *cis*-regulatory elements in mouse livers. These co-bound loci specifically link to genes important for glucose and lipid metabolism, supporting the notion that E47 is involved the transcriptional regulation of genes by GR.

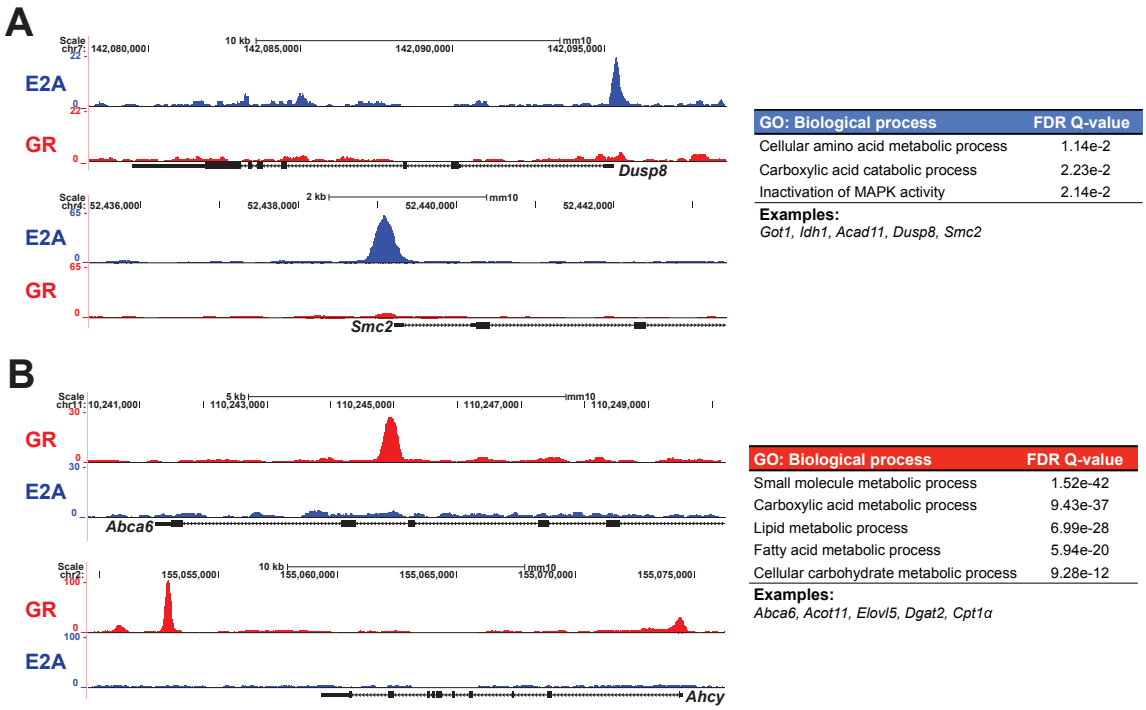

GO: Biological process	FDR Q-value
Cellular amino acid metabolic process	1.14e-2
Carboxylic acid catabolic process	2.23e-2
Inactivation of MAPK activity	2.14e-2

Examples:
Got1, Idh1, Acad11, Dusp8, Smc2

GO: Biological process	FDR Q-value
Small molecule metabolic process	1.52e-42
Carboxylic acid metabolic process	9.43e-37
Lipid metabolic process	6.99e-28
Fatty acid metabolic process	5.94e-20
Cellular carbohydrate metabolic process	9.28e-12

Examples:
Abca6, Acot11, Elovl5, Dgat2, Cpt1α

Figure 16: Pathway annotation of GR and E2A-specific peaks.
A: Analogous representation of E2A-specific occupancy and functional annotation of target genes. **B:** ChIP-Sequencing tracks display GR-specific occupancy at hepatic promoters and enhancers and functional annotation of GR-specific target genes by gene ontology (GO) analysis.

4.2 Characterization of *in vivo* loss of function mouse models

4.2.1 *E47-/-* mice are resistant to Dex-induced hyperglycemia

ChIP-Seq revealed the E47 motif to be enriched together with GR in liver and both factors to co-occupy a subset of metabolic genes. This prompted the hypothesis that E47 is needed for the transcriptional regulation of these metabolic target genes by GR. For this reason, one would expect an altered phenotypic response *in vivo* in response to GCs upon loss of E47. Besides its known role in B and T cell differentiation homozygous *E47* knockout mice had previously not been assayed for a metabolic phenotype.

Long-term GC-treatment in humans is known to result in hyperglycemia, frequently referred to as “steroid diabetes” (van Raalte and Diamant, 2014). Similarly, after three weeks of Dex-supplementation in the drinking water, wildtype mice displayed a mild hyperglycemia when subjected to a glucose tolerance test. Dex-treated *E47*-/- mice, on the other hand, showed significantly lower blood glucose levels over time after injection of the glucose bolus (**Fig. 17A**).

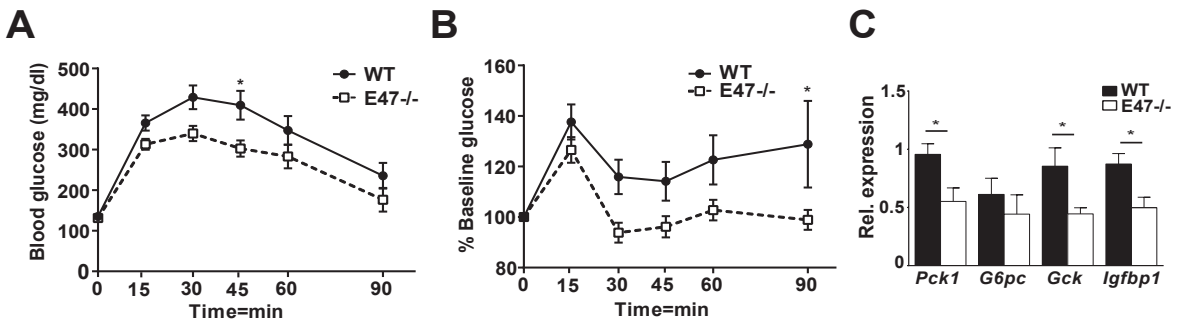

Figure 17: *E47-/-* mice display improved glucose tolerance upon GC treatment.
A: Glucose tolerance test i.p. (GTT) and pyruvate tolerance test i.p. (PTT) (**B**) of *E47-/-* and wildtype mice after 3 weeks of Dex treatment in drinking water. Data were analyzed by ANOVA and Bonferroni's multiple comparison test. Data are shown as mean ± SEM. Asterisks indicate significance, (*) P<0.05, n= 10 per genotype (GTT); n= 7 (WT) & 9 (E47-/-) (PTT), i.p.= intraperitoneal. **C:** qRT-PCR of gluconeogenic genes in Dex-treated livers, normalized to *U36b4;* data are mean ± SEM (*) P < 0.05, Student's t-test. n= 6 (WT) & 5-6 (E47-/-).

Furthermore, a pyruvate tolerance test also resulted in lower values in *E47-/-* mice compared to their wildtype littermates, suggesting reduced hepatic gluconeogenesis (**Fig. 17B**) in response to GCs. In accordance with liver-specific *GR* mutant mice, which show an impaired transcriptional activation of gluconeogenic genes (Opherk et al., 2004), expression of the key GR target genes *Pck1*, *Gck* and *Igfbp1* were diminished in *E47-/-* mice (**Fig 17C**).

This protective effect was a specific response to Dex treatment, since both glucose and pyruvate tolerance was the same in untreated wildtype and *E47-/-* mice (**Fig 18A&B**). Moreover, *E47-/-* mice displayed similar body weight and a percentage of body fat compared to wildtype littermates (**Fig 18C&D**). Gene expression of *E12*, the alternatively spliced variant of *E2A*, was comparable in Dex-treated livers of *E47-/-* mice, excluding a possible functional compensation (**Fig. 18E**).

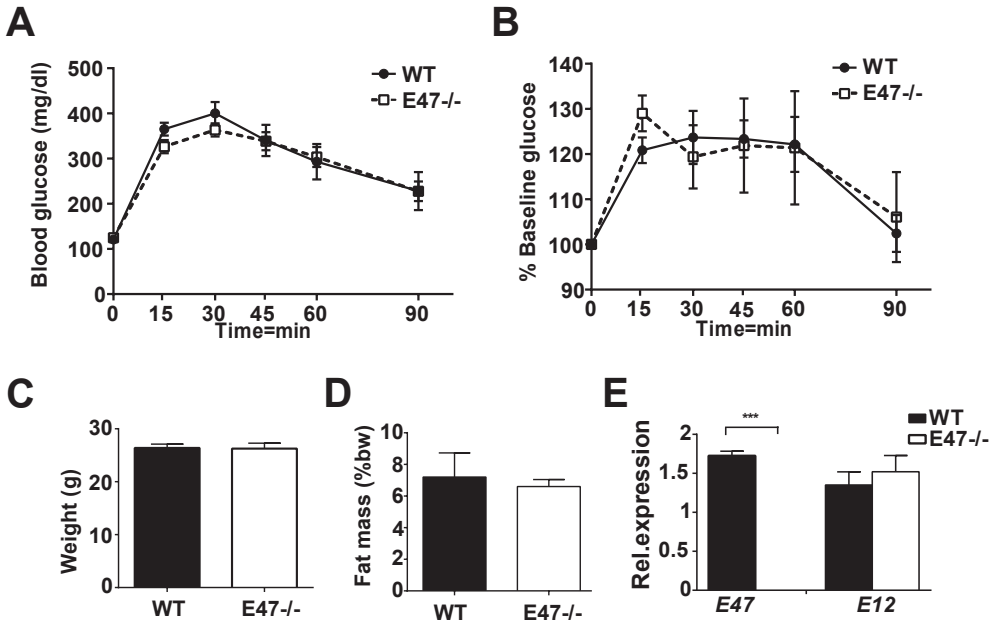

Figure 18: *E47-/-* mice are not affected metabolically in the basal state.
A: Glucose tolerance test i.p. (GTT) and pyruvate tolerance test i.p. (PTT) (**B**) in untreated *E47-/-* and wildtype mice. Data were analyzed by ANOVA and Bonferroni's multiple comparison test, n=9 (WT) & 15 (E47-/-)(GTT); n= 6 (WT) & 7 (E47-/-) (PTT); data for PTT is shown as % of baseline glucose (timepoint 0). **C:** Body weight of untreated *E47-/-* and wildtype mice in grams. Data are mean ± SEM, n=7 (WT) & 9 (E47-/-). **D:** Fast mass shown as percentage of body weight (%bw) in untreated *E47-/-* and wildtype mice. Data are mean ± SEM, n=8 (WT) & 11 (E47-/-). **E:** qRT-PCR of *E47* and *E12* expression in mouse livers after Dex treatment, normalized to *U36B4*. Data are expressed as mean ± SEM, (***) P<0.001, Student's t-test, n=10 (WT) & 7 (E47-/-).

4.2.2 *E47-/-* mice are protected from the development of hepatic steatosis

In order to study disturbances in lipid metabolism in response to GCs, another protocol of GC treatment was used. Chronic administration of corticosterone (Cort), the rodent Cortisol, was previously shown to induce comorbidities of the Metabolic Syndrome, including hepatic steatosis (Karatsoreos et al., 2010, Fransson et al., 2013). After three weeks of Cort administered via the drinking water, wildtype mice developed as steatotic phenotype in the liver as seen by accumulation of lipid droplets on Oil red O and H&E stainings (**Fig. 19A**). In contrast, *E47-/-* mice showed a noticeably diminished accumulation of lipids (**Fig. 19A**). Consistent with the stainings in liver, measurement of liver and plasma triglycerides showed lower levels for *E47-/-* mice compared to wildtype mice (**Fig. 19B**).

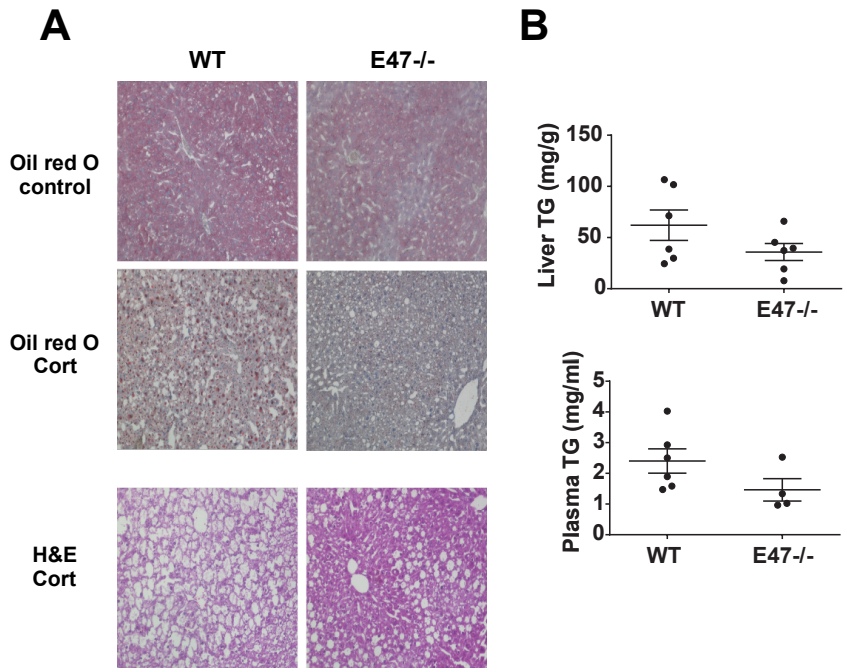

Figure 19: *E47 -/-* mice are protected from Cort-induced hepatic steatosis.
A: Liver sections (6um) stained with Oil Red O and hematoxylin and eosin (H&E) before and after Cort treatment for 3 weeks in drinking water. 20x magnification; representative image from n=3 per group. **B:** Measurement of liver and plasma triglycerides in mice treated with Cort for 3 weeks. Data are shown as mean ± SEM, n=6 (WT) & 4-6 (E47-/-).

Again, this effect was a specific response to GC treatment since untreated *E47-/-* and wildtype mice had comparable liver triglycerides, although plasma triglycerides were also lower (**Fig. 20A**). Apart from an overall state of dyslipidemia, obesity is a hallmark of the Metabolic Syndrome and Cort treatment was shown to result in increased central fat deposits in mice (Fransson et al., 2013, Karatsoreos et al., 2010). However, as measured by Echo-NMR, fat mass gain upon Cort treatment was similar *E47-/-* and wildtype mice. This indicated that protection from metabolic side effects was restricted to the liver (Fig. **20B**).

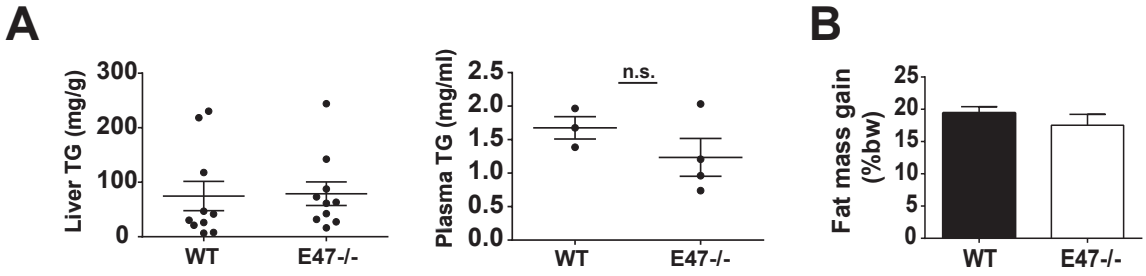

Figure 20: *E47-/-* mice do not display dyslipidemia in the basal state.
A: Measurement of liver and plasma triglycerides in untreated mice. Data are mean ± SEM, Liver: n= 10 per genotype; Plasma: n=3 (WT) & 4 (E47-/-); n.s.= not significant **B:** Fat mass gain shown as percentage of body weight (%bw) after 3 weeks of Cort treatment. Data are mean ± SEM, n=6 per genotype.

4.2.3 *E47-/-* mice display deregulated hepatic gene expression programs

To gain mechanistic insight into the altered response to GCs, gene expression profiles in *E47-/-* livers, were analyzed by RNA-seq in Cort and Dex-treated mice (**Supplemental Tables 3&4**). Reads were mapped to the mouse genome mm10 and differential expression analysis was performed using DESeq2. In Dex-treated livers, 302 genes were differentially expressed, whereas in Cort-treated livers 914 genes were identified as differentially expressed (**Fig. 21**). The criterion for differential expression were defined as fold change of 1.3 and a p-value <0.05.

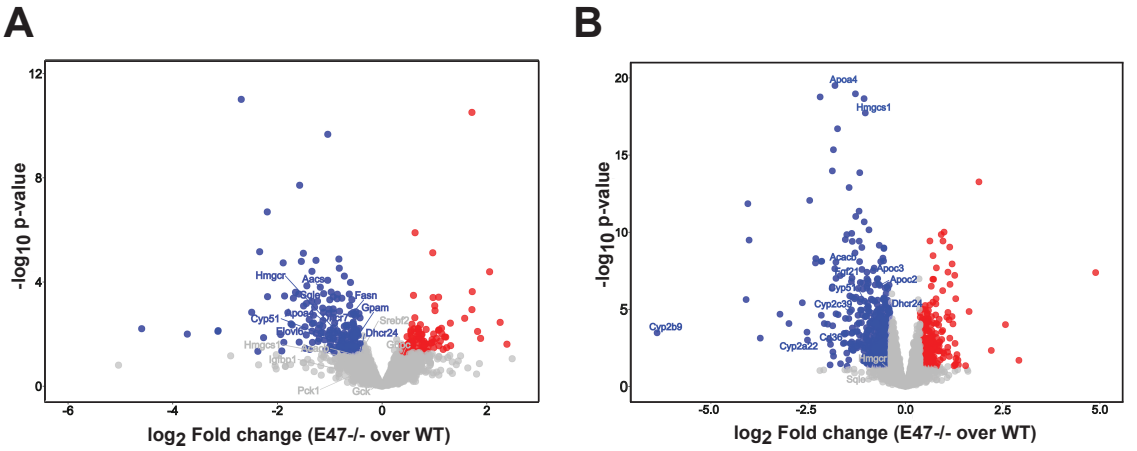

GO Biological process	FDR Q-value
Lipid metabolic process	1.77e-10
Monocarboxylic acid metabolic process	2.47e-6
Fatty acid metabolic process	1.35e-5
Cholesterol metabolic process	3.66e-4
Developmental process	1.30e-3

Examples:
Dhcr24, Dhcr7, Acacb, Gpam, Fasn, Aacs, Sqle, Cyp51, Elovl6, Apoa4, Hmgcs1, Hmgcr

GO Biological process	FDR Q-value
Small molecule metabolic process	2.45e-8
Lipid metabolic process	7.99e-8
Cholesterol metabolic process	5.20e-4
Lipid catabolic process	3.39e-3
Triglyceride metabolic process	4.85e-2

Examples:
Dhcr24, Acacb, Cyp2a22, Cy2c39, Cyp2b9, Fgf21, Cd36, Apoc2, Apoc3, Cyp51, Apoa4, Hmgcs1

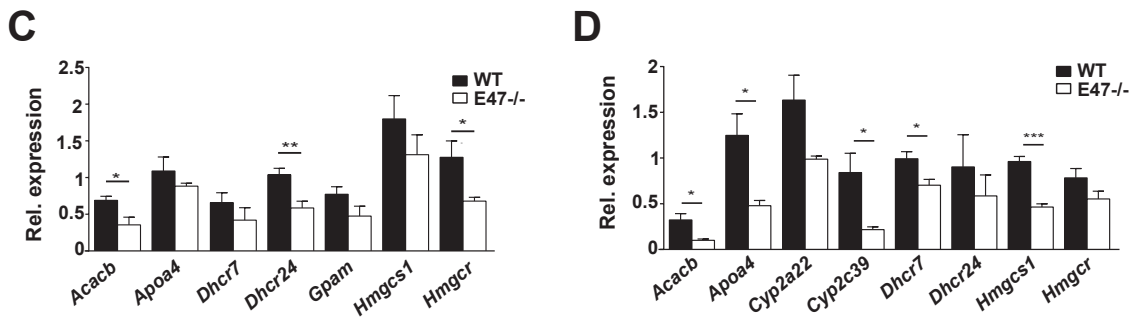

Figure 21: Livers of *E47-/-* mice reveal deregulated gene expression.
A-B: RNA-Seq data from Dex-treated **(A)** and Cort-treated **(B)** wildtype and *E47-/-* livers was visualized in volcano plots (blue= down-; red=up-regulated, fold change=1.3, p-value<0.05). Volcano plots show the log2 of fold change of gene expression between the (Dex/Cort) treated *E47* mutant group and control group versus log10 of p-value from t-test. GO analysis of differentially expressed genes is shown below each volcano plot. For GO analysis a base mean cutoff >200 was used. **C:** qRT-PCR of differentially expressed liver genes after Dex treatment, normalized to *U36B4*. Data are mean ± SEM, (*) P < 0.05, Student's t-test, n=5-7 (WT) & 4-7 (E47-/-). **D:** qRT-PCR of differentially expressed genes in livers after Cort treatment, normalized to *U36B4*. Data are mean ± SEM, n=4 per genotype.

Gene ontology (GO) analysis of differentially expressed genes in mutant livers receiving Dex (**Fig. 21A**) or Cort (**Fig. 21B**) identified globally deregulated expression profiles. These linked to pathways involved in regulation of lipid, triglyceride and cholesterol metabolism. Interestingly, genes affected by loss of E47 were mainly downregulated. This argues for an inability of GR to efficiently activate its target genes when E47 is lost and underlines E47's predominant role as a transcriptional activator. The differential expression of genes affected by the loss of E47 was confirmed by qRT-PCR. Among the genes showing reduced expression were e.g. *Dhcr24* (*24-dehydrocholesterol reductase*) and *Dhcr7* (*7-dehydrocholesterol reductase*), which are involved in cholesterol biosynthesis. Other genes included *Apoa4* (*apolipoprotein A4*), important for lipid transport and tissue uptake, and *Acacb* (*acetyl-CoA carboxylase beta*), which is the rate limiting enzyme catalyzing fatty acid synthesis (**Fig. 21C&D)**. This is in accordance with the data from the *in vivo* loss of function mouse model showing protection from hepatic steatosis and reduced levels of circulating triglycerides (**Fig. 19**). Therefore, the genes affected by the loss of E47 in liver in response to Dex and Cort treatment might explain the observed phenotype of reduced lipid accumulation and gluconeogenesis.

Importantly, RNA-Seq data from livers of untreated *E47*-/- only revealed very few changes in gene expression and failed to result in any functionally enriched pathways (**Fig. 22A; Supplemental Table 5**). This again demonstrated that altered gene expression upon loss of E47 is a GC-specific effect. Moreover, gene expression profiles in Dex-treated quadriceps muscle (**Fig. 22B; Supplemental Table 6**) and white adipose tissue (**Fig. 22C; Supplemental Table 7**) revealed no prominent differences in metabolic gene expression which could explain the improved glucose tolerance or reduced lipid droplet accumulation in liver. E47 had previously been reported to play a role in the regulation of *adiponectin* expression during development *in vitro* (Doran et al., 2008, Rahmouni and Sigmund, 2008). However, *Adipoq* mRNA levels in Dex-treated white adipose tissue were not significantly altered in *E47*-/- mice (**Fig. 22D**).

The differential gene expression profiles from RNA-Seq in Dex- and Cort-treated livers support the *in vivo* data form *E47* knockout mice. Loss of E47 results in a reduced metabolic gene expression, which would in turn protect from GC-induced side effects due to impaired upregulation of important gluconeogenic and lipid utilization genes.

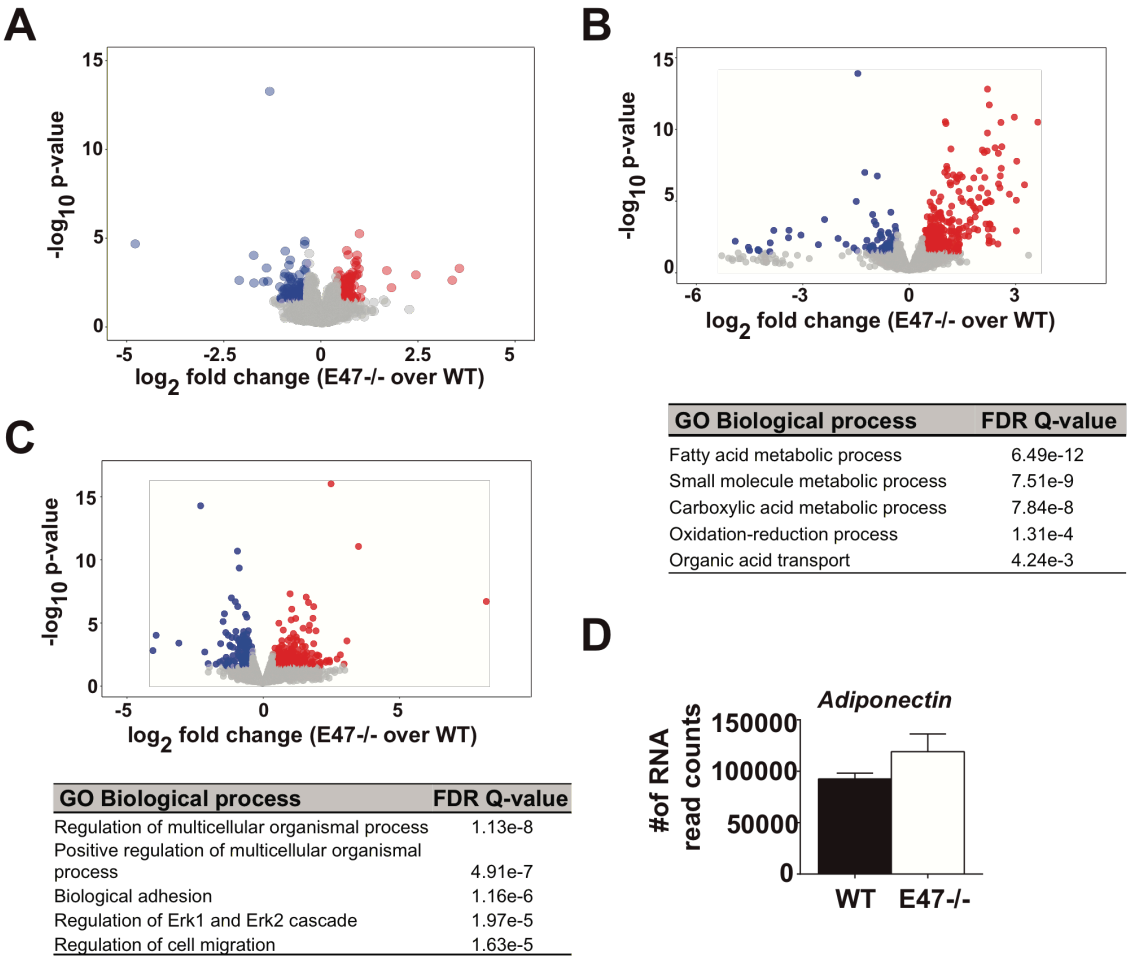

GO Biological process	FDR Q-value
Fatty acid metabolic process	6.49e-12
Small molecule metabolic process	7.51e-9
Carboxylic acid metabolic process	7.84e-8
Oxidation-reduction process	1.31e-4
Organic acid transport	4.24e-3

GO Biological process	FDR Q-value
Regulation of multicellular organismal process	1.13e-8
Positive regulation of multicellular organismal process	4.91e-7
Biological adhesion	1.16e-6
Regulation of Erk1 and Erk2 cascade	1.97e-5
Regulation of cell migration	1.63e-5

Figure 22: Changes in metabolic gene expression are specific to GC-treatment in liver.
A-C: RNA-Seq data from untreated mouse livers (**A**), Dex-treated skeletal quadriceps muscle (SM) (**B**) and Dex-treated white adipose tissue (DeFuria et al.) (**C**) was visualized in volcano plots (blue= down-; red=up-regulated, fold change 1.3, p-value<0.05). Volcano plots show the log2 of fold change of gene expression between the (*E47* mutant group and control group versus log10 of p-value from t-test. GO analysis of differentially expressed genes is shown below each volcano blot. For untreated liver, GO analysis did not result in functionally enriched pathways. For GO analysis a base mean cutoff >200 was used. Liver: n=5 (WT) & 6 (E47-/-); SM: n=2 (WT) & 4 (E47-/-); WAT: n=2 per genotype. **D:** Average number of normalized NGS read counts for *Adipoq* in Dex-treated white adipose tissue. Data are mean ±STDEV, n.s.= not significant, n=2 per genotype.

Fasting in mice over a prolonged period of time induces a rise in glucocorticoids due to their physiological function in the body to maintain glucose homeostasis (Vegiopoulos and Herzig, 2007). To examine whether the fasting-response mediated by GR is affected upon loss of E47, *E47-/-* mice and their wildtype littermates were fasted for a period of 16 hrs overnight. In the liver, expression levels of genes involved in the response to prolonged fasting were examined by qRT-PCR. Among these were gluconeogenic genes, e.g. *Pck1, G6pc* and *Gck* and genes important for lipid mobilization, e.g. *Fasn and Srebp1c*. Here, some gluconeogenic genes, e.g. *Pck1, G6pc and Gck,* showed a diminished expression in mutant mice in response to fasting (**Fig. 23**). This would point towards a mild fasting phenotype in

E47-/- mice. However, basal glucose levels were similar in untreated *E47-/-* and wildtype mice after overnight fasting and overall glucose tolerance was unchanged (**Fig. 17A**).

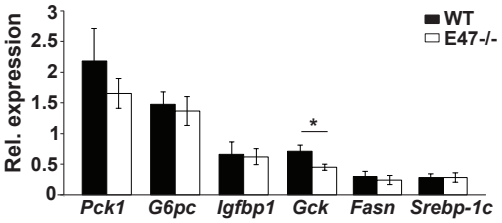

Figure 23: Gene expression changes in response to fasting in *E47-/-* livers.
qRT-PCR in livers of untreated fasted mice (16 hrs overnight), normalized to *U36b4.* Data are mean ± SEM (*) P<0.05, Student's t-test, n=6 (WT) & 6-7 (*E47-/-).*

Taken together, loss of E47 mildly affected the endogenous response to a state of prolonged fasting. This effect was, however, only observed on hepatic gene expression of gluconeogenic genes since fasting glucose levels were unchanged between in *E47-/-* mice and wildtype littermates. For the phenotypic difference of reduced hepatic gluconeogenesis to become apparent upon loss of E47, additional exposure to exogenous GCs is needed. This data again underlines the specific role, which E47 has in the regulation of GR target genes in liver in response to treatment with high levels of GCs.

4.2.4 Immunosuppressive effects of Dex are retained in *E47-/-* mice

Treatment with glucocorticoids is highly valued in the clinic for its important anti-inflammatory effects. This is due to GR's potent transcriptional repression of pro-inflammatory genes and activation of anti-inflammatory genes. To test if immunosuppressive GC action was retained in the absence of E47, bone marrow-derived macrophages were isolated from wildtype and *E47-/-* mice. For a pro-inflammatory stimulus, macrophages were activated by LPS and then suppressed by treatment with Dex stimulus. Treatment with Dex resulted in the induction of GR targets, e.g. *Per1* and *Gilz* and, more importantly, repression of inflammatory targets, e.g. *Ccl2* and *Il6* in both *E47-/-* and wildtype macrophages (**Fig. 24)**. Of note, expression of E47 in macrophages is significantly lower than in other tissues and the GR cistrome in macrophages does not harbor E47 motifs near GREs (Uhlenhaut et al., 2013).

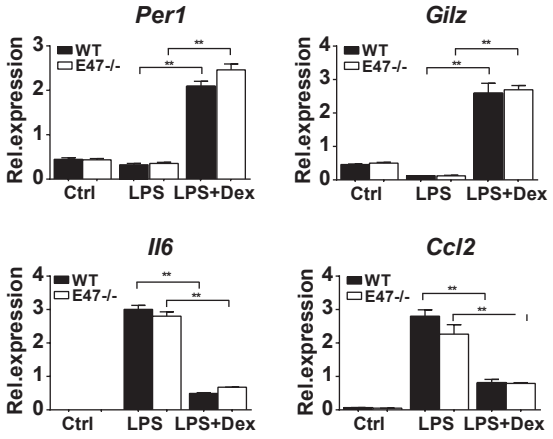

Figure 24: *E47-/-* mice remain responsive to the immunosuppressive effects of Dex.
qRT-PCR of Dex target genes in macrophages from *E47-/-* and wildtype mice, normalized to *U36B4*. Macrophages were treated with LPS or LPS+Dex. Data are mean ± STDEV (**) P<0.01, (***) P<0.001, Student's t-test, n=2 replicates per genotype.

Glucocorticoids are secreted under the control of the hypothalamic-pituitary-adrenal (HPA) Axis. In a classical negative feedback loop, GCs can limit their own production (Chung et al., 2011). To examine whether the HPA axis was intact in *E47-/-* mice, a Dexamethasone-suppression test was performed. Here, an acute injection of a high dose of Dex is administered to assess the suppression of ACTH secretion by the pituitary as an integral part of the negative feedback loop. This test is commonly used as a first diagnosis of Cushing's syndrome since effective suppression is absence in these cases. *E47-*/- mice displayed slightly elevated basal corticosterone levels, albeit not significant (**Fig. 25**).

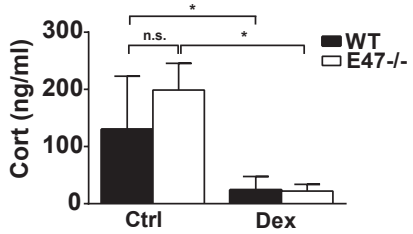

Figure 25: The HPA axis is functionally intact in *E47-/-* mice.
Plasma corticosterone was measured in mice 6hrs after injection of 1mg/kg Dex or vehicle. Data are mean ± SEM, n=10 (WT) & 11 (E47-/-), n.s.= not significant.

However, in response to an acute injection of Dex, mutant mice suppressed endogenous corticosterone production equally well compared to wildtype mice as shown in **Fig. 25**. The slight hypercorticolism in the basal state might be explained by a minor compensatory mechanism of a general GC-affected pathway. However, this was not sufficient to result in classical symptoms of Cushing's syndrome in the basal and untreated state.

Taken together, the data showed that important anti-inflammatory effects of Dex are maintained in *E47-*/- mice and that regulation of the HPA axis remains intact.

4.2.5 Hepatocyte-specific loss of E47 implicates liver as the target tissue

Data from RNA-Sequencing and metabolic phenotyping of global *E47-/-* mice strongly suggested a role for E47 in gene regulation of hepatic metabolism. Furthermore, the liver was implicated to be the target tissue for a potential crosstalk between E47 and GR and to mediate protection from hyperglycemia and hyperlipidemia. To confirm, liver-specific *E47* knockout mice were generated by crossing *E47* floxed alleles with the Albumin-Cre line (specified as $E47^{\Delta LKO}$) and metabolically phenotyped in response to GC treatment. After three weeks of Dex supplementation in the drinking water, $E47^{\Delta LKO}$ displayed improved glucose tolerance (**Fig. 26A**), as previously seen in global *E47-/-* mice. Resistance to the development of steroid diabetes was again accompanied by a reduced expression of key gluconeogenic genes such as *Pck1* and *G6pc* in livers of $E47^{\Delta LKO}$ mice (**Fig. 26B**).

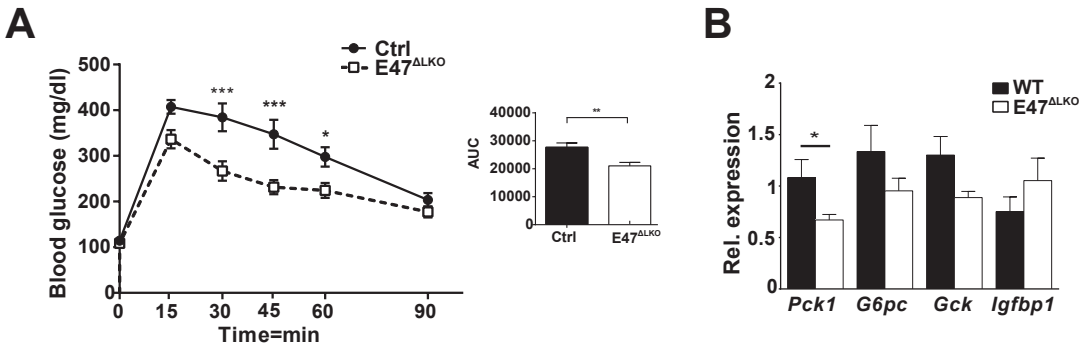

Figure 26: Liver-specific *E47-/-* mice are resistant to Dex-induced hyperglycemia.
A: Glucose tolerance test i.p. (GTT) in *Albumin-Cre* x $E47^{flox/flox}$ ($E47^{\Delta LKO}$) and control mice after 3 weeks of Dex treatment. Data were analyzed by ANOVA and Bonferroni's multiple comparison test. Data are shown as mean ± SEM. Asterisks indicate significance, (*) P<0.05, (**) P<0.01, (***) P<0.001, n=11 per genotype. **B:** qRT-PCR of gluconeogenic genes in livers on Dex normalized to *U36b4*. Data are mean ± SEM, (*) P<0.05, Student's t-test, n=6 per genotype.

Analogous to the global *E47* knockout model, untreated $E47^{\Delta LKO}$ displayed similar basal glucose tolerance, comparable body weight, slightly lower but not significant basal body fat mass and no compensatory expression of *E12* in Dex-treated livers (**Fig. 27A-D**).

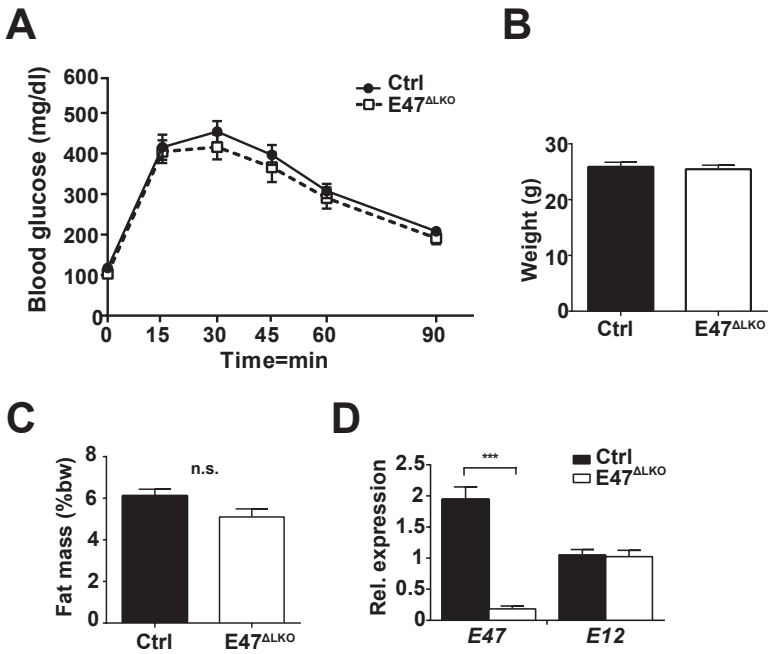

Figure 27: Liver-specific *E47-/-* mice are metabolically unaffected in the basal state.
A: Glucose tolerance test i.p. in untreated E47$^{\Delta LKO}$ and control mice. Data were analyzed by ANOVA and Bonferroni's multiple comparison test and are mean ± SEM, n=11 per genotype. **B:** Body weight of untreated E47 $^{\Delta LKO}$ and control mice. Data are mean ± SEM, n=7 per genotype. **C:** Fat mass shown as percentage of body weight (%bw) in untreated E47$^{\Delta LKO}$ and control mice. Data are mean ± SEM, n=7 per genotype. **D:** qRT-PCR of *E47* and *E12* expression in livers after Dex treatment, normalized to *U36B4*. Data are mean ± SEM, (***) P<0.0001, Student's t-test, n=7 (Ctrl) & 5 (E47$^{\Delta LKO}$).

The protective effect from GC-induced side effects was confirmed after treatment with Cort. Here, liver histology and measurements of liver and plasma triglycerides showed protection from hepatic steatosis and dyslipidemia in *E47$^{\Delta LKO}$* mice (**Fig. 28A&B**). By qRT-PCR, expression levels of gene important for lipid and cholesterol biosynthesis and utilization, e.g. *Acacb, Dhcr7*, *Dhcr24,* were examined. Consistent with data from global *E47-/-* mice, these genes were downregulated in livers of *E47$^{\Delta LKO}$* mice, thereby confirming the deregulated liver metabolism (**Fig. 28C**). Similar to *E47-/-* mice, liver-specific deletion of E47 had no impact on the increase of fat mass as measured by Echo-NMR (**Fig. 28D)**.

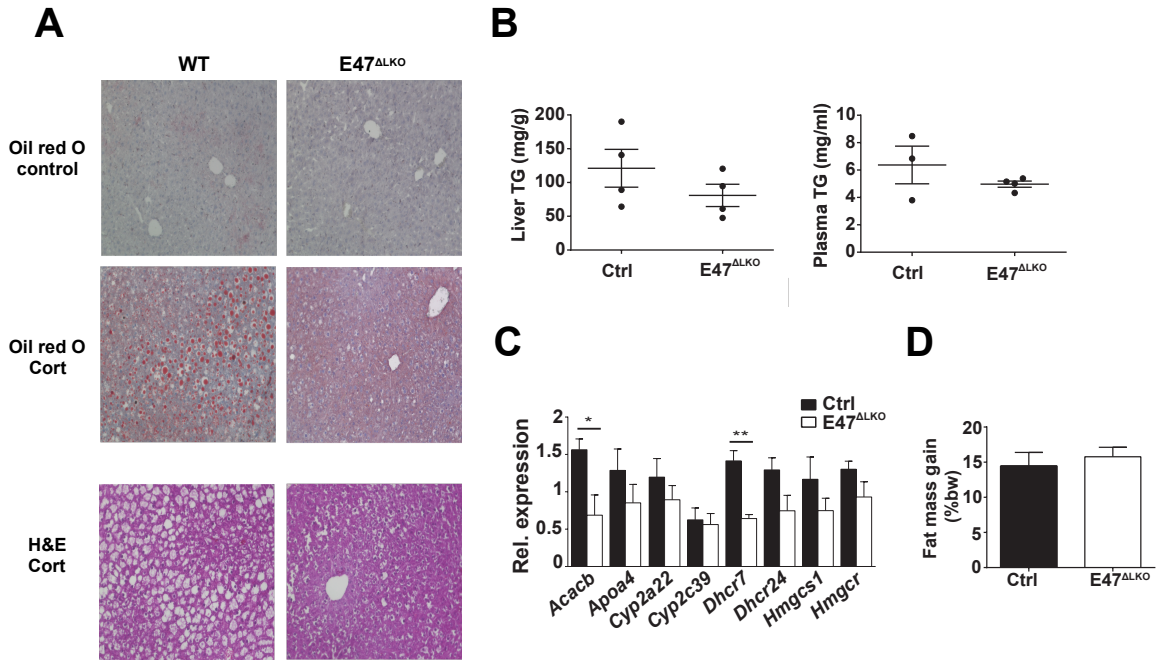

Figure 28: Liver-specific *E47-/-* mice are protected from Cort-induced hepatic steatosis.
A: Liver sections (6um) stained with Oil Red O and hematoxylin and eosin (H&E) before and after Cort treatment for 3 weeks. 20x magnification. **B:** Measurement of liver and plasma triglycerides in E47$^{\Delta LKO}$ and control mice treated with Cort. Data are shown as mean ± SEM, n=4 per genotype. **C:** qRT-PCR of differentially expressed genes in livers after Cort treatment, normalized to *U36B4*. Data are mean ± SEM, (*) P<0.05, Student's t-test, n=5 per genotype. **D:** Fat mass gain shown as percentage of body weight (%bw) after Cort treatment. Data are mean ± SEM, n=8 per genotype.

Physiological effects of glucocorticoids and GR are widespread and extend beyond causing disturbances in hepatic metabolism (Schacke et al., 2002). Therefore, long-term treatment with a high dose of any glucocorticoid will likely have additional pathological changes. To elicit acute gene expression responses, *E47$^{\Delta LKO}$* were injected with a high dose of Dex and sacrificed one hour later (**Fig. 29**). This approach would also avoid secondary and indirect comorbidities of long-term treatment with steroids. The Dex-injected wildtype and *E47* mutant livers were subsequently used for RNA-Sequencing. Reads were mapped to the mouse genome mm10 and differential expression analysis was performed using DESeq2 (Love et al., 2014). In Dex-injected livers, 208 genes were identified as differentially expressed using the criterion of fold change 1.3 and p-value <0.05. As an acute response to high availability of Dex, GO analysis of differentially expressed genes in short-term treated *E47$^{\Delta LKO}$* livers linked to lipid and fatty acid metabolic processes and cholesterol transport (**Fig. 29; Supplemental Table 8**). In this context, pathway annotations of genes coincided with the RNA-Seq data from global *E47-/-* mice (**Fig. 22A&B**). Among the genes differentially expressed in response to short-term Dex exposure were known metabolic genes, e.g. *Apoa4*, Cd36 and *Srebp1c.*

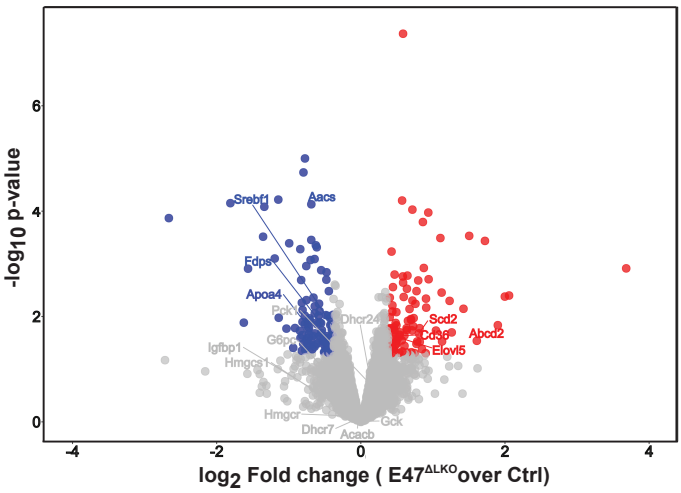

Figure 29: Acute Dex response on differential gene expression in *E47*$^{\Delta LKO}$ mice.
RNA Seq data from 1 hr Dex-injected *E47*$^{\Delta LKO}$ livers was visualized in a volcano plot (blue= down-; red=up-regulated, fold change 1.3, p-value<0.05). Volcano plot shows the log2 of fold change of gene expression between the *E47*$^{\Delta LKO}$ and control group versus p-value from the t-test. GO analysis of differentially expressed genes is shown below. For GO analysis a base mean cutoff >200 was used, (n=3 per genotype).

GO Biological process	FDR Q-value
Lipid metabolic process	7.01e-3
Monocarboxylic acid metabolic process	4.66e-2
Steroid metabolic process	5.87e-2
Positive regulation of fatty acid metabolic process	2.37e-1
Cholesterol transport	3.32e-1

Examples:
Apoa4, Cd36, Aacs, Srebf1, Elovl5, Abcd2

Importantly, the majority of differentially expressed transcripts from *E47* mutant mice treated with either Cort or Dex (**Fig. 21A&B, Fig. 29**) were shown to be GR target genes (**Fig. 30**). Here, all transcripts with a nearby GR peak are defined as a target gene. Between 63% (Cort longterm) to 85% (Dex longterm and acute Dex) of transcripts expressed in *E47* mutant livers could therefore be classified as bound and regulated by GR. Among the differentially expressed genes identified to harbor a GR peak were metabolic genes such as *Dhcr24, Hmgcs1 Acacb, Gpam and Apoa4.* This, once more, emphasizes the specific role of E47 in transcriptional regulation by GR in response to GCs.

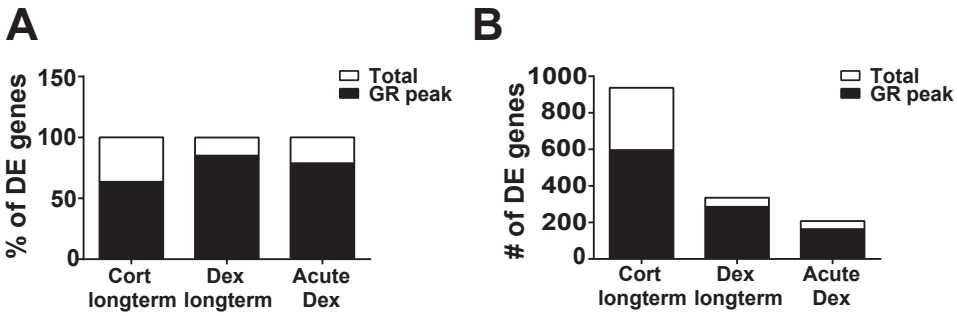

Figure 30: Differentially expressed genes in *E47* mutant livers are GR target genes.
A-B: Percentage **(A)** and number **(B)** of differentially expressed genes in *E47* mutant mice, which harbor a detectable GR ChIP peak nearby. RNA-Seq data from Fig. 21A&B and Fig. 29.

Taken together, metabolic phenotyping of hepatocyte-specific *E47*$^{\Delta LKO}$ mice confirmed the preceding *in vivo* data from global *E47* mutant mice. Loss of E47 affects GR-mediated hepatic metabolism, resulting in protection from GC-induced hyperglycemia and dyslipidemia and emphasizes the liver to be the focal point of E47 action.

4.2.6 Loss of E47 does not affect progression of diet-induced obesity

Many of the pathologies commonly seen with long-term GC-treatment or in Cushing's patients resemble the Metabolic Syndrome including obesity, glucose intolerance and dyslipidemia (Wang, 2005). Since previous data linked E47 to lipid and glucose metabolism regulation by GR in response to GC treatment, the development of diet-induced obesity and its comorbidities was studied in the *E47* mutant mouse models.

Global mutant mice were fed a high-fat diet (HFD) for 12 weeks. At the end of the feeding regime, *E47-/-* mice showed improved glucose tolerance as seen in a glucose tolerance test (**Fig. 31A**). Whereas, obese wildtype mice revealed the expected excess accumulation of hepatic triglycerides, *E47-/-* mice had slightly lower liver triglycerides with no differences in plasma triglycerides (**Fig. 31B**). This was confirmed by Oil red O and H&E staining on liver tissue, since HFD feeding resulted in a prominent hepatic steatosis in wildtype mice (**Fig. 31C**). Liver tissue of *E47-/-* mice also showed a diminished accumulation of lipids on Oil red O staining, but no difference in the presence of large lipid vacuoles on H&E staining (**Fig. 31C**). Moreover, weight gain on HFD was comparable between both groups (**Fig. 31D**).

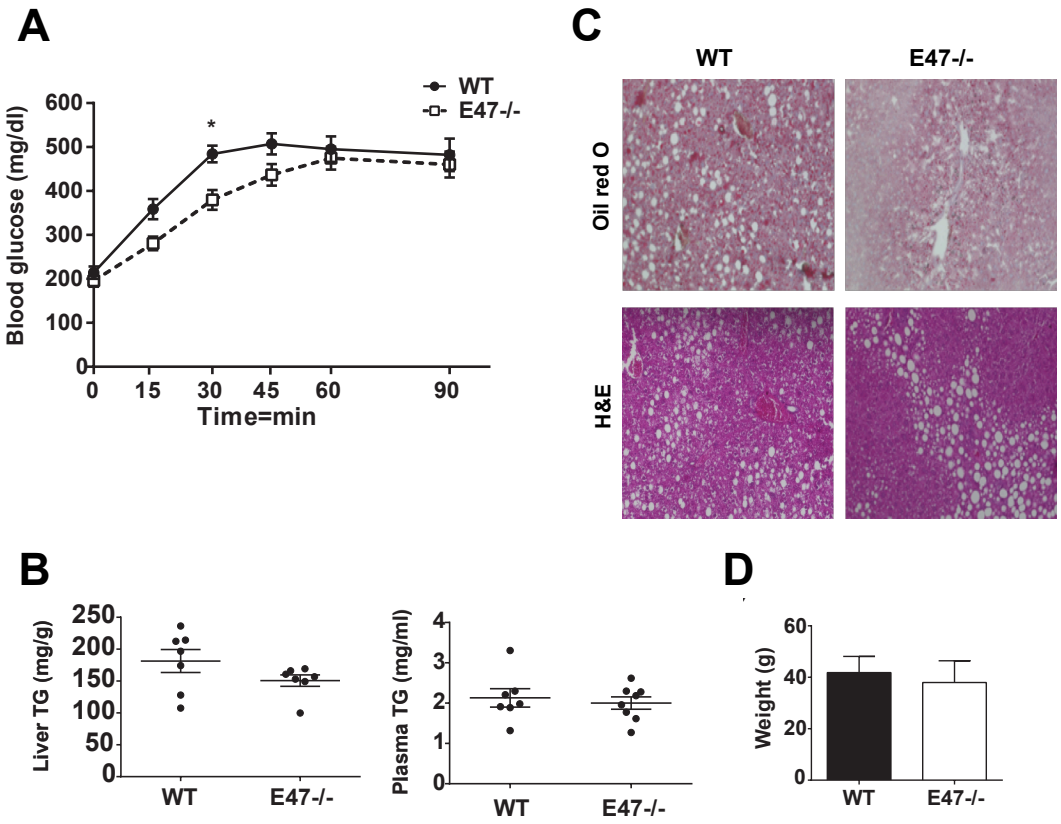

Figure 31: Metabolic phenotyping of HFD-fed *E47-/-* mice.
A: Glucose tolerance test i.p. (GTT) of *E47-/-* and wildtype mice after 12 weeks of high fat diet (HFD) feeding. Data were analyzed by ANOVA and Bonferroni's multiple comparison tests. Data are shown as mean ± SEM. n= 9 per genotype; i.p.= intraperitoneal. **B:** Measurement of liver and plasma triglycerides in *E47-/-* and wildtype mice after 12 weeks of HFD. Data are shown as mean ± SEM, Liver: n=7 per genotype, Plasma: n=7 (WT) & 8 (E47-/-). **C:** Liver sections (6µm) were stained with Oil Red O and hematoxylin and eosin (H&E) after 12 weeks of HFD; 20x magnification, brightfield microscopy, representative image from n=2 per genotype **D:** Body weight of *E47-/-* and wildtype mice in grams after 12 weeks of HFD. Data are mean ± SEM, n=9 per genotype.

Overall, data from HFD-fed *E47-/-* mice revealed an attenuated development of some of the classical side effects seen with HFD feeding, in particular in the development of hepatic steatosis.

As mentioned before, *E47*-/- mice have a complete lack of mature B cells and a partial early block in T-lymphocyte development (Beck et al., 2009b). A previous study had shown that obese mice lacking B cells (B^{null} mice) or mice with depleted B cell reservoirs had an improved glucose tolerance and insulin sensitivity on HFD compared to obese wildtype mice (Winer et al., 2011). This was accompanied by a comparable body weight gain on HFD (Winer et al., 2011). In order to exclude the lack of mature immune cells as a factor for protection from HFD-induced comorbidities, $E47^{\Delta LKO}$ were fed a HFD for 12 weeks. A glucose tolerance test showed no differences between $E47^{\Delta LKO}$ and control littermates (**Fig. 32A**). Liver as well as plasma triglycerides were equally elevated in $E47^{\Delta LKO}$ and control mice

(**Fig. 32B**) which was also reflected in a similar accumulation of lipid droplets and development of a steatotic phenotype as shown on histological stainings of liver tissue (**Fig. 32C**). In addition, *E47*$^{\Delta LKO}$ and control mice showed the same body weight gain on HFD (**Fig. 32D**).

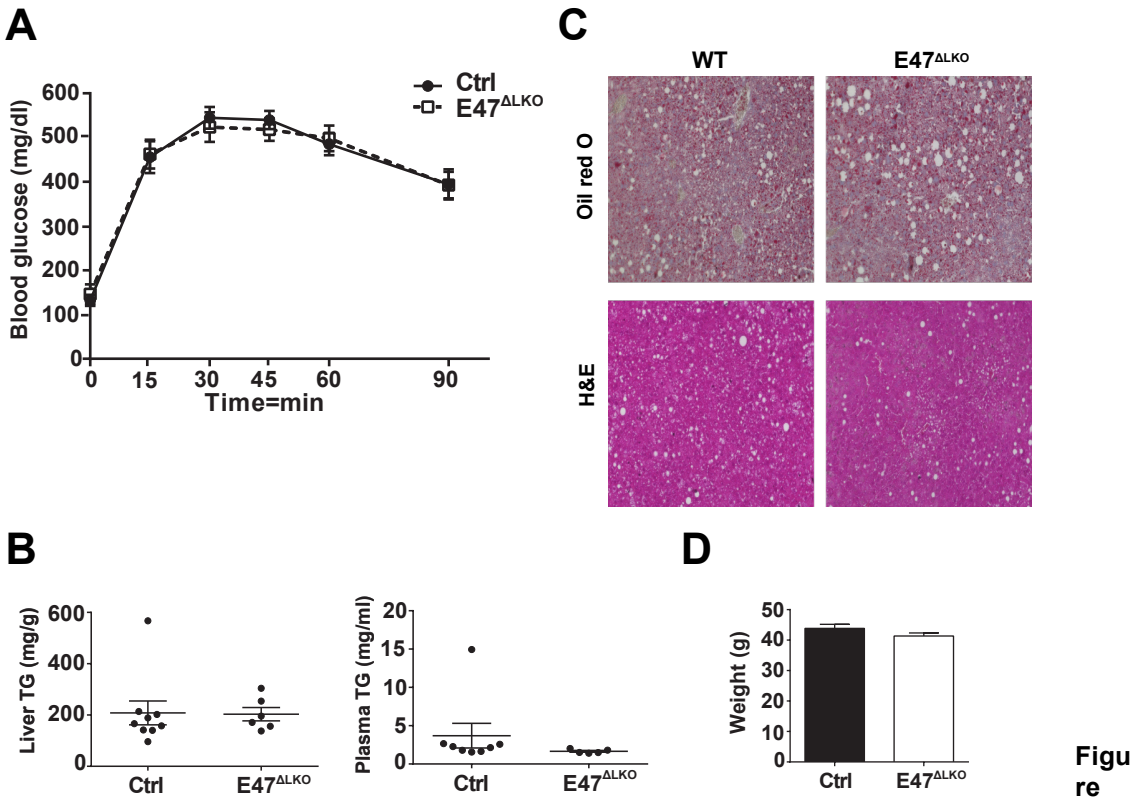

Figure 32: *E47*$^{\Delta LKO}$ mice are not protected from HFD-induced metabolic disturbances.
A: Glucose tolerance test i.p. (GTT) of *E47*$^{\Delta LKO}$ and control mice after 12 weeks of high fat diet (HFD) feeding. Data were analyzed by ANOVA and Bonferroni's multiple comparison tests. Data are shown as mean ± SEM. n=9 (Ctrl) & 6 (*E47*$^{\Delta LKO}$); i.p.= intraperionteal. **B:** Measurement of liver and plasma triglycerides in *E47*$^{\Delta LKO}$ and control mice after 12 weeks of HFD. Data are shown as mean ± SEM, Liver: n=9 (Ctrl) & 6 (*E47*$^{\Delta LKO}$), Plasma: n=8 (Ctrl) & 5 (*E47*$^{\Delta LKO}$). **C:** Liver sections (6µm) were stained with Oil Red O after 12 weeks of HFD; 20x magnification, brightfield microscopy, representative image of n=3. **D:** Body weight of *E47*$^{\Delta LKO}$ and control mice in grams after 12 weeks of HFD. Data are mean ± SEM, n=9 (Ctrl) & 6 (*E47*$^{\Delta LKO}$).

The data from HFD-fed mutant mice suggest that loss of E47 does not affect the development of diet-induced obesity and its metabolic abnormalities. Any observed partial protection from the development of hyperglycemia or hepatic steatosis seen in HFD-fed *E47-/-* mice might be explained by the reduced inflammatory profile originating from the lack of mature immune cells. This was confirmed in *E47*$^{\Delta LKO}$ mice, which fail to show any protection from diet-induced metabolic disturbances since they retain their full immune cell potential.

Taken together, the role E47 plays in the regulation of metabolic genes in hepatocytes seems to be a specific response to high exogenous GC levels and does not reflect a general metabolic function of E47 in the liver.

4.3 Mechanistic insight into chromatin crosstalk between GR and E2A in liver

4.3.1 GR's interactome in liver is affected by loss of E47

The ChIP-Seq data showed that GR and E2A bind and regulate a common set of target genes linked to glucose and lipid metabolism in liver. The genetic loss of *E47* protected from steroid-induced side effects with diminished transcriptional activation of metabolic genes. This observation could potentially be explained by an impaired function of GR itself. In order to test this, nuclear localization of GR in Dex-injected *E47* mutant livers was examined (**Fig. 33**).

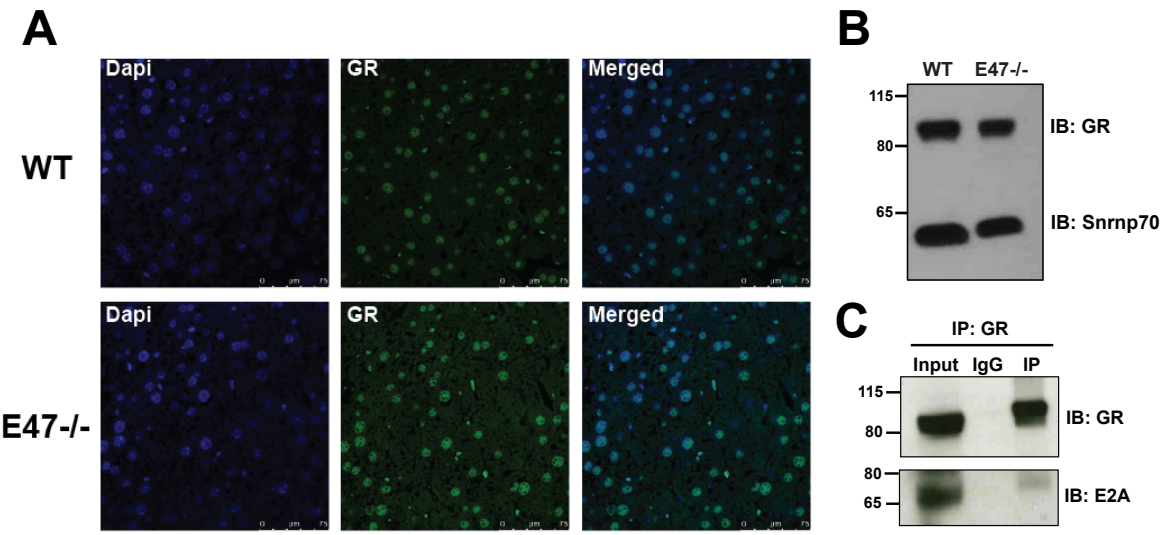

Figure 33: Expression and nuclear localization of GR is unchanged in *E47-/-* livers.
A: Immunofluorescence of GR in Dex-injected *E47*-/- and WT livers. Liver sections of 6µm were stained with α-GR antibody, co-stained with DAPI and visualized using confocal microscopy, scale bar: 75 µm, magnification of 63x. **B:** Western blot of nuclear extracts from Dex-treated WT and E47-/- livers. Immunoblot (IB) for GR and Snrp70. **C:** Co-immunoprecipitation of GR and E2A from liver nuclear extracts of WT mice treated with longterm Dex. 30% input and IP against GR and E2A are shown. Immunoblot (IB) for GR and E2A.

By fluorescent immunostaining and confocal microscopy, nuclear GR was shown to be unaffected by the loss of E47 (**Fig. 33A**). In addition, protein levels of GR in nuclear extracts of Dex-treated wildtype and E47 mutant liver were comparable (**Fig. 33B**). The data confirmed that the phenotype could not be explained by a reduced expression or nuclear import of the GR itself. For this reason, protein-protein interaction studies were performed, to functionally characterize the role of E47 as a crucial part of the GR interactome in liver. Endogenous co-immunoprecipitation of GR from liver nuclear extracts revealed a weak band for E2A on Western blot indicating a putative physical interaction between GR and E2A (**Fig. 33C**). This is supported by two predicted LXXLL motifs in the E2A protein sequence. LXXLL

motifs mediate interaction between nuclear receptors and transcription factors (Savkur and Burris, 2004).

To purify the transcriptional complex assembled by GR in hepatocytes, ChIP coupled to mass spectrometry (ChIP-MS) for GR was performed in Dex-injected *E47*$^{\Delta LKO}$ and control livers. Significantly enriched proteins in IP samples from control and *E47* mutant liver samples were plotted as fold enrichment of GR versus the negative control IgG (**Fig. 34**). In control livers, GR was enriched together with c/EBPs, SRCs, HNF4α, RXR, FoxO1, Mediator subunits MED16 MED23 and MED24, chromatin remodelers and histone modifiers (**Fig. 34A**). c/EBP, HNF4α, RXR and Fox factors are among the footprints identified in the present GR ChIP-Seq data set (**Fig. 11**) and have been published before to co-localize together with GR at hepatic *cis*-regulatory elements (Lim et al., 2015, Grontved et al., 2013, Phuc Le et al., 2005). Interestingly, FoxO1 and the Mediator subunits MED16 and MED23 were not present anymore together with GR in E47 mutant livers (**Fig. 34B**). Peptide counts for the selected proteins shown below are listed in Supplemental Table 9. MED23, MED24 and MED16 are all components of the multisubunit Mediator complex. By facilitating interactions between gene-specific transcription factors and the RNA polymerase II machinery, Mediator enables transcription at target genes (Malik and Roeder, 2005). FoxO1, on the other hand, is part of the superfamily of Forkhead transcription factors and a direct transcriptional regulator of gluconeogenesis (Puigserver et al., 2003).

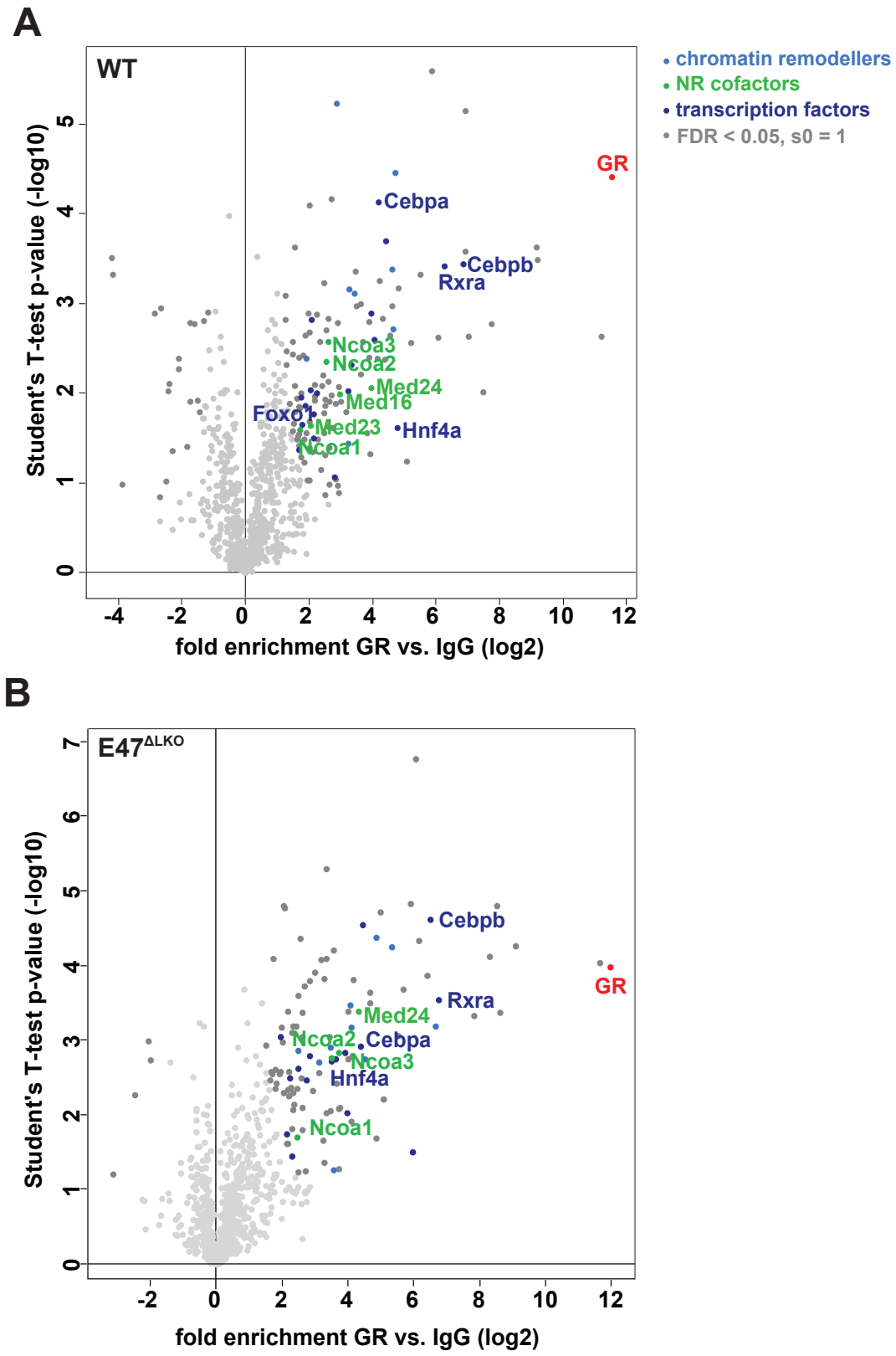

Figure 34: The GR interactome in liver changes upon loss of E47.
A: ChIP-MS was performed for GR in Dex-injected wildtype livers and Dex-injected *E47*$^{\Delta LKO}$ livers (**B**). Volcano plot showing selected significantly enriched proteins in GR IP samples versus IgG. P-values versus the log2 fold enrichment between GR over IgG are plotted. Pale blue: chromatin remodelers (GO Biol. Process); green: NR coregulators; dark blue: sequence specific DNA binding transcription factor activity (GO Mol. Function); dark grey: significant outliers derived by Fisher's exact test (FDR<0.05, s0=1), n=3 per genotype.

4.3.2 E47 is needed for recruitment of GR and coregulators to target genes

A potential molecular mechanism explaining the phenotype might be crosstalk of GR and E47 at certain hepatic loci. Close proximity of both factors would be needed to efficiently recruit and assemble a critical “mass" of transcriptional regulators required for the subsequent activation of gene expression. Loss of E47 in mutant livers therefore results in a reduced number of transcriptional regulators below a certain threshold to ensure sufficient transcriptional activation. In this regard, Mediator and FoxO1 both constitute important regulators of transcription. Of note, the phenotype could not be explained by reduced expression of either Mediator subunits, FoxO1, GR or the nuclear receptors LXRα and LXRβ in *E47* mutant tissue (**Fig. 35)**. The LXR receptors have been implicated before in mediating GC-induced side effects (Patel et al., 2011) (see Chapter 5.3).

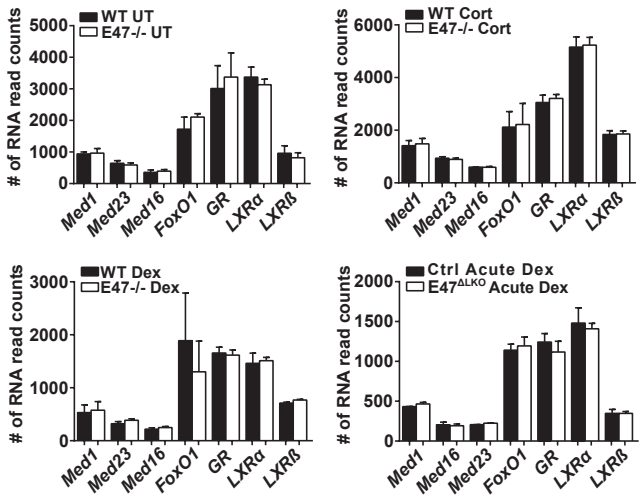

Figure 35: Expression of *GR*, *Med1* and *FoxO1* is unchanged in mutant livers.
Number of normalized read counts for *Med1, Med23, Med16, Foxo1, GR, Lxrα* and *Lxrβ* from RNA-Seq data in untreated (UT), Cort or Dex treated or Dex-injected livers.

Testing this hypothesis, ChIP-qPCR experiments for GR, MED1 and FoxO1 were performed on hepatic *cis*-regulatory elements in wildtype and *E47* mutant livers. MED1 was chosen since it constitutes the core component of the Mediator complex. Promoter and enhancer sites of metabolic genes discussed above were selected. These loci are co-bound by GR and E2A in liver and were shown to have a diminished expression in *E47* mutant livers in response to GCs (**Fig. 21**). Among these were *Apoa4, Dhcr7, Dhcr24, Gpam, Hmgcr, Hmgcs1* or *Pck1.*

For Dex-treated wildtype livers, a robust recruitment of GR to promoters and enhancers of shared target sites was found at all selected loci (**Fig. 36A**). Occupancy of GR was, however,

markedly decreased in *E47* mutant livers. Interestingly, most of the sites also exhibited a reduced binding for MED1 (**Fig. 36B**) and, to some extent, FoxO1 (**Fig. 36C**). These included the same sites as for GR, namely *Apoa4*, *Dhcr7*, *Dhcr24*, *Hmgcs1* and *Pck1*. For the *Acacb* locus, occupancy of MED1 and FoxO1 was not reduced.

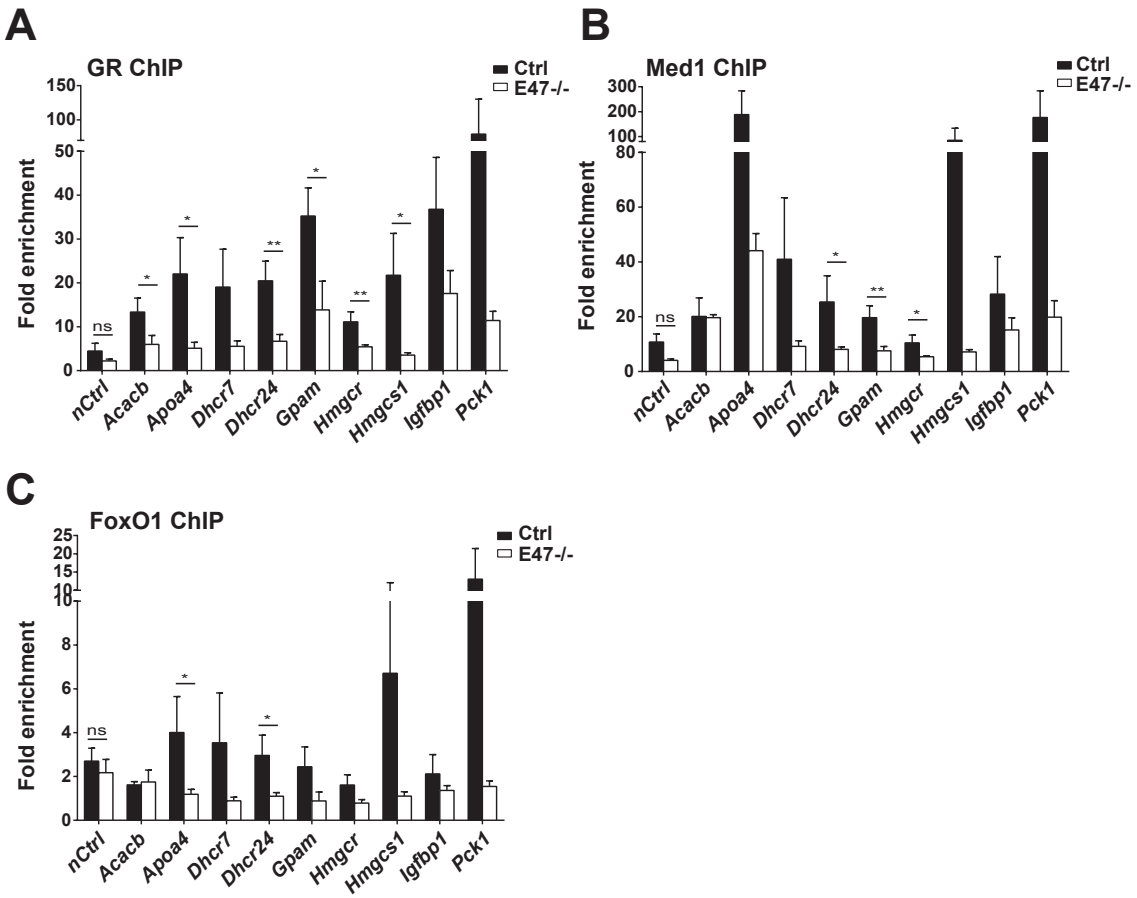

Figure 36: Loss of E47 results in reduced recruitment and binding of GR in Dex-treated livers.
A: ChIP-qPCR in Dex-treated *E47-/-* and control livers shows binding of GR, MED1 **(B)** and FoxO1 **(C)** at metabolic promoters and enhancers. Data are shown as fold enrichment over IgG. A negative control region is displayed (nCtrl) (n=6 per genotype, data are mean ±SEM).

Reduced occupancy of GR and coregulators such as FoxO1 and Mediator might therefore be the underlying mechanism explaining the phenotypic response of *E47* mutant mice. This is in agreement with the data from the loss of function mouse models (see Chapter 4.2). Diminished activation of metabolic genes in liver, e.g. *Pck1*, *Igfbp1*, *Gpam* and *Dhcr24*, as seen in *E47* mutant mice, would result in a reduced side effect profile upon GC treatment. Since protection from hepatic steatosis and dyslipidemia was examined with Cort treatment, additional ChIP qPCRs for GR and MED1 were performed in Cort-treated wildtype and mutant livers. Concordantly, promoters and enhancers of key genes involved in cholesterol

biosynthesis or fatty acid syntehsis, e.g. *Dhcr7*, *Dhcr24, Acacb* and *Cyp2c39* showed reduced occupancy of GR and MED1 in *E47* mutant livers **(Fig. 37A&B).**

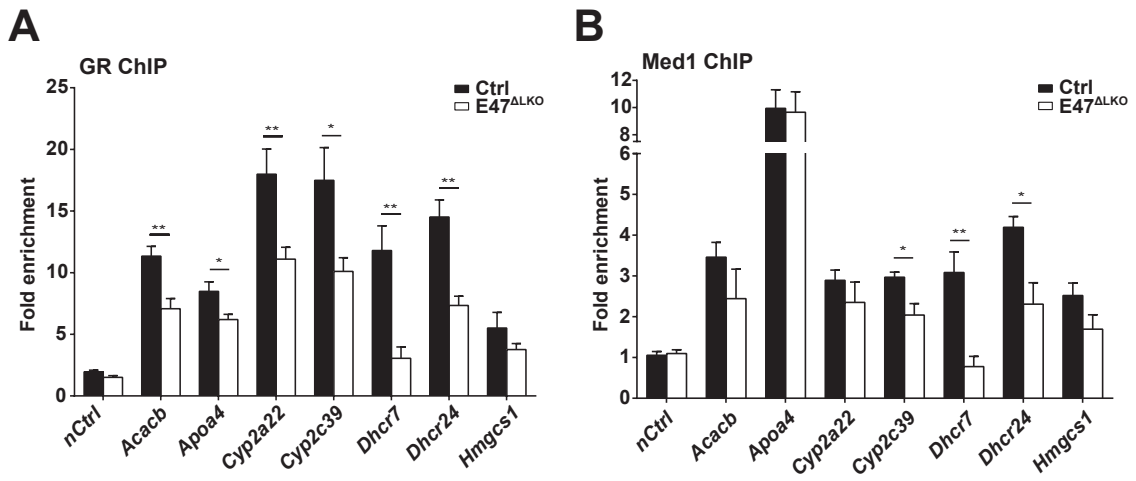

Figure 37: GR and MED1 show reduced occupancy at lipid sites in Cort-treated livers.
A: ChIP-qPCR in Cort-treated *E47*$^{\Delta LKO}$ and control livers shows binding of GR and Med1 **(B)** at metabolic promoters and enhancers. Data are shown as fold enrichment over IgG and was normalized to a negative control region (n=6 per genotype, data are mean ±SEM).

These data strongly suggest that at a subset of hepatic cis-regulatory elements the presence of E47 is required for sufficient binding of GR itself. By allowing occupancy of GR, FoxO1 and Mediator can be recruited and transcriptional activation of key metabolic genes is facilitated in response to GCs. Loss of E47, on the other hand, would markedly reduce binding of GR and its coregulators. Protection from GC-induced side effects, e.g. hyperglycemia, hepatic steatosis and dyslipidemia, might therefore stem from the attenuated expression of these metabolic target genes.

4.4 Identifying features of GR regulation conserved in humans

4.4.1 E47 and GR cooperate in the transcriptional activation of human GR targets

To test whether the findings from the mouse model might be therapeutically relevant for human disease, a set of 162 human *cis*-regulatory elements were screened in a high throughput luciferase reporter approach. In this cell-based system, CV-1 cells were transiently transfected with human promoter and enhancer reporter constructs predicted to be regulated by GR. CV-1 cells are derived from kidney fibroblast and are non-steroidogenic. This cell line was chosen since it is suitable for transfection experiments involving GCs and to decipher the molecular action of GR. CV-1 cells were cultured in medium supplemented

with vehicle, Cortisol or Dexamethasone. Luciferase activity of reporters was measured and normalized to β-Gal activity for transfection efficiency. Fold change over empty vector with vehicle was calculated and reporter sequences were then classified into those responding with either activation or repression (or not responding) upon addition of GCs (**Fig. 38).** Supplemental table 10a&b lists clustered reporter sequences based on fold changes. Overrepresented motifs in up- and downregulated reporters were identified using a binding site prediction tool (OTFBS). Of the 162 human *cis*-regulatory elements tested, around 40 were downregulated, while more than 80 were induced at least twofold by GCs (**Fig. 38A**). In both upregulated and downregulated reporter elements, classical GRE consensus sequences were enriched (**Fig. 38B**).

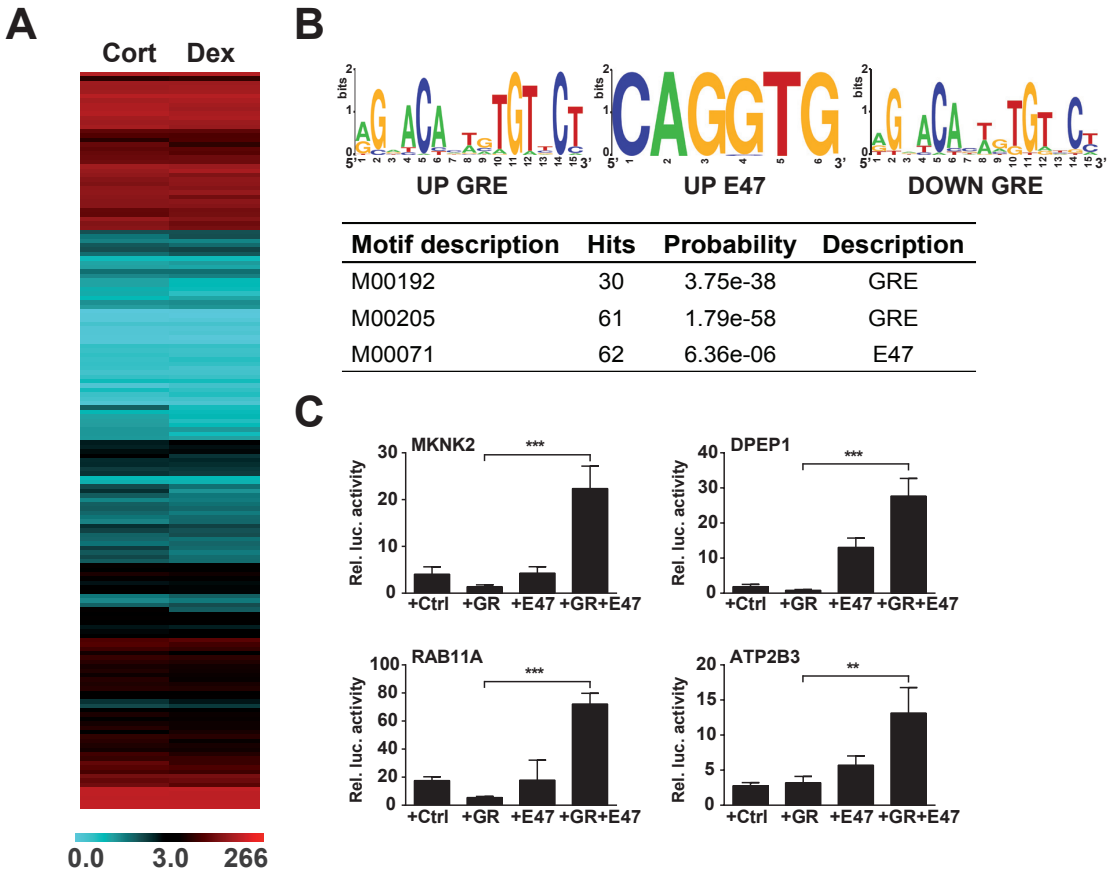

Motif description	Hits	Probability	Description
M00192	30	3.75e-38	GRE
M00205	61	1.79e-58	GRE
M00071	62	6.36e-06	E47

Figure 38: The E47 motif is enriched near GREs in human cis-regulatory elements.
A: Relative luciferase activity of 162 human reporter constructs regulated by GR was clustered into up- and downregulated reporters. Data from biological triplicates were normalized for transfection efficiency and to empty vector with vehicle. Reporters activated by GR plus ligand (Cort(isol) or Dex(amethasone)) appear red, repressed reporters appear blue. **B:** Motif analyses on corresponding DNA sequences show identical GRE consensus motifs in both activated and repressed reporters (UP & DOWN GREs). Upregulated reporter sequences are enriched for E47 consensus binding sites (UP E47). **C:** Luciferase assays of selected reporters from the screen were co-transfected with human GR and E47 expression vectors in CV-1 cells treated with Dex.

Interestingly, the E-Box motif (CAGGTG) for E47 was significantly enriched near GREs in positive sequences (**Fig. 38B**). The E47 motif was specifically associated with transcriptional

activation by GR since it occurred in 47% of all GR-upregulated reporter elements. The presence of E47 near GREs in human *cis*-regulatory sequences suggests a possible conservation of E47 function in human GC responses.

In order to validate the motif prediction, expression vectors for human GR and human E47 were either transfected alone or together with selected reporter elements from the initial screen. In the presence of Dex, reporters only showed a robust induction of luciferase activity when both transcription factors were present (**Fig. 38C**). Next, the predicted E-Box motifs in selected reporters were mutated to TTGGCC. Activation of luciferase activity in the presence of both factors was now abolished demonstrating that GR requires binding of E47 to regulate the activation of human targets (**Fig. 39A**). Furthermore, an expression vector for the human E47 inhibitor ID protein ID3 was transfected together with GR and E47. By binding to E47, ID3 inhibits E47 from binding and activating its E-Box. As shown for the *DPEP1* promoter, co-transfection of ID3 abrogated any induction of luciferase activity demonstrating that GR and E47 regulate human targets in a cooperative manner (**Fig. 39B**).

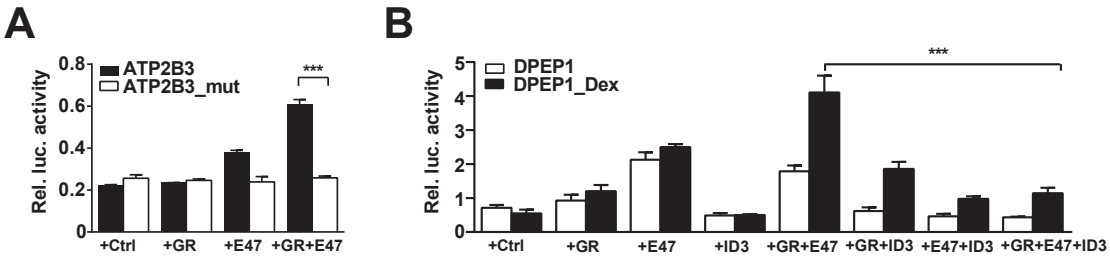

Figure 39: Binding of E47 is needed for the transcriptional activation of human targets.
A: The two predicted E-Boxes in the *ATP2B3* regulatory element were mutated and a luciferase acitivty was measured. Data are shown as mean ± SEM, (***) P<0.001, Student's t-test, n=3 replicates. **B:** The *DPEP1* reporter was co-transfected with expression vectors for human GR, human E47 and human ID3 in CV-1 cells. Cells were treated with vehicle or Dex and luciferase activity of transfected constructs was measured and normalized. Data are shown as mean ± SEM, (***) P<0.001, Student's t-test, n=3 replicates; rel. luc. activity = relative luciferase activity.

Taken together, the data from luciferase reporters suggests a conserved function for E47 in the transcriptional activation of certain human targets by GCs. The cooperative regulation of human targets could be of significance for translating these findings into the clinic.

5. Discussion

5.1 The GR-E47 axis controls distinct aspects of hepatic metabolism

This thesis identified the transcription factor E47 as a novel partner for GR in hepatocytes. E47 specifically cooperates in the transcriptional activation of metabolic gene networks in response to GCs. The loss of E47 in mutant mice therefore results in a protection from GC-induced hyperglycemia, hyperlipidemia and hepatic steatosis. To determine the molecular basis for the observed phenotypic changes, RNA-Seq was performed in *E47* mutant livers in response to GCs. Here, distinct gene networks were differentially expressed upon loss of E47 (**Fig. 21**). The majority of genes affected in response to Dex or Cort show reduced expression, which is in line with E47's predominant role as a transcriptional activator. Deregulated genes can be clustered into pathways relating to lipid, triglyceride and cholesterol metabolism. Elevated circulating GC levels upon steroid treatment are known to cause lipid accumulation in the liver and whole-body dyslipidemia (Vegiopoulos and Herzig, 2007). GR-controlled gluconeogenesis and resulting hyperglycemia has a well-established link to the upregulation of gluconeogenic genes, such as *Pck1* and *G6pc*. However, the exact molecular mechanism of how GR controls other aspects of hepatic metabolism, e.g. lipid metabolism, remains to be clarified. In this regard, the collaborative interaction with partnering transcription factors and coregulators adds an additional layer of regulation to GR's function in hepatic metabolism (de Guia and Herzig, 2015). Accumulating genomic and proteomic analyses have increased the pool of potential partners necessary for GR to regulate different gene networks in the liver (Phuc Le et al., 2005, Wang et al., 2012). In the ChIP-MS data presented here, several Mediator subunits, FoxO1, SRCs, c/EBPs, RXR and HNF4α were enriched together with GR in Dex-treated wildtype livers. In *E47* mutant livers, the Mediator subunits MED16 and MED23 as well as FoxO1 were not present anymore (**Fig. 34B**). Furthermore, ChIP qPCR in GC-treated livers revealed a diminished recruitment and binding of GR itself, MED1 and FoxO1 to enhancers and promoters induced by GCs upon loss of E47 (**Fig 36&37**).

Mediator is a multisubunit complex comprising a head, middle and tail module. Most transcription factors are unable to directly interact with RNA polymerase II (Pol II). The Mediator complex fills this gap by acting as a bridging factor. By binding directly to the RNA Pol II, it integrates and relays signals from enhancer-bound transcription factors to the transcriptional start site (Kornberg, 2005, Youn et al., 2016). Here, the basal transcription machinery is assembled and consists of the RNA Pol II and general transcription factors, e.g. TFIIB, TFIID, TDIIE, TDIIF, and TFIIH, important for the initiation of transcription (Youn et al.,

2016).

MED1 constitutes a core component and was shown to directly interact with multiple transcription factors in liver including GR, PGC1α and nuclear receptors PPARα and PPARγ and have an essential function in the metabolic signaling of these factors (Jia et al., 2014). By binding directly to GR via both LXXLL motifs, MED1 has an established link to GR-mediated transcription of genes in a ligand-dependent manner. Using a *Med1-/-* mouse embryonic fibroblast line, the authors show that MED1 is required for enhancing GR-mediated gene transcription. Consequently, mutations in the LXXLL motif greatly reduce gene transcription by GR (Chen and Roeder, 2007). Interestingly, the requirement of MED1 for initiation of transcription depends on different GR targets (Chen and Roeder, 2007). This selective gene function was also reported when levels of *Med1* and *Med14*, another subunit of the tail module, were reduced via small interfering RNAs in an osteosarcoma cell line. Depending on the gene in question, either MED1 or MED14 are differentially required by GR to activate gene transcription (Chen et al., 2006). The above-mentioned *in vitro* studies demonstrate that MED1 holds an important co-regulatory role in gene expression mediated by GR and is used in a gene-specific manner. Liver-specific *Med1* mutant mice are protected from the development of Dex-induced hepatic steatosis (Jia et al., 2009). Dex-treatment would normally repress enzymes involved in fatty acid oxidation. However, in liver-specific *Med1* mutant mice, deficiency of MED1 results in normalized levels of these genes and a diminished occurrence of lipid accumulation in the liver (Jia et al., 2009).

Besides MED1, knockout models for other distinct Mediator subunits have been described and revealed links to glucose and lipid metabolism. MED23 is a subunit of the tail module and was initially identified in the ChIP-MS data set as one of the factors lost in *E47* mutant livers. In liver-specific *Med23* knockout mice, glucose tolerance and the lipid profile is significantly improved. When challenged with a HFD diet, knockout mice are protected from diet-induced obesity. Moreover, ablation of *Med23* using adenovirus-expressing shRNA significantly improves metabolic parameters such as glucose tolerance and plasma cholesterol and triglyceride levels in db/db mice (Chu et al., 2014). In *Med23*-deficient primary hepatocytes, this protective effect is mediated via a reduced recruitment of RNA Pol II to target genes of FoxO1, which subsequently attenuates their expression (Chu et al., 2014). Thus, by affecting the transcriptional activity of FoxO1, loss of MED23 results in an improved glucose tolerance and lipid profile (Chu et al., 2014).

With its crucial role in facilitating gene transcription, many of the distinct Mediator subunits have unveiled specificity for different transcription factors and pathways (Youn et al., 2016)

(**Fig. 40**). Modulation of individual subunits would therefore offer a mechanism for a tissue- and gene selective regulation.

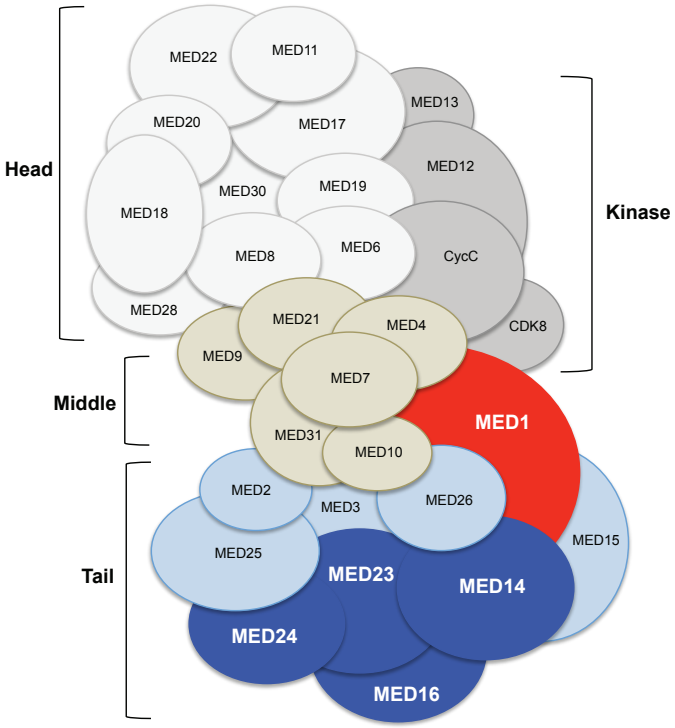

Figure 40: Graphical representation of the different Mediator subunits.
The Mediator complex consists of a head module, a middle module, a tail module and a transiently associated kinase module. Mediator subunits discussed here are highlighted. MED1 (in red) represents a core subunit likely situated between the middle and tail modules. Subunits highlighted in blue (MED14, MED16, MED23, MED24) are part of the tail module. The relative location of the subunits within the complex are based on previous publications but have yet to be precisely mapped. Picture modified from (Malik and Roeder, 2010)

The ChIP-MS data revealed FoxO1 to be among the transcription factors enriched with GR but lost in *E47* mutant livers (**Fig. 34**). The Fox consensus motif was also identified in both the GR and E2A cistromes presented here (**Fig. 11**) and is found among the footprints of transcription factors enriched with GREs (Lim et al., 2015, Grontved et al., 2013, Phuc Le et al., 2005). Although the previous datasets have shown occupancy of FoxA factors, it is entirely likely that FoxO1 recognizes this motif. A link between GR and FoxO1 has long been established in the upregulation of the *Pck1* gene. Besides the GRE itself, the *Pck1* promoter harbors a collection of binding sites for other transcription factors, among them FoxO1 (Vegiopoulos and Herzig, 2007). Together with c/EBP, HNF4α, RXR and FoxA2, FoxO1 exerts important accessory function in facilitating full induction of the *Pck1* by enabling GR recruitment to the site (Hall et al., 2000, Chakravarty et al., 2005).

FoxO1 is part of the superfamily of Forkhead transcription factors, which is implicated in a wide range of developmental processes and human diseases (Hannenhalli and Kaestner, 2009). The FoxO factors FoxO1, FoxO3 and FoxO4 all play important roles in the

homeostasis of glucose signaling. Liver-specific deletion of *FoxO1/3/4* collectively results in lower blood glucose levels and improved glucose and pyruvate tolerance (Xiong et al., 2013). FoxO1 is known as a key regulator of hepatic gluconeogenesis in response to insulin signaling (Puigserver et al., 2003, Gross et al., 2008). In the fasted state, FoxO1 promotes hepatic gluconeogenesis by up-regulating the expression of, the two key genes *Pck1* and *G6pc*. Upon feeding, insulin is secreted from the pancreas and FoxO1 is phosphorylated. Phospohrylated FoxO1, in turn, is excluded from the nucleus and therefore unable to activate hepatic gluconeogenic gene expression (Puigserver et al., 2003). In situations of metabolic dysfunction, e.g. in diabetic patients, the significance of FoxO1 action becomes evident. Here, hepatic gluconeogenesis is inappropriately activated which is thought to be promoted by FoxO1 resulting in hyperglycemia and glucose intolerance (Gross et al., 2008). Liver-specific deletion of FoxO1 results in an overall improvement of glucose metabolism. At birth, *FoxO1* mutant mice show a drastic reduction of glucose levels, which is maintained upon prolonged fasting in adult life (Matsumoto et al., 2007). In fasted *FoxO1* mutant livers, gluconeogenic gene expression is severely diminished (Matsumoto et al., 2007). This introduces the loss of FoxO1 or inhibition of FoxO1 in liver, respectively, as an appealing approach to undertake new therapeutic routes in the treatment of hyperglycemia and progression to diabetes (Matsumoto et al., 2007).

The data from liver-specific *FoxO1* mutant mice is in agreement with data from *E47* mutant livers. Here, reduced binding of FoxO1 due to the loss of E47 results in attenuated upregulation of gluconeogenic GR target genes upon GC-treatment. E47 has previously been identified in a common pathway with FoxO1, albeit upstream of FoxO1 signaling since E2A binding sites in enhancer and promoter regions of the *FoxO1* locus were identified (Welinder et al., 2011). These studies were performed in B cells, since the majority of what is known about E47 concentrates on its involvement in immune cell differentiation and maturation. Nevertheless, it coincides with the data presented here and suggests a potential role for E47 in FoxO1 function in liver. Interestingly, microarray analyses in a lymphoma cell line overexpressing E47 have also presented a possible role for E47 in the regulation of genes in lipid metabolism (Schwartz et al., 2006). Here, the expression of a subset of genes involved in lipid biosynthesis is induced by targeted expression of E47 (Schwartz et al., 2006).

Taken together, the interplay of GR, FoxO1 and E47 is likely responsible for the efficient activation of gluconeogenic and lipid gene programs in the liver. In the present model, GR requires E47 at a shared subset of *cis*-regulatory elements overlapping with FoxO1. Subsequent recruitment of the Mediator complex is needed for the transcriptional activation

of metabolic genes. In the absence of E47, occupancy of GR and FoxO1 at metabolic genes is reduced and loading of Mediator and the basal transcriptional machinery is also impaired. In response to GC treatment, *E47* mutant mice would therefore be protected from hepatic steatosis and hyperglycemia due to diminished mRNA expression of these co-bound metabolic genes (**Fig. 41**).

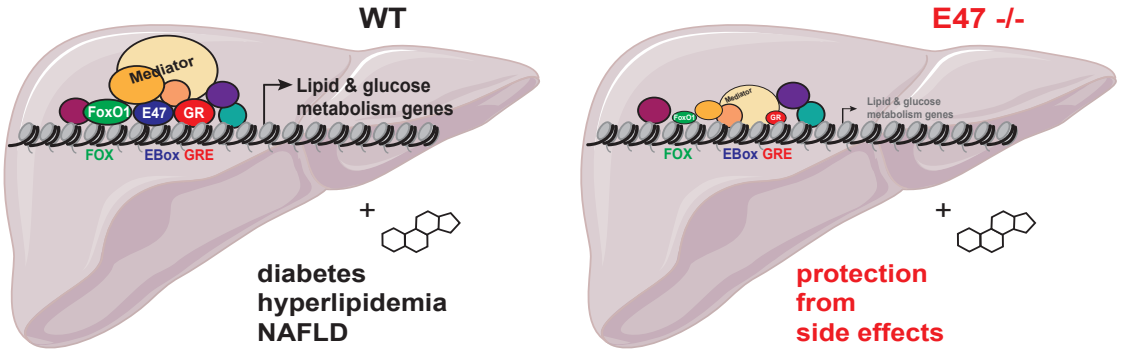

Figure 41: Modulation of hepatic GR function by E47.
In wildtype livers, E47 binds together with GR at a subset of *cis*-regulatory elements, which are overlapping with FoxO1. As a response to GCs, the Mediator complex is recruited resulting in the transcriptional activation of certain metabolic genes. In *E47* mutant livers, absence of E47 results in reduced binding of GR and FoxO1 causing a reduction the recruitment of Mediator. Subsequently, mRNA expression levels of these metabolic genes are diminished. *E47-/-* mice are therefore protected from the development of GC-induced hyperglycemia and hepatic steatosis. Liver cartoon was taken from Servier Medical Art, licensed under a Creative Common Attribution 3.0 Generic License, <http://smart.servier.com/>.

5.2 E47 and the specification of lineage

The present thesis identified the E47 as a potentiating transcription factor for GR to activate metabolic gene programs in liver. Moreover, it was demonstrated that E47 needs to be present at distinct *cis*-regulatory sites to ensure GR and its co-regulators can efficiently access and bind in the genome. This argues for E47 to have a lineage-specific function and to determine chromatin accessibility for other factors.

Genome-wide location analyses have unveiled that in most cases only a fraction of all potential binding sites for a given transcription factor in the genome are actually bound; the majority of binding sites remain unoccupied due to inaccessible DNA (Zaret and Carroll, 2011). GR action is highly cell-type and locus-specific and GR relies on open and accessible chromatin in order to bind to its target genes (Grontved et al., 2013, Biddie et al., 2011, John et al., 2011). Comparing GR binding sites between different mouse cells shows that only a small proportion of GR-bound sites in liver can be identified in other cistromes and the

majority was indeed liver-specific (Grontved et al., 2013) (**Fig. 6**). In this context, the existence of lineage-determining transcription factors have long been known. Lineage-determining factors change chromatin accessibility and “prime” the chromatin landscape for other signal-dependent factors to be directed to target sites in a tissue-specific manner (Zhang and Glass, 2013, Drouin, 2014). The pivotal role of these lineage factors lies in the “opening” of closed chromatin by binding first and recruiting chromatin-remodeling enzymes, e.g. histone acetylases, to establish a cell-type specific enhancer landscape (Greulich et al., 2016). Once the cell-type-specific enhancer landscape is established, signal-dependent transcription factors such as GR and their associated partners can access their binding sites. Among the parameters to define where in the genome a transcription factor will likely bind are histone modifications, which render chromatin accessible. One such histone mark is H3K4 methylation, either monomethylation at enhancers or trimethylated at promoters (Heintzman et al., 2007). In addition, the presence of certain histone-acetylases, such as p300, at enhancers indicates whether this specific binding site will likely be bound by its transcription factor (Zaret and Carroll, 2011). Several lineage-determining factors have previously been identified. Among them are HNF4α, HNF6, c/EBP and the FoxA proteins, respectively. All factors were shown to be required for the development of the hepatocyte lineage (Park et al., 1993, Hall et al., 1995, Wang et al., 1996, Hall et al., 2000). In addition, their footprints have been found in different GR ChIP-Seq data sets (Lim et al., 2015, Grontved et al., 2013, Phuc Le et al., 2005)(**Fig.11**). FoxA1 is known to function as a lineage-determining factor for members of the nuclear hormone receptor family. Binding of the estrogen receptor (ER) and the androgen receptor (AR), respectively, correlates with occupancy of FoxA1 in different cancer cell lines (Hurtado et al., 2011, Sahu et al., 2011). ChIP-Seq for ER identified the presence of FoxA1 sites at the majority of ER binding sites in the genome, demonstrating that FoxA1 regulates chromatin accessibility for subsequent recruitment of ER (Carroll et al., 2005).

The E proteins E47 and E12 have a well-established function in the commitment to the lymphocyte cell lineage, specifically by favoring specification of B lymphocyte commitment and differentiation over the myeloid lineage (de Pooter and Kee, 2010). Indeed, E47 was reported to exert lineage-determining functions in the maturation of B cells (Heinz et al., 2010). PU.1 together with c/EBP is essential for the development and “priming” of the myeloid lineage (Heinz et al., 2010, Iwasaki et al., 2005) (Heinz et al., 2010, Jin et al., 2011). Moreover, binding of PU.1 depends on the presence of other lineage-determining factors and occurs in the vicinity of these motifs (Heinz et al., 2010). In the case of B cell development, the presence of E47, EBF1, Pax5 and Oct2 was shown to be crucial in defining whether PU.1 can bind B cell-specific genomic sites (Heinz et al., 2010). Interestingly, in pro-B cells,

E2A binds together with EBF and FoxO1 in a synchronized manner to a wide range of different *cis*-regulatory sites (Lin et al., 2010). In addition, ChIP-Seq for FoxO1 in pro-B cells shows enrichment for composite E2A and FoxO1 sites and patterns of H3K4 monomethylation (marking active enhancers), on the other hand, are heavily correlated with occupancy of E2A (Lin et al., 2010).

E2A was also shown to interact and recruit histone acetylases, such as CBP, p300 and PCAF, in pre B-cells via its two N-terminal activation domains AD1 and AD2 (Bradney et al., 2003). As ubiquitously expressed co-activators, CBP and its paralog p300 hold crucial roles in regulating gene transcription. They are recruited to enhancers and promoters through interactions with DNA-bound transcription factors and the basal transcription machinery and are able to catalyze acetylation of histones and facilitate gene transcription (Kalkhoven, 2004). E47 and E12 bind directly to CBP/p300 through specific acetylation sites in AD1, which first enables recruitment followed by transcriptional activation (Hyndman et al., 2012b). Moreover, the histone acetyltransferase activity of CBP and p300 is significantly increased by direct association with specific residues in the transcriptional domain of E47/E12 (Hyndman et al., 2012a). This raises the possibility that E47 makes direct contact with enzymes involved in chromatin modification and underlines the factor's decisive role in determining binding of associated factors.

Taken together, E47's previously described role as a lineage-determining factor in B cell development can likely be conveyed to its interaction with GR at specific target gene sites in liver. In this model, GR requires E47 for recruitment of CBP/p300 and its histone acetyltransferase function to define points of chromatin access. Chromatin accessibility would then enable GR and FoxO1 to occupy its sites in the DNA and, in a cooperative manner, recruit the Mediator complex and activate gene transcription.

5.3 Anatgonism of E47: a new therapeutic avenue?

Despite the 70 years since the discovery of GCs, novel aspects of GC-mediated gene regulation are continuously being uncovered (De Bosscher and Haegeman, 2009). Due to their powerful potential to dissolve inflammatory processes, GCs have become one of the most used drugs in the clinic nowadays. Unfortunately, so has the need to treat the severe side effects accompanying their long-term use. These frequently include the development of hyperglycemia, dyslipidemia, obesity, muscle wasting and osteoporosis (Schacke et al., 2002). In the past decade, the therapeutic benefits of GC treatment have been attributed to the repression of inflammatory genes. On the other hand, activation of genes was made

accountable for the development of many of the side effects, specifically concerning the metabolism (Sundahl et al., 2015). For this reason, separating the two transcriptional mechanisms of action had taken center stage to improve the overall therapeutic ratio of synthetic GCs.

One promising approach had previously been the development of compounds which would act as ligands or modulators for GR and largely favor the repressive function whilst exhibiting a reduced activating potential (Sundahl et al., 2015). Multiple of these compounds, frequently designated as dissociated compounds or selective GR agonists and modulators (SEGRAMs), have been reported in the past years (Schacke et al., 2007, De Bosscher, 2010). Among the first generation of published dissociated GR ligands with a steroidal backbone was RU24858. RU24858 exhibited promising dissociation *in vitro* in a rat asthma model with only a minor residual activating activity (Belvisi et al., 2001). However, it quickly became clear that *in vivo* RU24858 would still induce typical steroid side effects, e.g. induction of osteoporosis (Belvisi et al., 2001). The lack of success of selective steroidal GR agonists *in vivo* has led to a refocus towards non-steroidal GR modulators. This would largely bypass the possibility that derivatives are metabolized in a way that they behave similar to GCs (De Bosscher, 2010, Schacke et al., 2007). AL-438, as a modified progestin, was able to retain its ability to efficiently inhibit NFκB activated genes, e.g. Il6, in a rat asthma model *in vivo* (Coghlan et al., 2003). The compound exhibited a diminished induction of blood glucose, which is associated with activation of metabolic genes (Coghlan et al., 2003). Interestingly, AL-438 seemed to affect the association of GR with its different co-regulators. AL-438-activated GR was still able to interact with SRC2 (GRIP1) previously implicated in the suppression of inflammatory genes. However, association with PGC-1, a co-activator important for hepatic glucose metabolism, was attenuated (De Bosscher and Haegeman, 2009). It is still unknown whether this specific cofactor association is selective and stringent enough to predict the side effect outcome (De Bosscher and Haegeman, 2009). In addition, more studies are needed to conclude whether the improved side-effect profile of AL-438 is present in other inflammatory models.

It quickly became clear that the traditional model of a dissociated GR effect on different tissues, whether desired or detrimental, could not be attributed to the exclusive transcriptional outcome of either activation or repression. In this regard, the activation of many anti-inflammatory genes by GR, e.g. *IκBα, Gilz, Dusp1* or *Dusp14*, constitutes an integral part of the receptor's anti-inflammatory function (Beck et al., 2009a, De Bosscher and Haegeman, 2009). By eliminating GR-driven gene activation, this important component of the therapeutic action of GR in immune cells would be lost. Furthermore, a large number

of side effects do indeed result from GR-mediated activation of genes, e.g. hyperglycemia. However, many also arise due to GR's repressive action, e.g. suppression of the HPA axis, and are often the results of a combination of both mechanisms, e.g. osteoporosis (Schacke et al., 2002). The fact that side effects are subjected to more than one mechanism underlines, once more, the complexity of pathways regulated by GR in different tissues. In the past, a clear separation of gene repression versus activation to reduce side effects has proven to be less successful. However, the selective modulation of GR action is still believed to provide an entry point into developing safer GC treatment (Sundahl et al., 2015). By focusing on cell-type specific factors defining the transcriptional complex at target sites, the "context-dependent" regulation of genes by GR needs to be considered when designing safer GC ligands (Beck et al., 2009a).

A more tissue-selective modulation of GR signaling was suggested by combining administration of a steroid together with a compound, which is not directly targeting GR. This would alleviate a portion of GR-induced side effects without affecting its anti-inflammatory potential (Patel et al., 2017). The liver X receptors (LXRα and LXRβ) are also members of the nuclear hormone receptor family. They are activated by cholesterol metabolites and exert important functions in cholesterol metabolism and fatty acid synthesis (Patel et al., 2014, Patel et al., 2017). Importantly, GR and LXR are both involved in gluconeogenesis and the suppression of inflammation and share a common set of genes (Patel et al., 2017). Patel et al. had previously shown that *Lxrβ-/-* mice are protected from the development of commonly seen metabolic side effects, e.g. hyperglycemia, hyperinsulinemia and hepatic steatosis when treated with Dex (Patel et al., 2011). Importantly, *Lxrβ -/-* mice remain sensitive to the anti-inflammatory action of Dex. Prominent suppression of pro-inflammatory genes in LPS-activated macrophages is retained arguing for an LXR-independent response to GCs in immune cells (Patel et al., 2011). Mechanistically, the authors demonstrated that LXR is required for efficient recruitment of Dex-activated GR to the *Pck1* promoter. The *Pck1* promoter entails binding sites for transcription factors needed to facilitate full gene induction including FoxO1 and PGC1α (Chakravarty et al., 2005). In *Lxrα/β-/-* mice, prominent downregulation of *Pck1* expression in liver is accompanied by equally diminished up-regulation of *Foxo1* and *Pgc1α* (Patel et al., 2011).

On the basis of the *Lxrβ null* mice, Patel et al. speculated if the protective effect could be exploited therapeutically by inhibiting LXR exogenously (Patel et al., 2017). In this context, GSK2033 was introduced as a LXR antagonist. Treatment with GSK2033, a pan LXR antagonist, shows suppression of gluconeogenic genes in mouse livers when administered in combination with Dex. In accordance with data from *Lxrβ -/-* mice, co-administration of

GSK2033 with Dex results in a diminished recruitment of GR to the *Pck1* promoter. Additionally, known accessory factors MED1, c/EBPβ and RNA Pol II also fail to efficiently bind to their respective sites in the *Pck1* locus (Patel et al., 2017). More importantly, antagonism with GSK2033 is specific to LXRβ and has no effect on the expression of anti-inflammatory genes in LPS-treated macrophages, therefore preserving the immunosuppressive effect of GC-treatment (Patel et al., 2017).

Antagonism of LXRß demonstrates that dissociating the activation of gluconeogenic genes and repression of inflammatory genes by GR is feasible. Separation occurs in a tissue- and target gene-specific manner and exemplifies once again the requirement to view gene regulation by GR in its cell-type specific context. Interestingly, the protection from GC-induced side effects in *Lxrβ -/-* mice mirrors the results from GC-treated *E47-/-* and *E47*$^{\Delta LKO}$ mice. Similarly to *LXR* mutant mice, GR action in immune cells is also not affected by the loss of E47. Anti-inflammatory genes, e.g. *Il6* and *Ccl2*, are effectively repressed in macrophages treated with Dex (**Fig. 24**). Both the GR and the E2A cistrome harbor the nuclear receptor DR1 motif, which constitutes the binding site for the retinoid X receptor, RXR. RXR was co-purified with GR in the present ChIP-MS data set from wildtype livers (**Fig. 31**) and is known to serve as a heterodimer partner for LXR. In addition, expression of both *Lxrα* and *Lxrβ* mRNA is not changed in *E47* mutant livers (**Fig. 35**). By measures of affecting and essentially destabilizing the transcriptional complex assembled by GR at target genes, loss of E47 or LXRβ might therefore exert its beneficial effects via a comparable mechanism. GR, E47 and LXR might act within a shared transcriptional complex and overlap in the regulation of metabolic target genes such as *Pck1* (**Fig. 42**).

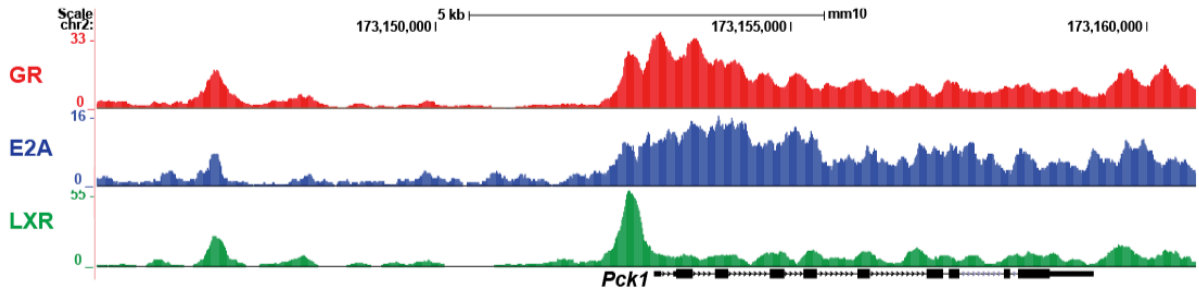

Figure 42: GR, E2A and LXR share binding sites in liver.
ChIP-Seq tracks showing the overlapping binding of GR, E2A and LXR at the *Pck1* locus in mouse liver. ChIP-Seq for LXR was performed in female mouse livers treated with the LXR agonist T0901317 (Boergesen et al., 2012). Data was obtained from NCBI GEO (accession number: GSE3526).

Analogous to using the LXR antagonist GSK2033 to selectively minimize GC-induced side effect profile, antagonizing E47 function could be a potential therapeutic approach. Interestingly, data from the human luciferase screen suggests a conserved function for E47 in the transcriptional activation of certain human targets by GCs. Here, the ID proteins come into focus. By heterodimerization, E proteins are prevented from binding DNA since ID proteins lack a basic region. This way, ID proteins serve as endogenous inhibitors and impact gene regulation (Massari and Murre, 2000, Benezra et al., 1990, Kee, 2009). Modulation of dosage and activity of E2A via ID proteins, specifically ID2 and ID3, is important in determining B- and T-cell lineages (Lazorchak et al., 2005, Engel and Murre, 2001, Murre, 2005). Moreover, knockout mouse models of some ID proteins results in an aberrant lipid and glucose metabolism (Wang and Baker, 2015). In this regard, preliminary data has shown that ID3 can be selectively overexpressed in liver via the tail vein using an adeno-associated virus vector system. Upon long-term Dex treatment, ID3-injected mice revealed a tendency towards lower blood glucose in a glucose tolerance test compared to control-injected mice. Here, the liver-specific inhibition of E47 using a virus system serves as a possibility of how activity of E47 could potentially be targeted and modulated exogenously.

As a factor required for activation of lipid and glucose by GR in hepatocytes, *E47* mutant mice are protected from GC-induced hyperglycemia and hepatic steatosis. Importantly, loss of E47 does not affect GR-mediated repression of immunogenic target genes. In this way, targeting E47 could potentially provide a new approach to tissue-specifically ameliorate side effects of long-term GC treatment without interfering with the beneficial anti-inflammatory effects of GCs.

6. Concluding remarks and future perspective

In this thesis, I have identified a novel role for the bHLH factor E47 in hepatic metabolism in response to GCs.

The conundrum how the action of a single receptor can lead to transcriptional activation versus repression of genes depending on the cell type is still unknown. With the wealth of genomic data on hand, it has become clear that gene regulation by GR is greatly influenced by a myriad of interacting transcription factors and coregulators that affect gene regulation. GR binding across the genome is highly cell-type specific. Using genomics and proteomics, I demonstrated that E47 is needed for GR and collaborating factors such as Mediator and FoxO1 to occupy its binding sites in hepatic enhancers and promoters. Consequently, loss of E47 protects mice from the development of GC-induced hyperglycemia, hepatic steatosis and dyslipidemia. As a lineage-determining factor for GR in liver, E47 facilitates chromatin access for GR and collaborating transcription factors at a subset of genes thereby shaping distinct hepatocyte and locus-specific GC responses.

GCs are highly valued in the clinic for their immunosuppressive properties but their use is restricted by side effects, which are often linked to aberrant activation of metabolic gene expression in the liver. The therapeutic potential of targeting E47 to eliminate certain metabolic side effects would lie in the hepatocyte-specific modulation of the GC response while retaining important anti-inflammatory properties in immune cells. Since crosstalk between GR and E47 is conserved on several human promoters and enhancers, interfering with or abolishing expression levels of E47 might influence patient's susceptibility to GC-induced side effects or relieve the burden of Cushing's disease.

Developing novel GC treatment regimes with reduced adverse effects has proven to be difficult. Elucidating the distinct molecular mechanisms by which GR influences tissue-specific gene expression and side effect progression presents a major step towards safer steroid treatment.

References

BAIN, G., ENGEL, I., ROBANUS MAANDAG, E. C., TE RIELE, H. P., VOLAND, J. R., SHARP, L. L., CHUN, J., HUEY, B., PINKEL, D. & MURRE, C. 1997a. E2A deficiency leads to abnormalities in alphabeta T-cell development and to rapid development of T-cell lymphomas. *Mol Cell Biol,* 17**,** 4782-91.

BAIN, G., MAANDAG, E. C., IZON, D. J., AMSEN, D., KRUISBEEK, A. M., WEINTRAUB, B. C., KROP, I., SCHLISSEL, M. S., FEENEY, A. J., VAN ROON, M. & ET AL. 1994. E2A proteins are required for proper B cell development and initiation of immunoglobulin gene rearrangements. *Cell,* 79**,** 885-92.

BAIN, G., ROBANUS MAANDAG, E. C., TE RIELE, H. P., FEENEY, A. J., SHEEHY, A., SCHLISSEL, M., SHINTON, S. A., HARDY, R. R. & MURRE, C. 1997b. Both E12 and E47 allow commitment to the B cell lineage. *Immunity,* 6**,** 145-54.

BARNES, P. J. 1998. Anti-inflammatory actions of glucocorticoids: molecular mechanisms. *Clin Sci (Lond),* 94**,** 557-72.

BEAUDRY, J. B., PIERREUX, C. E., HAYHURST, G. P., PLUMB-RUDEWIEZ, N., WEISS, M. C., ROUSSEAU, G. G. & LEMAIGRE, F. P. 2006. Threshold levels of hepatocyte nuclear factor 6 (HNF-6) acting in synergy with HNF-4 and PGC-1alpha are required for time-specific gene expression during liver development. *Mol Cell Biol,* 26**,** 6037-46.

BECK, I. M., VANDEN BERGHE, W., VERMEULEN, L., YAMAMOTO, K. R., HAEGEMAN, G. & DE BOSSCHER, K. 2009a. Crosstalk in inflammation: the interplay of glucocorticoid receptor-based mechanisms and kinases and phosphatases. *Endocr Rev,* 30**,** 830-82.

BECK, K., PEAK, M. M., OTA, T., NEMAZEE, D. & MURRE, C. 2009b. Distinct roles for E12 and E47 in B cell specification and the sequential rearrangement of immunoglobulin light chain loci. *J Exp Med,* 206**,** 2271-84.

BELVISI, M. G., WICKS, S. L., BATTRAM, C. H., BOTTOMS, S. E., REDFORD, J. E., WOODMAN, P., BROWN, T. J., WEBBER, S. E. & FOSTER, M. L. 2001. Therapeutic benefit of a dissociated glucocorticoid and the relevance of in vitro separation of transrepression from transactivation activity. *J Immunol,* 166**,** 1975-82.

BENEZRA, R., DAVIS, R. L., LOCKSHON, D., TURNER, D. L. & WEINTRAUB, H. 1990. The protein Id: a negative regulator of helix-loop-helix DNA binding proteins. *Cell,* 61**,** 49-59.

BIDDIE, S. C., JOHN, S., SABO, P. J., THURMAN, R. E., JOHNSON, T. A., SCHILTZ, R. L., MIRANDA, T. B., SUNG, M. H., TRUMP, S., LIGHTMAN, S. L., VINSON, C., STAMATOYANNOPOULOS, J. A. & HAGER, G. L. 2011. Transcription factor AP1 potentiates chromatin accessibility and glucocorticoid receptor binding. *Mol Cell,* 43**,** 145-55.

BOERGESEN, M., PEDERSEN, T. A., GROSS, B., VAN HEERINGEN, S. J., HAGENBEEK, D., BINDESBOLL, C., CARON, S., LALLOYER, F., STEFFENSEN, K. R., NEBB, H. I., GUSTAFSSON, J. A., STUNNENBERG, H. G., STAELS, B. & MANDRUP, S. 2012. Genome-wide profiling of liver X receptor, retinoid X receptor, and peroxisome proliferator-activated receptor alpha in mouse liver reveals extensive sharing of binding sites. *Mol Cell Biol,* 32**,** 852-67.

BOOKOUT, A. L., JEONG, Y., DOWNES, M., YU, R. T., EVANS, R. M. & MANGELSDORF, D. J. 2006. Anatomical profiling of nuclear receptor expression reveals a hierarchical transcriptional network. *Cell,* 126**,** 789-99.

BRADNEY, C., HJELMELAND, M., KOMATSU, Y., YOSHIDA, M., YAO, T. P. & ZHUANG, Y. 2003. Regulation of E2A activities by histone acetyltransferases in B lymphocyte development. *J Biol Chem,* 278**,** 2370-6.

BURNS, C. M. 2016. The History of Cortisone Discovery and Development. *Rheum Dis Clin North Am,* 42**,** 1-14, vii.

CARROLL, J. S., LIU, X. S., BRODSKY, A. S., LI, W., MEYER, C. A., SZARY, A. J., EECKHOUTE, J., SHAO, W., HESTERMANN, E. V., GEISTLINGER, T. R., FOX, E. A., SILVER, P. A. & BROWN, M. 2005. Chromosome-wide mapping of estrogen receptor binding reveals long-range regulation requiring the forkhead protein FoxA1. *Cell,* 122**,** 33-43.

CHAKRAVARTY, K., CASSUTO, H., RESHEF, L. & HANSON, R. W. 2005. Factors that control the tissue-specific transcription of the gene for phosphoenolpyruvate carboxykinase-C. *Crit Rev Biochem Mol Biol,* 40**,** 129-54.

CHEN, W. & ROEDER, R. G. 2007. The Mediator subunit MED1/TRAP220 is required for optimal glucocorticoid receptor-mediated transcription activation. *Nucleic Acids Res,* 35**,** 6161-9.

CHEN, W., ROGATSKY, I. & GARABEDIAN, M. J. 2006. MED14 and MED1 differentially regulate target-specific gene activation by the glucocorticoid receptor. *Mol Endocrinol,* 20**,** 560-72.

CHU, Y., GOMEZ ROSSO, L., HUANG, P., WANG, Z., XU, Y., YAO, X., BAO, M., YAN, J., SONG, H. & WANG, G. 2014. Liver Med23 ablation improves glucose and lipid metabolism through modulating FOXO1 activity. *Cell Res,* 24**,** 1250-65.

CHUNG, S., SON, G. H. & KIM, K. 2011. Circadian rhythm of adrenal glucocorticoid: its regulation and clinical implications. *Biochim Biophys Acta,* 1812**,** 581-91.

COGHLAN, M. J., JACOBSON, P. B., LANE, B., NAKANE, M., LIN, C. W., ELMORE, S. W., KYM, P. R., LULY, J. R., CARTER, G. W., TURNER, R., TYREE, C. M., HU, J., ELGORT, M., ROSEN, J. & MINER, J. N. 2003. A novel antiinflammatory maintains glucocorticoid efficacy with reduced side effects. *Mol Endocrinol,* 17**,** 860-9.

COX, J., HEIN, M. Y., LUBER, C. A., PARON, I., NAGARAJ, N. & MANN, M. 2014. Accurate proteome-wide label-free quantification by delayed normalization and maximal peptide ratio extraction, termed MaxLFQ. *Mol Cell Proteomics,* 13**,** 2513-26.

DAHLMAN-WRIGHT, K., SILTALA-ROOS, H., CARLSTEDT-DUKE, J. & GUSTAFSSON, J. A. 1990. Protein-protein interactions facilitate DNA binding by the glucocorticoid receptor DNA-binding domain. *J Biol Chem,* 265**,** 14030-5.

DAHLMAN-WRIGHT, K., WRIGHT, A., GUSTAFSSON, J. A. & CARLSTEDT-DUKE, J. 1991. Interaction of the glucocorticoid receptor DNA-binding domain with DNA as a dimer is mediated by a short segment of five amino acids. *J Biol Chem,* 266**,** 3107-12.

DE BOSSCHER, K. 2010. Selective Glucocorticoid Receptor modulators. *J Steroid Biochem Mol Biol,* 120**,** 96-104.

DE BOSSCHER, K. & HAEGEMAN, G. 2009. Minireview: latest perspectives on antiinflammatory actions of glucocorticoids. *Mol Endocrinol,* 23**,** 281-91.

DE GUIA, R. M. & HERZIG, S. 2015. How Do Glucocorticoids Regulate Lipid Metabolism? *Adv Exp Med Biol,* 872**,** 127-44.

DE POOTER, R. F. & KEE, B. L. 2010. E proteins and the regulation of early lymphocyte development. *Immunol Rev,* 238**,** 93-109.

DEFURIA, J., BELKINA, A. C., JAGANNATHAN-BOGDAN, M., SNYDER-CAPPIONE, J., CARR, J. D., NERSESOVA, Y. R., MARKHAM, D., STRISSEL, K. J., WATKINS, A. A., ZHU, M., ALLEN, J., BOUCHARD, J., TORALDO, G., JASUJA, R., OBIN, M. S., MCDONNELL, M. E., APOVIAN, C., DENIS, G. V. & NIKOLAJCZYK, B. S. 2013. B cells promote inflammation in obesity and type 2 diabetes through regulation of T-cell function and an inflammatory cytokine profile. *Proc Natl Acad Sci U S A,* 110**,** 5133-8.

DENNIS, D. J., HAN, S. & SCHUURMANS, C. 2018. bHLH transcription factors in neural development, disease, and reprogramming. *Brain Res*.

DESMET, S. J. & DE BOSSCHER, K. 2017. Glucocorticoid receptors: finding the middle ground. *J Clin Invest,* 127**,** 1136-1145.

DIAMOND, M. I., MINER, J. N., YOSHINAGA, S. K. & YAMAMOTO, K. R. 1990. Transcription factor interactions: selectors of positive or negative regulation from a single DNA element. *Science,* 249**,** 1266-72.

DOBIN, A., DAVIS, C. A., SCHLESINGER, F., DRENKOW, J., ZALESKI, C., JHA, S., BATUT, P., CHAISSON, M. & GINGERAS, T. R. 2013. STAR: ultrafast universal RNA-seq aligner. *Bioinformatics,* 29**,** 15-21.

DORAN, A. C., MELLER, N., CUTCHINS, A., DELIRI, H., SLAYTON, R. P., OLDHAM, S. N., KIM, J. B., KELLER, S. R. & MCNAMARA, C. A. 2008. The helix-loop-helix factors Id3 and E47 are novel regulators of adiponectin. *Circ Res,* 103**,** 624-34.

DROUIN, J. 2014. Minireview: pioneer transcription factors in cell fate specification. *Mol Endocrinol,* 28**,** 989-98.

DURINCK, S., SPELLMAN, P. T., BIRNEY, E. & HUBER, W. 2009. Mapping identifiers for the integration of genomic datasets with the R/Bioconductor package biomaRt. *Nat Protoc,* 4**,** 1184-91.

EDEN, E., NAVON, R., STEINFELD, I., LIPSON, D. & YAKHINI, Z. 2009. GOrilla: a tool for discovery and visualization of enriched GO terms in ranked gene lists. *BMC Bioinformatics,* 10**,** 48.

ENGEL, I. & MURRE, C. 2001. The function of E- and Id proteins in lymphocyte development. *Nat Rev Immunol,* 1**,** 193-9.

EPHRUSSI, A., CHURCH, G. M., TONEGAWA, S. & GILBERT, W. 1985. B lineage--specific interactions of an immunoglobulin enhancer with cellular factors in vivo. *Science,* 227**,** 134-40.

EVANS, R. M. 1988. The steroid and thyroid hormone receptor superfamily. *Science,* 240**,** 889-95.

EVANS, R. M. & MANGELSDORF, D. J. 2014. Nuclear Receptors, RXR, and the Big Bang. *Cell,* 157**,** 255-66.

FRANSSON, L., FRANZEN, S., ROSENGREN, V., WOLBERT, P., SJOHOLM, A. & ORTSATER, H. 2013. beta-Cell adaptation in a mouse model of glucocorticoid-induced metabolic syndrome. *J Endocrinol,* 219**,** 231-41.

FRENKEL, B., WHITE, W. & TUCKERMANN, J. 2015. Glucocorticoid-Induced Osteoporosis. *Adv Exp Med Biol,* 872**,** 179-215.

GARABEDIAN, M. J., HARRIS, C. A. & JEANNETEAU, F. 2017. Glucocorticoid receptor action in metabolic and neuronal function. *F1000Res,* 6**,** 1208.

GEER, E. B., ISLAM, J. & BUETTNER, C. 2014. Mechanisms of glucocorticoid-induced insulin resistance: focus on adipose tissue function and lipid metabolism. *Endocrinol Metab Clin North Am,* 43**,** 75-102.

GLASS, C. K. & SAIJO, K. 2010. Nuclear receptor transrepression pathways that regulate inflammation in macrophages and T cells. *Nat Rev Immunol,* 10**,** 365-76.

GRANNER, D. K., WANG, J. C. & YAMAMOTO, K. R. 2015. Regulatory Actions of Glucocorticoid Hormones: From Organisms to Mechanisms. *Adv Exp Med Biol,* 872**,** 3-31.

GREEN, S., WALTER, P., KUMAR, V., KRUST, A., BORNERT, J. M., ARGOS, P. & CHAMBON, P. 1986. Human oestrogen receptor cDNA: sequence, expression and homology to v-erb-A. *Nature,* 320**,** 134-9.

GREULICH, F., HEMMER, M. C., ROLLINS, D. A., ROGATSKY, I. & UHLENHAUT, N. H. 2016. There goes the neighborhood: Assembly of transcriptional complexes during the regulation of metabolism and inflammation by the glucocorticoid receptor. *Steroids,* 114**,** 7-15.

GRONTVED, L., JOHN, S., BAEK, S., LIU, Y., BUCKLEY, J. R., VINSON, C., AGUILERA, G. & HAGER, G. L. 2013. C/EBP maintains chromatin accessibility in liver and facilitates glucocorticoid receptor recruitment to steroid response elements. *EMBO J,* 32**,** 1568-83.

GROSS, D. N., VAN DEN HEUVEL, A. P. & BIRNBAUM, M. J. 2008. The role of FoxO in the regulation of metabolism. *Oncogene,* 27**,** 2320-36.

GUALDI, R., BOSSARD, P., ZHENG, M., HAMADA, Y., COLEMAN, J. R. & ZARET, K. S. 1996. Hepatic specification of the gut endoderm in vitro: cell signaling and transcriptional control. *Genes Dev,* 10**,** 1670-82.

HALL, R. K., SLADEK, F. M. & GRANNER, D. K. 1995. The orphan receptors COUP-TF and HNF-4 serve as accessory factors required for induction of phosphoenolpyruvate carboxykinase gene transcription by glucocorticoids. *Proc Natl Acad Sci U S A,* 92**,** 412-6.

HALL, R. K., YAMASAKI, T., KUCERA, T., WALTNER-LAW, M., O'BRIEN, R. & GRANNER, D. K. 2000. Regulation of phosphoenolpyruvate carboxykinase and insulin-like growth factor-binding protein-1 gene expression by insulin. The role of winged helix/forkhead proteins. *J Biol Chem,* 275**,** 30169-75.

HANNENHALLI, S. & KAESTNER, K. H. 2009. The evolution of Fox genes and their role in development and disease. *Nat Rev Genet,* 10**,** 233-40.

HAO, H., ALLEN, D. L. & HARDIN, P. E. 1997. A circadian enhancer mediates PER-dependent mRNA cycling in Drosophila melanogaster. *Mol Cell Biol,* 17**,** 3687-93.

HAYHURST, G. P., LEE, Y. H., LAMBERT, G., WARD, J. M. & GONZALEZ, F. J. 2001. Hepatocyte nuclear factor 4alpha (nuclear receptor 2A1) is essential for maintenance of hepatic gene expression and lipid homeostasis. *Mol Cell Biol,* 21**,** 1393-403.

HEIN, M. Y., HUBNER, N. C., POSER, I., COX, J., NAGARAJ, N., TOYODA, Y., GAK, I. A., WEISSWANGE, I., MANSFELD, J., BUCHHOLZ, F., HYMAN, A. A. & MANN, M. 2015. A human interactome in three quantitative dimensions organized by stoichiometries and abundances. *Cell,* 163**,** 712-23.

HEINTZMAN, N. D., STUART, R. K., HON, G., FU, Y., CHING, C. W., HAWKINS, R. D., BARRERA, L. O., VAN CALCAR, S., QU, C., CHING, K. A., WANG, W., WENG, Z., GREEN, R. D., CRAWFORD, G. E. & REN, B. 2007. Distinct and predictive chromatin signatures of transcriptional promoters and enhancers in the human genome. *Nat Genet,* 39**,** 311-8.

HEINZ, S., BENNER, C., SPANN, N., BERTOLINO, E., LIN, Y. C., LASLO, P., CHENG, J. X., MURRE, C., SINGH, H. & GLASS, C. K. 2010. Simple combinations of lineage-determining transcription factors prime cis-regulatory elements required for macrophage and B cell identities. *Mol Cell,* 38**,** 576-89.

HENCH, P. S., KENDALL, E. C. & ET AL. 1949. The effect of a hormone of the adrenal cortex (17-hydroxy-11-dehydrocorticosterone; compound E) and of pituitary adrenocorticotropic hormone on rheumatoid arthritis. *Proc Staff Meet Mayo Clin,* 24**,** 181-97.

HENTHORN, P., KILEDJIAN, M. & KADESCH, T. 1990. Two distinct transcription factors that bind the immunoglobulin enhancer microE5/kappa 2 motif. *Science,* 247**,** 467-70.

HERMAN, J. P., MCKLVEEN, J. M., GHOSAL, S., KOPP, B., WULSIN, A., MAKINSON, R., SCHEIMANN, J. & MYERS, B. 2016. Regulation of the Hypothalamic-Pituitary-Adrenocortical Stress Response. *Compr Physiol,* 6**,** 603-21.

HEROLD, M. J., MCPHERSON, K. G. & REICHARDT, H. M. 2006. Glucocorticoids in T cell apoptosis and function. *Cell Mol Life Sci,* 63**,** 60-72.

HOLLENBERG, S. M., WEINBERGER, C., ONG, E. S., CERELLI, G., ORO, A., LEBO, R., THOMPSON, E. B., ROSENFELD, M. G. & EVANS, R. M. 1985. Primary structure and expression of a functional human glucocorticoid receptor cDNA. *Nature,* 318**,** 635-41.

HURTADO, A., HOLMES, K. A., ROSS-INNES, C. S., SCHMIDT, D. & CARROLL, J. S. 2011. FOXA1 is a key determinant of estrogen receptor function and endocrine response. *Nat Genet,* 43**,** 27-33.

HYNDMAN, B. D., THOMPSON, P., BAYLY, R., COTE, G. P. & LEBRUN, D. P. 2012a. E2A proteins enhance the histone acetyltransferase activity of the transcriptional co-activators CBP and p300. *Biochim Biophys Acta,* 1819**,** 446-53.

HYNDMAN, B. D., THOMPSON, P., DENIS, C. M., CHITAYAT, S., BAYLY, R., SMITH, S. P. & LEBRUN, D. P. 2012b. Mapping acetylation sites in E2A identifies a conserved lysine residue in activation domain 1 that promotes CBP/p300 recruitment and transcriptional activation. *Biochim Biophys Acta,* 1819**,** 375-81.

IMAI, E., STROMSTEDT, P. E., QUINN, P. G., CARLSTEDT-DUKE, J., GUSTAFSSON, J. A. & GRANNER, D. K. 1990. Characterization of a complex glucocorticoid response unit in the phosphoenolpyruvate carboxykinase gene. *Mol Cell Biol,* 10**,** 4712-9.

IWASAKI, H., SOMOZA, C., SHIGEMATSU, H., DUPREZ, E. A., IWASAKI-ARAI, J., MIZUNO, S., ARINOBU, Y., GEARY, K., ZHANG, P., DAYARAM, T., FENYUS, M. L., ELF, S., CHAN, S., KASTNER, P., HUETTNER, C. S., MURRAY, R., TENEN, D. G. & AKASHI, K. 2005. Distinctive and indispensable roles of PU.1 in maintenance of hematopoietic stem cells and their differentiation. *Blood,* 106**,** 1590-600.

JIA, Y., VISWAKARMA, N., FU, T., YU, S., RAO, M. S., BORENSZTAJN, J. & REDDY, J. K. 2009. Conditional ablation of mediator subunit MED1 (MED1/PPARBP) gene in mouse liver attenuates glucocorticoid receptor agonist dexamethasone-induced hepatic steatosis. *Gene Expr,* 14**,** 291-306.

JIA, Y., VISWAKARMA, N. & REDDY, J. K. 2014. Med1 subunit of the mediator complex in nuclear receptor-regulated energy metabolism, liver regeneration, and hepatocarcinogenesis. *Gene Expr,* 16**,** 63-75.

JIN, F., LI, Y., REN, B. & NATARAJAN, R. 2011. PU.1 and C/EBP(alpha) synergistically program distinct response to NF-kappaB activation through establishing monocyte specific enhancers. *Proc Natl Acad Sci U S A,* 108**,** 5290-5.

JOHN, S., SABO, P. J., THURMAN, R. E., SUNG, M. H., BIDDIE, S. C., JOHNSON, T. A., HAGER, G. L. & STAMATOYANNOPOULOS, J. A. 2011. Chromatin accessibility pre-determines glucocorticoid receptor binding patterns. *Nat Genet,* 43**,** 264-8.

JONES, S. 2004. An overview of the basic helix-loop-helix proteins. *Genome Biol,* 5**,** 226.

KALKHOVEN, E. 2004. CBP and p300: HATs for different occasions. *Biochem Pharmacol,* 68**,** 1145-55.

KARATSOREOS, I. N., BHAGAT, S. M., BOWLES, N. P., WEIL, Z. M., PFAFF, D. W. & MCEWEN, B. S. 2010. Endocrine and physiological changes in response to chronic corticosterone: a potential model of the metabolic syndrome in mouse. *Endocrinology,* 151**,** 2117-27.

KEE, B. L. 2009. E and ID proteins branch out. *Nat Rev Immunol,* 9**,** 175-84.

KLEIMAN, A., HUBNER, S., RODRIGUEZ PARKITNA, J. M., NEUMANN, A., HOFER, S., WEIGAND, M. A., BAUER, M., SCHMID, W., SCHUTZ, G., LIBERT, C., REICHARDT, H. M. & TUCKERMANN, J. P. 2012. Glucocorticoid receptor dimerization is required for survival in septic shock via suppression of interleukin-1 in macrophages. *FASEB J,* 26**,** 722-9.

KORNBERG, R. D. 2005. Mediator and the mechanism of transcriptional activation. *Trends Biochem Sci,* 30**,** 235-9.

KUMAR, R. & THOMPSON, E. B. 2005. Gene regulation by the glucocorticoid receptor: structure:function relationship. *J Steroid Biochem Mol Biol,* 94**,** 383-94.

LANGLAIS, D., COUTURE, C., BALSALOBRE, A. & DROUIN, J. 2012. The Stat3/GR interaction code: predictive value of direct/indirect DNA recruitment for transcription outcome. *Mol Cell,* 47**,** 38-49.

LASSAR, A. B., BUSKIN, J. N., LOCKSHON, D., DAVIS, R. L., APONE, S., HAUSCHKA, S. D. & WEINTRAUB, H. 1989. MyoD is a sequence-specific DNA binding protein requiring a region of myc homology to bind to the muscle creatine kinase enhancer. *Cell,* 58**,** 823-31.

LASSAR, A. B., DAVIS, R. L., WRIGHT, W. E., KADESCH, T., MURRE, C., VORONOVA, A., BALTIMORE, D. & WEINTRAUB, H. 1991. Functional activity of myogenic HLH proteins requires hetero-oligomerization with E12/E47-like proteins in vivo. *Cell,* 66**,** 305-15.

LAZORCHAK, A., JONES, M. E. & ZHUANG, Y. 2005. New insights into E-protein function in lymphocyte development. *Trends Immunol,* 26**,** 334-8.

LEE, C. S., FRIEDMAN, J. R., FULMER, J. T. & KAESTNER, K. H. 2005. The initiation of liver development is dependent on Foxa transcription factors. *Nature,* 435**,** 944-7.

LEMKE, U., KRONES-HERZIG, A., BERRIEL DIAZ, M., NARVEKAR, P., ZIEGLER, A., VEGIOPOULOS, A., CATO, A. C., BOHL, S., KLINGMULLER, U., SCREATON, R. A., MULLER-DECKER, K., KERSTEN, S. & HERZIG, S. 2008. The glucocorticoid receptor controls hepatic dyslipidemia through Hes1. *Cell Metab,* 8**,** 212-23.

LI, H. & DURBIN, R. 2010. Fast and accurate long-read alignment with Burrows-Wheeler transform. *Bioinformatics,* 26**,** 589-95.

LI, H., HANDSAKER, B., WYSOKER, A., FENNELL, T., RUAN, J., HOMER, N., MARTH, G., ABECASIS, G. & DURBIN, R. 2009. The Sequence Alignment/Map format and SAMtools. *Bioinformatics,* 25**,** 2078-9.

LI, J., NING, G. & DUNCAN, S. A. 2000. Mammalian hepatocyte differentiation requires the transcription factor HNF-4alpha. *Genes Dev,* 14**,** 464-74.

LIM, H. W., UHLENHAUT, N. H., RAUCH, A., WEINER, J., HUBNER, S., HUBNER, N., WON, K. J., LAZAR, M. A., TUCKERMANN, J. & STEGER, D. J. 2015. Genomic redistribution of GR monomers and dimers mediates transcriptional response to exogenous glucocorticoid in vivo. *Genome Res,* 25**,** 836-44.

LIN, Y. C., JHUNJHUNWALA, S., BENNER, C., HEINZ, S., WELINDER, E., MANSSON, R., SIGVARDSSON, M., HAGMAN, J., ESPINOZA, C. A., DUTKOWSKI, J., IDEKER, T., GLASS, C. K. & MURRE, C. 2010. A global network of transcription factors, involving E2A, EBF1 and Foxo1, that orchestrates B cell fate. *Nat Immunol,* 11**,** 635-43.

LOVE, M. I., HUBER, W. & ANDERS, S. 2014. Moderated estimation of fold change and dispersion for RNA-seq data with DESeq2. *Genome Biol,* 15**,** 550.

MALIK, S. & ROEDER, R. G. 2005. Dynamic regulation of pol II transcription by the mammalian Mediator complex. *Trends Biochem Sci,* 30**,** 256-63.

MALIK, S. & ROEDER, R. G. 2010. The metazoan Mediator co-activator complex as an integrative hub for transcriptional regulation. *Nat Rev Genet,* 11**,** 761-72.

MANGELSDORF, D. J., THUMMEL, C., BEATO, M., HERRLICH, P., SCHUTZ, G., UMESONO, K., BLUMBERG, B., KASTNER, P., MARK, M., CHAMBON, P. & EVANS, R. M. 1995. The nuclear receptor superfamily: the second decade. *Cell,* 83**,** 835-9.

MARGAGLIOTTI, S., CLOTMAN, F., PIERREUX, C. E., BEAUDRY, J. B., JACQUEMIN, P., ROUSSEAU, G. G. & LEMAIGRE, F. P. 2007. The Onecut transcription factors HNF-6/OC-1

and OC-2 regulate early liver expansion by controlling hepatoblast migration. *Dev Biol,* 311**,** 579-89.

MASSARI, M. E. & MURRE, C. 2000. Helix-loop-helix proteins: regulators of transcription in eucaryotic organisms. *Mol Cell Biol,* 20**,** 429-40.

MATSUMOTO, M., POCAI, A., ROSSETTI, L., DEPINHO, R. A. & ACCILI, D. 2007. Impaired regulation of hepatic glucose production in mice lacking the forkhead transcription factor Foxo1 in liver. *Cell Metab,* 6**,** 208-16.

MCLEAN, C. Y., BRISTOR, D., HILLER, M., CLARKE, S. L., SCHAAR, B. T., LOWE, C. B., WENGER, A. M. & BEJERANO, G. 2010. GREAT improves functional interpretation of cis-regulatory regions. *Nat Biotechnol,* 28**,** 495-501.

MIRANDA, T. B., MORRIS, S. A. & HAGER, G. L. 2013. Complex genomic interactions in the dynamic regulation of transcription by the glucocorticoid receptor. *Mol Cell Endocrinol,* 380**,** 16-24.

MORRISON, N. & EISMAN, J. 1993. Role of the negative glucocorticoid regulatory element in glucocorticoid repression of the human osteocalcin promoter. *J Bone Miner Res,* 8**,** 969-75.

MUNOZ, E., BREWER, M. & BALER, R. 2002. Circadian Transcription. Thinking outside the E-Box. *J Biol Chem,* 277**,** 36009-17.

MURRE, C. 2005. Helix-loop-helix proteins and lymphocyte development. *Nat Immunol,* 6**,** 1079-86.

MURRE, C., BAIN, G., VAN DIJK, M. A., ENGEL, I., FURNARI, B. A., MASSARI, M. E., MATTHEWS, J. R., QUONG, M. W., RIVERA, R. R. & STUIVER, M. H. 1994. Structure and function of helix-loop-helix proteins. *Biochim Biophys Acta,* 1218**,** 129-35.

MURRE, C., MCCAW, P. S. & BALTIMORE, D. 1989a. A new DNA binding and dimerization motif in immunoglobulin enhancer binding, daughterless, MyoD, and myc proteins. *Cell,* 56**,** 777-83.

MURRE, C., MCCAW, P. S., VAESSIN, H., CAUDY, M., JAN, L. Y., JAN, Y. N., CABRERA, C. V., BUSKIN, J. N., HAUSCHKA, S. D., LASSAR, A. B. & ET AL. 1989b. Interactions between heterologous helix-loop-helix proteins generate complexes that bind specifically to a common DNA sequence. *Cell,* 58**,** 537-44.

NAYA, F. J., HUANG, H. P., QIU, Y., MUTOH, H., DEMAYO, F. J., LEITER, A. B. & TSAI, M. J. 1997. Diabetes, defective pancreatic morphogenesis, and abnormal enteroendocrine differentiation in BETA2/neuroD-deficient mice. *Genes Dev,* 11**,** 2323-34.

NAYA, F. J., STELLRECHT, C. M. & TSAI, M. J. 1995. Tissue-specific regulation of the insulin gene by a novel basic helix-loop-helix transcription factor. *Genes Dev,* 9**,** 1009-19.

NECELA, B. M. & CIDLOWSKI, J. A. 2004. Mechanisms of glucocorticoid receptor action in noninflammatory and inflammatory cells. *Proc Am Thorac Soc,* 1**,** 239-46.

OAKLEY, R. H. & CIDLOWSKI, J. A. 2011. Cellular processing of the glucocorticoid receptor gene and protein: new mechanisms for generating tissue-specific actions of glucocorticoids. *J Biol Chem,* 286**,** 3177-84.

OAKLEY, R. H. & CIDLOWSKI, J. A. 2013. The biology of the glucocorticoid receptor: new signaling mechanisms in health and disease. *J Allergy Clin Immunol,* 132**,** 1033-44.

OGAWA, S., LOZACH, J., BENNER, C., PASCUAL, G., TANGIRALA, R. K., WESTIN, S., HOFFMANN, A., SUBRAMANIAM, S., DAVID, M., ROSENFELD, M. G. & GLASS, C. K. 2005. Molecular determinants of crosstalk between nuclear receptors and toll-like receptors. *Cell,* 122**,** 707-21.

OPHERK, C., TRONCHE, F., KELLENDONK, C., KOHLMULLER, D., SCHULZE, A., SCHMID, W. & SCHUTZ, G. 2004. Inactivation of the glucocorticoid receptor in hepatocytes leads to fasting hypoglycemia and ameliorates hyperglycemia in streptozotocin-induced diabetes mellitus. *Mol Endocrinol,* 18**,** 1346-53.

OSTUNI, R., PICCOLO, V., BAROZZI, I., POLLETTI, S., TERMANINI, A., BONIFACIO, S., CURINA, A., PROSPERINI, E., GHISLETTI, S. & NATOLI, G. 2013. Latent enhancers activated by stimulation in differentiated cells. *Cell,* 152**,** 157-71.

OVERMAN, R. A., YEH, J. Y. & DEAL, C. L. 2013. Prevalence of oral glucocorticoid usage in the United States: a general population perspective. *Arthritis Care Res (Hoboken),* 65**,** 294-8.

PARK, E. A., GURNEY, A. L., NIZIELSKI, S. E., HAKIMI, P., CAO, Z., MOORMAN, A. & HANSON, R. W. 1993. Relative roles of CCAAT/enhancer-binding protein beta and cAMP regulatory element-binding protein in controlling transcription of the gene for phosphoenolpyruvate carboxykinase (GTP). *J Biol Chem,* 268**,** 613-9.

PARTCH, C. L., GREEN, C. B. & TAKAHASHI, J. S. 2014. Molecular architecture of the mammalian circadian clock. *Trends Cell Biol,* 24**,** 90-9.

PATEL, R., MAGOMEDOVA, L., TSAI, R., ANGERS, S., ORELLANA, A. & CUMMINS, C. L. 2017. Separating the Anti-Inflammatory and Diabetogenic Effects of Glucocorticoids Through LXRbeta Antagonism. *Endocrinology,* 158**,** 1034-1047.

PATEL, R., PATEL, M., TSAI, R., LIN, V., BOOKOUT, A. L., ZHANG, Y., MAGOMEDOVA, L., LI, T., CHAN, J. F., BUDD, C., MANGELSDORF, D. J. & CUMMINS, C. L. 2011. LXRbeta is required for glucocorticoid-induced hyperglycemia and hepatosteatosis in mice. *J Clin Invest,* 121**,** 431-41.

PATEL, R., WILLIAMS-DAUTOVICH, J. & CUMMINS, C. L. 2014. Minireview: new molecular mediators of glucocorticoid receptor activity in metabolic tissues. *Mol Endocrinol,* 28**,** 999-1011.

PHUC LE, P., FRIEDMAN, J. R., SCHUG, J., BRESTELLI, J. E., PARKER, J. B., BOCHKIS, I. M. & KAESTNER, K. H. 2005. Glucocorticoid receptor-dependent gene regulatory networks. *PLoS Genet,* 1**,** e16.

PRATT, W. B. & TOFT, D. O. 1997. Steroid receptor interactions with heat shock protein and immunophilin chaperones. *Endocr Rev,* 18**,** 306-60.

PUIGSERVER, P., RHEE, J., DONOVAN, J., WALKEY, C. J., YOON, J. C., ORIENTE, F., KITAMURA, Y., ALTOMONTE, J., DONG, H., ACCILI, D. & SPIEGELMAN, B. M. 2003. Insulin-regulated hepatic gluconeogenesis through FOXO1-PGC-1alpha interaction. *Nature,* 423**,** 550-5.

RAHMOUNI, K. & SIGMUND, C. D. 2008. Id3, E47, and SREBP-1c: fat factors controlling adiponectin expression. *Circ Res,* 103**,** 565-7.

REVOLLO, J. R., OAKLEY, R. H., LU, N. Z., KADMIEL, M., GANDHAVADI, M. & CIDLOWSKI, J. A. 2013. HES1 is a master regulator of glucocorticoid receptor-dependent gene expression. *Sci Signal,* 6**,** ra103.

ROSE, A. J. & HERZIG, S. 2013. Metabolic control through glucocorticoid hormones: an update. *Mol Cell Endocrinol,* 380**,** 65-78.

RUDIGER, J. J., ROTH, M., BIHL, M. P., CORNELIUS, B. C., JOHNSON, M., ZIESCHE, R. & BLOCK, L. H. 2002. Interaction of C/EBPalpha and the glucocorticoid receptor in vivo and in nontransformed human cells. *Faseb j,* 16**,** 177-84.

SACTA, M. A., CHINENOV, Y. & ROGATSKY, I. 2016. Glucocorticoid Signaling: An Update from a Genomic Perspective. *Annu Rev Physiol,* 78**,** 155-80.

SAHU, B., LAAKSO, M., OVASKA, K., MIRTTI, T., LUNDIN, J., RANNIKKO, A., SANKILA, A., TURUNEN, J. P., LUNDIN, M., KONSTI, J., VESTERINEN, T., NORDLING, S., KALLIONIEMI, O., HAUTANIEMI, S. & JANNE, O. A. 2011. Dual role of FoxA1 in androgen receptor binding to chromatin, androgen signalling and prostate cancer. *Embo j,* 30**,** 3962-76.

SAPOLSKY, R. M., ROMERO, L. M. & MUNCK, A. U. 2000. How do glucocorticoids influence stress responses? Integrating permissive, suppressive, stimulatory, and preparative actions. *Endocr Rev,* 21**,** 55-89.

SAVKUR, R. S. & BURRIS, T. P. 2004. The coactivator LXXLL nuclear receptor recognition motif. *J Pept Res,* 63**,** 207-12.

SCHACKE, H., BERGER, M., REHWINKEL, H. & ASADULLAH, K. 2007. Selective glucocorticoid receptor agonists (SEGRAs): novel ligands with an improved therapeutic index. *Mol Cell Endocrinol,* 275**,** 109-17.

SCHACKE, H., DOCKE, W. D. & ASADULLAH, K. 2002. Mechanisms involved in the side effects of glucocorticoids. *Pharmacol Ther,* 96**,** 23-43.

SCHELTEMA, R. A., HAUSCHILD, J. P., LANGE, O., HORNBURG, D., DENISOV, E., DAMOC, E., KUEHN, A., MAKAROV, A. & MANN, M. 2014. The Q Exactive HF, a Benchtop mass spectrometer with a pre-filter, high-performance quadrupole and an ultra-high-field Orbitrap analyzer. *Mol Cell Proteomics,* 13**,** 3698-708.

SCHWARTZ, R., ENGEL, I., FALLAHI-SICHANI, M., PETRIE, H. T. & MURRE, C. 2006. Gene expression patterns define novel roles for E47 in cell cycle progression, cytokine-mediated signaling, and T lineage development. *Proc Natl Acad Sci U S A,* 103**,** 9976-81.

SHIBLI-RAHHAL, A., VAN BEEK, M. & SCHLECHTE, J. A. 2006. Cushing's syndrome. *Clin Dermatol,* 24**,** 260-5.

SKINNER, M. K., RAWLS, A., WILSON-RAWLS, J. & ROALSON, E. H. 2010. Basic helix-loop-helix transcription factor gene family phylogenetics and nomenclature. *Differentiation,* 80**,** 1-8.

SPIGA, F., WALKER, J. J., TERRY, J. R. & LIGHTMAN, S. L. 2014. HPA axis-rhythms. *Compr Physiol,* 4**,** 1273-98.

SPRAGUE, R. G., POWER, M. H. & MASON, H. L. 1950. Physiological effects of cortisone and pituitary adrenocorticotropic hormone (ACTH) in man. *J Am Med Assoc,* 144**,** 1341-7.

STARICK, S. R., IBN-SALEM, J., JURK, M., HERNANDEZ, C., LOVE, M. I., CHUNG, H. R., VINGRON, M., THOMAS-CHOLLIER, M. & MEIJSING, S. H. 2015. ChIP-exo signal associated with DNA-binding motifs provides insight into the genomic binding of the glucocorticoid receptor and cooperating transcription factors. *Genome Res,* 25**,** 825-35.

STAUDT, L. M. & LENARDO, M. J. 1991. Immunoglobulin gene transcription. *Annu Rev Immunol,* 9**,** 373-98.

SUN, X. H. & BALTIMORE, D. 1991. An inhibitory domain of E12 transcription factor prevents DNA binding in E12 homodimers but not in E12 heterodimers. *Cell,* 64**,** 459-70.

SUNDAHL, N., BRIDELANCE, J., LIBERT, C., DE BOSSCHER, K. & BECK, I. M. 2015. Selective glucocorticoid receptor modulation: New directions with non-steroidal scaffolds. *Pharmacol Ther,* 152**,** 28-41.

SURJIT, M., GANTI, K. P., MUKHERJI, A., YE, T., HUA, G., METZGER, D., LI, M. & CHAMBON, P. 2011. Widespread negative response elements mediate direct repression by agonist-liganded glucocorticoid receptor. *Cell,* 145**,** 224-41.

TUCKERMANN, J. P., KLEIMAN, A., MORIGGL, R., SPANBROEK, R., NEUMANN, A., ILLING, A., CLAUSEN, B. E., STRIDE, B., FORSTER, I., HABENICHT, A. J., REICHARDT, H. M., TRONCHE, F., SCHMID, W. & SCHUTZ, G. 2007. Macrophages and neutrophils are the targets for immune suppression by glucocorticoids in contact allergy. *J Clin Invest,* 117**,** 1381-90.

UHLENHAUT, N. H., BARISH, G. D., YU, R. T., DOWNES, M., KARUNASIRI, M., LIDDLE, C., SCHWALIE, P., HUBNER, N. & EVANS, R. M. 2013. Insights into negative regulation by the

glucocorticoid receptor from genome-wide profiling of inflammatory cistromes. *Mol Cell,* 49**,** 158-71.

VAN RAALTE, D. H. & DIAMANT, M. 2014. Steroid diabetes: from mechanism to treatment? *Neth J Med,* 72**,** 62-72.

VANDER KOOI, B. T., ONUMA, H., OESER, J. K., SVITEK, C. A., ALLEN, S. R., VANDER KOOI, C. W., CHAZIN, W. J. & O'BRIEN, R. M. 2005. The glucose-6-phosphatase catalytic subunit gene promoter contains both positive and negative glucocorticoid response elements. *Mol Endocrinol,* 19**,** 3001-22.

VANDEVYVER, S., DEJAGER, L., TUCKERMANN, J. & LIBERT, C. 2013. New insights into the anti-inflammatory mechanisms of glucocorticoids: an emerging role for glucocorticoid-receptor-mediated transactivation. *Endocrinology,* 154**,** 993-1007.

VEGIOPOULOS, A. & HERZIG, S. 2007. Glucocorticoids, metabolism and metabolic diseases. *Mol Cell Endocrinol,* 275**,** 43-61.

WALKER, B. R. 2007. Glucocorticoids and cardiovascular disease. *Eur J Endocrinol,* 157**,** 545-59.

WANG, J. C., GRAY, N. E., KUO, T. & HARRIS, C. A. 2012. Regulation of triglyceride metabolism by glucocorticoid receptor. *Cell Biosci,* 2**,** 19.

WANG, J. C., STROMSTEDT, P. E., O'BRIEN, R. M. & GRANNER, D. K. 1996. Hepatic nuclear factor 3 is an accessory factor required for the stimulation of phosphoenolpyruvate carboxykinase gene transcription by glucocorticoids. *Mol Endocrinol,* 10**,** 794-800.

WANG, L. H. & BAKER, N. E. 2015. E Proteins and ID Proteins: Helix-Loop-Helix Partners in Development and Disease. *Dev Cell,* 35**,** 269-80.

WANG, M. 2005. The role of glucocorticoid action in the pathophysiology of the Metabolic Syndrome. *Nutr Metab (Lond),* 2**,** 3.

WELINDER, E., MANSSON, R., MERCER, E. M., BRYDER, D., SIGVARDSSON, M. & MURRE, C. 2011. The transcription factors E2A and HEB act in concert to induce the expression of FOXO1 in the common lymphoid progenitor. *Proc Natl Acad Sci U S A,* 108**,** 17402-7.

WINER, D. A., WINER, S., SHEN, L., WADIA, P. P., YANTHA, J., PALTSER, G., TSUI, H., WU, P., DAVIDSON, M. G., ALONSO, M. N., LEONG, H. X., GLASSFORD, A., CAIMOL, M., KENKEL, J. A., TEDDER, T. F., MCLAUGHLIN, T., MIKLOS, D. B., DOSCH, H. M. & ENGLEMAN, E. G. 2011. B cells promote insulin resistance through modulation of T cells and production of pathogenic IgG antibodies. *Nat Med,* 17**,** 610-7.

XIONG, X., TAO, R., DEPINHO, R. A. & DONG, X. C. 2013. Deletion of hepatic FoxO1/3/4 genes in mice significantly impacts on glucose metabolism through downregulation of gluconeogenesis and upregulation of glycolysis. *PLoS One,* 8**,** e74340.

YOUN, D. Y., XIAOLI, A. M., PESSIN, J. E. & YANG, F. 2016. Regulation of metabolism by the Mediator complex. *Biophys Rep,* 2**,** 69-77.

YUE, F., CHENG, Y., BRESCHI, A., VIERSTRA, J., WU, W., RYBA, T., SANDSTROM, R., MA, Z., DAVIS, C., POPE, B. D., SHEN, Y., PERVOUCHINE, D. D., DJEBALI, S., THURMAN, R. E., KAUL, R., RYNES, E., KIRILUSHA, A., MARINOV, G. K., WILLIAMS, B. A., TROUT, D., AMRHEIN, H., FISHER-AYLOR, K., ANTOSHECHKIN, I., DESALVO, G., SEE, L. H., FASTUCA, M., DRENKOW, J., ZALESKI, C., DOBIN, A., PRIETO, P., LAGARDE, J., BUSSOTTI, G., TANZER, A., DENAS, O., LI, K., BENDER, M. A., ZHANG, M., BYRON, R., GROUDINE, M. T., MCCLEARY, D., PHAM, L., YE, Z., KUAN, S., EDSALL, L., WU, Y. C., RASMUSSEN, M. D., BANSAL, M. S., KELLIS, M., KELLER, C. A., MORRISSEY, C. S., MISHRA, T., JAIN, D., DOGAN, N., HARRIS, R. S., CAYTING, P., KAWLI, T., BOYLE, A. P., EUSKIRCHEN, G., KUNDAJE, A., LIN, S., LIN, Y., JANSEN, C., MALLADI, V. S., CLINE, M. S., ERICKSON, D. T., KIRKUP, V. M., LEARNED, K., SLOAN, C. A., ROSENBLOOM, K. R., LACERDA DE SOUSA, B., BEAL, K., PIGNATELLI, M., FLICEK, P., LIAN, J., KAHVECI, T.,

LEE, D., KENT, W. J., RAMALHO SANTOS, M., HERRERO, J., NOTREDAME, C., JOHNSON, A., VONG, S., LEE, K., BATES, D., NERI, F., DIEGEL, M., CANFIELD, T., SABO, P. J., WILKEN, M. S., REH, T. A., GISTE, E., SHAFER, A., KUTYAVIN, T., HAUGEN, E., DUNN, D., REYNOLDS, A. P., NEPH, S., HUMBERT, R., HANSEN, R. S., DE BRUIJN, M., et al. 2014. A comparative encyclopedia of DNA elements in the mouse genome. *Nature,* 515**,** 355-64.

ZARET, K. S. & CARROLL, J. S. 2011. Pioneer transcription factors: establishing competence for gene expression. *Genes Dev,* 25**,** 2227-41.

ZHANG, D. X. & GLASS, C. K. 2013. Towards an understanding of cell-specific functions of signal-dependent transcription factors. *J Mol Endocrinol,* 51**,** T37-50.

ZHANG, Y., LIU, T., MEYER, C. A., EECKHOUTE, J., JOHNSON, D. S., BERNSTEIN, B. E., NUSBAUM, C., MYERS, R. M., BROWN, M., LI, W. & LIU, X. S. 2008. Model-based analysis of ChIP-Seq (MACS). *Genome Biol,* 9**,** R137.

ZHUANG, Y., SORIANO, P. & WEINTRAUB, H. 1994. The helix-loop-helix gene E2A is required for B cell formation. *Cell,* 79**,** 875-84.

Supplement data

Supplemental Table 1: ChIP-Sequencing raw reads.

ChIP sample	# reads processed	# reads uniquely mapped (paired-end)
GR replicate 1	36552517	29641799
GR replicate 2	40180888	33246622
E2A replicate 1	41481309	26052840
E2A replicate 2	30346951	22700288

Supplemental Table 2: GR ChIP-Sequencing peaks in liver.
GR ChIP-Seq data from Dex-treated liver is shown. Selected peaks discussed above are listed. Data represents n=1.

Peak	Start	End	Annotation	Distance to TSS	Symbol	Gene name
chr2	173153073	173154459	Promoter (<=1kb)	0	Pck1	phosphoenolpyruvate carboxykinase 1, cytosolic
chr2	155059312	155074497	Distal Intergenic	17653	Ahcy	S-adenosylhomocysteine hydrolase
chr4	106561038	106589113	Intron (uc008tyl.1/74754, intron 2 of 8)	4135	Dhcr24	24-dehydrocholesterol reductase
chr5	114165518	114250758	Intron (uc008yzi.2/100705, intron 1 of 51)	7435	Acacb	acetyl-Coenzyme A carboxylase beta
chr6	5483351	5496278	3' UTR	10852	Pdk4	pyruvate dehydrogenase kinase, isoenzyme 4
chr7	26931631	26939386	Distal Intergenic	21896	Cyp2a22	cytochrome P450, family 2, subfamily a, polypeptide 22
chr7	143823167	143848410	Intron (uc009kqc.1/13360, intron 2 of 8)	10471	Dhcr7	7-dehydrocholesterol reductase
chr8	109990436	109999804	Distal Intergenic	13841	Tat	tyrosine aminotransferase
chr9	46240844	46243458	Promoter (1-2kb)	-1511	Apoa4	apolipoprotein A-IV
chr11	7197787	7202546	Distal Intergenic	-2711	Igfbp1	insulin-like growth factor binding protein 1
chr11	5900821	5915135	Promoter (<=1kb)	0	Gck	glucokinase
chr11	120805958	120824547	Promoter (<=1kb)	0	Fasn	fatty acid synthase
chr11	101367716	101377903	Distal Intergenic	-4982	G6pc	glucose-6-phosphatase, catalytic

chr11	69098956	69109957	Promoter (<=1kb)	0	Per1	period circadian clock 1
chr11	60199084	60220627	Distal Intergenic	-3859	Srebf1	sterol regulatory element binding transcription factor 1
chr11	110176821	110251776	Exon (uc007mdj.3/76184, exon 5 of 39)	6504	Abca6	ATP-binding cassette, sub-family A (ABC1), member 6
chr13	96648962	96670936	Distal Intergenic	-2888	Hmgcr	3-hydroxy-3-methylglutaryl-Coenzyme A reductase
chr13	119690351	119702186	Intron (uc007rzu.1/245269, intron 2 of 3)	25793	Hmgcs1	3-hydroxy-3-methylglutaryl-Coenzyme A synthase 1
chr19	39510822	39568529	Promoter (<=1kb)	0	Cyp2c39	cytochrome P450, family 2, subfamily c, polypeptide 39
chr19	55069734	55127216	Distal Intergenic	-4413	Gpam	glycerol-3-phosphate acyltransferase, mitochondrial

Supplemental Table 3: Genes differentially expressed in livers of Dex-treated *E47-/-* mice.
Results from RNA-Seq in liver indicating the fold change (FC) in gene expression as log2 (log2FC). The top 50 up and downregulated genes (FC1.3; p-value<0.05 and selected genes discussed above) are listed. Data represents n=2 (WT) & 3 (*E47-/-)*.

Ensembl gene	log2 FC	p-value	MGI (Mouse Genome Interactive) symbol
ENSMUSG00000037411	-4,93	0,00	Serpine1
ENSMUSG00000022376	-4,59	0,01	Adcy8
ENSMUSG00000038665	-3,72	0,01	Dgki
ENSMUSG00000026360	-3,14	0,01	Rgs2
ENSMUSG00000032899	-3,13	0,01	Styk1
ENSMUSG00000051439	-2,69	0,00	Cd14
ENSMUSG00000026012	-2,49	0,00	Cd28
ENSMUSG00000043013	-2,37	0,05	Onecut1
ENSMUSG00000040111	-2,34	0,00	Gramd1b
ENSMUSG00000041550	-2,26	0,01	Serpina5
ENSMUSG00000105703	-2,19	0,00	Gm43305
ENSMUSG00000009394	-2,19	0,00	Syn2
ENSMUSG00000025909	-1,94	0,01	Sntg1
ENSMUSG00000067279	-1,92	0,04	Ppp1r3c
ENSMUSG00000028195	-1,89	0,00	Cyr61
ENSMUSG00000092075	-1,88	0,02	Serpina4-ps1
ENSMUSG00000038349	-1,86	0,00	Plcl1
ENSMUSG00000033998	-1,80	0,00	Kcnk1
ENSMUSG00000078922	-1,74	0,00	Tgtp1
ENSMUSG00000059824	-1,72	0,00	Dbp
ENSMUSG00000041567	-1,70	0,00	Serpina12
ENSMUSG00000066477	-1,65	0,00	Gm16551
ENSMUSG00000026628	-1,59	0,00	Atf3
ENSMUSG00000006154	-1,58	0,02	Eps8l1
ENSMUSG00000059743	-1,58	0,00	Fdps
ENSMUSG00000020423	-1,54	0,00	Btg2
ENSMUSG00000026475	-1,50	0,00	Rgs16
ENSMUSG00000029381	-1,50	0,00	Shroom3
ENSMUSG00000047109	-1,47	0,01	Cldn14
ENSMUSG00000069892	-1,47	0,04	9930111J21Rik2
ENSMUSG00000084996	-1,45	0,01	Gm11419
ENSMUSG00000030256	-1,45	0,00	Bhlhe41
ENSMUSG00000020649	-1,44	0,00	Rrm2
ENSMUSG00000027954	-1,39	0,00	Efna1
ENSMUSG00000051361	-1,38	0,04	6030498E09Rik
ENSMUSG00000015451	-1,34	0,00	C4a
ENSMUSG00000068877	-1,34	0,00	Selenbp2
ENSMUSG00000021573	-1,34	0,01	Tppp
ENSMUSG00000020205	-1,33	0,00	Phlda1
ENSMUSG00000038530	-1,33	0,02	Rgs4
ENSMUSG00000034936	-1,31	0,00	Arl4d
ENSMUSG00000038415	-1,31	0,00	Foxq1
ENSMUSG00000003541	-1,29	0,00	Ier3

ENSMUSG00000027313	-1,26	0,00	Chac1
ENSMUSG00000019966	-1,26	0,01	Kitl
ENSMUSG00000022351	-1,23	0,00	Sqle
ENSMUSG00000089712	-1,22	0,02	Gm15889
ENSMUSG00000028681	-1,22	0,01	Ptch2
ENSMUSG00000058258	-1,20	0,02	Idi1
ENSMUSG00000020937	-1,19	0,00	Plcd3
ENSMUSG00000032080	-1,13	0,00	Apoa4
ENSMUSG00000021670	-0,84	0,01	Hmgcr
ENSMUSG00000058454	-0,77	0,01	Dhcr7
ENSMUSG00000093930	-0,74	0,07	Hmgcs1
ENSMUSG00000042010	-0,55	0,06	Acacb
ENSMUSG00000024978	-0,46	0,01	Gpam
ENSMUSG00000034926	-0,41	0,05	Dhcr24
ENSMUSG00000020429	-0,23	0,46	Igfbp1
ENSMUSG00000027513	-0,23	0,18	Pck1
ENSMUSG00000041798	-0,06	0,80	Gck
ENSMUSG00000078650	0,27	0,23	G6pc
ENSMUSG00000068086	0,38	0,03	Cyp2d9
ENSMUSG00000022821	0,38	0,04	Hgd
ENSMUSG00000045193	0,39	0,04	Cirbp
ENSMUSG00000027997	0,39	0,05	Casp6
ENSMUSG00000089960	0,40	0,03	Ugt1a1
ENSMUSG00000045374	0,41	0,04	Wdr81
ENSMUSG00000039450	0,42	0,03	Dcxr
ENSMUSG00000020919	0,44	0,04	Stat5b
ENSMUSG00000021236	0,44	0,03	Entpd5
ENSMUSG00000018427	0,44	0,04	Ypel2
ENSMUSG00000073147	0,45	0,05	5031425E22Rik
ENSMUSG00000069922	0,47	0,04	Ces3a
ENSMUSG00000052632	0,47	0,03	Asap2
ENSMUSG00000028863	0,48	0,04	Meaf6
ENSMUSG00000000275	0,48	0,01	Trim25
ENSMUSG00000056966	0,49	0,05	Gjc3
ENSMUSG00000031788	0,49	0,04	Kifc3
ENSMUSG00000037254	0,49	0,02	Itih2
ENSMUSG00000066319	0,50	0,02	Rtp3
ENSMUSG00000061353	0,51	0,03	Cxcl12
ENSMUSG00000025260	0,51	0,02	Hsd17b10
ENSMUSG00000024887	0,52	0,04	Asah2
ENSMUSG00000052062	0,53	0,02	Pard3b
ENSMUSG00000034837	0,53	0,04	Gnat1
ENSMUSG00000042248	0,53	0,03	Cyp2c37
ENSMUSG00000026489	0,53	0,02	Coq8a
ENSMUSG00000031147	0,54	0,03	Magix
ENSMUSG00000021884	0,55	0,01	Hacl1
ENSMUSG00000101939	0,55	0,01	Gm28438
ENSMUSG00000086628	0,56	0,01	Gm16157

ENSMUSG00000046532	0,57	0,04	Ar
ENSMUSG00000032724	0,57	0,00	Abtb2
ENSMUSG00000039202	0,57	0,01	Abhd2
ENSMUSG00000027259	0,58	0,04	Adal
ENSMUSG00000020038	0,59	0,02	Cry1
ENSMUSG00000055116	0,59	0,02	Arntl
ENSMUSG00000040706	0,59	0,03	Agmat
ENSMUSG00000042453	0,59	0,02	Reln
ENSMUSG00000026272	0,60	0,00	Agxt
ENSMUSG00000036655	0,60	0,04	Colec11
ENSMUSG00000039395	0,61	0,01	Mreg
ENSMUSG00000020620	0,63	0,00	Abca8b
ENSMUSG00000015357	0,63	0,00	Clpx
ENSMUSG00000028150	0,65	0,02	Rorc
ENSMUSG00000033318	0,66	0,01	Gstt2
ENSMUSG00000010025	0,67	0,05	Aldh3a2
ENSMUSG00000097729	0,68	0,01	2310015A10Rik
ENSMUSG00000005677	0,68	0,01	Nr1i3
ENSMUSG00000090555	0,69	0,01	Gm8893
ENSMUSG00000023017	0,69	0,03	Asic1
ENSMUSG00000005413	0,69	0,01	Hmox1

Supplemental Table 4: Genes differentially expressed in livers of Cort-treated *E47-/-* mice.
Results from RNA-Seq in liver indicating the fold change (FC) in gene expression as log2 (log2FC). The top 50 up and downregulated genes (FC1.3; p-value<0.05 and selected genes discussed above) are listed. Data represents n=4 per genotype.

Ensembl gene	log2 FC	p-value	MGI (Mouse Genome Interactive) symbol
ENSMUSG00000040660	-6,38	0,00	Cyp2b9
ENSMUSG00000028664	-4,10	0,00	Ephb2
ENSMUSG00000050359	-4,05	0,00	Sprr1a
ENSMUSG00000034634	-4,02	0,00	Ly6d
ENSMUSG00000074254	-3,73	0,00	Cyp2a4
ENSMUSG00000029816	-3,22	0,00	Gpnmb
ENSMUSG00000029272	-2,99	0,00	Sult1e1
ENSMUSG00000053168	-2,65	0,00	9030619P08Rik
ENSMUSG00000067656	-2,53	0,00	Slc22a27
ENSMUSG00000091867	-2,52	0,00	Cyp2a22
ENSMUSG00000022947	-2,46	0,00	Cbr3
ENSMUSG00000040809	-2,30	0,00	Chil3
ENSMUSG00000004038	-2,19	0,00	Gstm3
ENSMUSG00000020037	-2,16	0,00	Rfx4
ENSMUSG00000106069	-2,15	0,00	Gm6135
ENSMUSG00000045502	-2,09	0,00	Hcar2
ENSMUSG00000035186	-2,00	0,00	Ubd
ENSMUSG00000006398	-1,95	0,00	Cdc20
ENSMUSG00000026691	-1,94	0,04	Fmo3

ENSMUSG00000074183	-1,93	0,00	Gsta1
ENSMUSG00000049493	-1,88	0,00	Pls1
ENSMUSG00000045934	-1,88	0,00	Mtmr11
ENSMUSG00000074179	-1,87	0,00	Gm10639
ENSMUSG00000037139	-1,86	0,01	Myom3
ENSMUSG00000037419	-1,85	0,00	Endod1
ENSMUSG00000049109	-1,85	0,01	Themis
ENSMUSG00000049723	-1,82	0,00	Mmp12
ENSMUSG00000032080	-1,81	0,00	Apoa4
ENSMUSG00000021208	-1,79	0,00	Ifi27l2b
ENSMUSG00000102813	-1,79	0,00	Gm37795
ENSMUSG00000029188	-1,78	0,00	Slc34a2
ENSMUSG00000031150	-1,75	0,00	Ccdc120
ENSMUSG00000024640	-1,73	0,00	Psat1
ENSMUSG00000041219	-1,68	0,00	Arhgap11a
ENSMUSG00000092008	-1,67	0,03	Cyp2c69
ENSMUSG00000002944	-1,60	0,00	Cd36
ENSMUSG00000012187	-1,57	0,00	Mogat1
ENSMUSG00000064246	-1,57	0,00	Chil1
ENSMUSG00000027699	-1,56	0,00	Ect2
ENSMUSG00000031271	-1,55	0,00	Serpina7
ENSMUSG00000017002	-1,54	0,00	Slpi
ENSMUSG00000028712	-1,52	0,00	Cyp4a31
ENSMUSG00000028555	-1,51	0,00	Ttc39a
ENSMUSG00000035385	-1,50	0,05	Ccl2
ENSMUSG00000019577	-1,46	0,02	Pdk4
ENSMUSG00000001228	-1,46	0,00	Uhrf1
ENSMUSG00000040562	-1,45	0,00	Gstm2
ENSMUSG00000035439	-1,43	0,00	Haus8
ENSMUSG00000025003	-1,43	0,00	Cyp2c39
ENSMUSG00000042010	-1,18	0,00	Acacb
ENSMUSG00000093930	-1,03	0,00	Hmgcs1
ENSMUSG00000034926	-0,59	0,00	Dhcr24
ENSMUSG00000058454	-0,40	0,03	Dhcr7
ENSMUSG00000020429	-0,33	0,54	Igfbp1
ENSMUSG00000041798	-0,26	0,16	Gck
ENSMUSG00000021670	-0,24	0,20	Hmgcr
ENSMUSG00000078650	-0,06	0,79	G6pc
ENSMUSG00000027513	0,21	0,16	Pck1
ENSMUSG00000052921	0,38	0,00	Arhgef15
ENSMUSG00000047867	0,38	0,02	Gimap6
ENSMUSG00000024055	0,38	0,00	Cyp4f13
ENSMUSG00000060036	0,38	0,03	Rpl3
ENSMUSG00000004655	0,38	0,00	Aqp1
ENSMUSG00000028776	0,38	0,00	Tinagl1
ENSMUSG00000036819	0,38	0,00	Jmjd4
ENSMUSG00000022091	0,38	0,04	Sorbs3
ENSMUSG00000087141	0,39	0,00	Plcxd2

ENSMUSG00000030087	0,39	0,02	Klf15
ENSMUSG00000027778	0,39	0,01	Ift80
ENSMUSG00000024151	0,39	0,01	Msh2
ENSMUSG00000031605	0,39	0,00	Klhl2
ENSMUSG00000034522	0,39	0,04	Zfp395
ENSMUSG00000027300	0,39	0,01	Ubox5
ENSMUSG00000054252	0,39	0,02	Fgfr3
ENSMUSG00000030067	0,39	0,00	Foxp1
ENSMUSG00000072620	0,39	0,01	Slfn2
ENSMUSG00000019966	0,39	0,03	Kitl
ENSMUSG00000027332	0,39	0,01	Ivd
ENSMUSG00000082536	0,39	0,01	Gm13456
ENSMUSG00000043065	0,39	0,02	Spice1
ENSMUSG00000057037	0,39	0,00	Cfhr1
ENSMUSG00000007872	0,39	0,04	Id3
ENSMUSG00000024440	0,40	0,03	Pcdh12
ENSMUSG00000022708	0,40	0,00	Zbtb20
ENSMUSG00000062619	0,40	0,00	2310039H08Rik
ENSMUSG00000004748	0,40	0,00	Mtfp1
ENSMUSG00000022353	0,40	0,01	Mtss1
ENSMUSG00000020644	0,40	0,03	Id2
ENSMUSG00000058396	0,40	0,00	Gpr182
ENSMUSG00000022610	0,40	0,02	Mapk12
ENSMUSG00000057842	0,40	0,01	Zfp595
ENSMUSG00000086825	0,40	0,00	Gm15675
ENSMUSG00000021134	0,41	0,00	Srsf5
ENSMUSG00000006464	0,41	0,03	Bbs1
ENSMUSG00000101397	0,41	0,00	Mug-ps1
ENSMUSG00000060301	0,41	0,00	2610008E11Rik
ENSMUSG00000044469	0,41	0,05	Tnfaip8l1
ENSMUSG00000024065	0,41	0,01	Ehd3
ENSMUSG00000034911	0,41	0,00	Ushbp1
ENSMUSG00000055862	0,41	0,00	Izumo4
ENSMUSG00000031365	0,41	0,02	Zfp275
ENSMUSG00000028381	0,41	0,00	Ugcg
ENSMUSG00000031167	0,41	0,01	Rbm3
ENSMUSG00000015656	0,42	0,01	Hspa8
ENSMUSG00000030424	0,42	0,04	Zfp939
ENSMUSG00000029471	0,42	0,01	Camkk2
ENSMUSG00000021947	0,42	0,00	Cryl1
ENSMUSG00000096971	0,42	0,03	4930556M19Rik
ENSMUSG00000071711	0,42	0,01	Mpst

Supplemental Table 5: Genes differentially expressed in livers of untreated *E47-/-* mice.
Results from RNA-Seq in liver indicating the fold change (FC) in gene expression as log2 (log2FC). The top 50 up and downregulated genes (FC1.3; p-value<0.05) are listed. Data represents n= 5 (WT) & 6 (E47-/-).

Ensembl gene	log2 FC	p-value	MGI (Mouse Genome Interactive) symbol
ENSMUSG00000088246	-4,81	0,00	Gm25911
ENSMUSG00000076258	-2,14	0,00	Gm23935
ENSMUSG00000020037	-1,76	0,00	Rfx4
ENSMUSG00000046229	-1,76	0,01	Scand1
ENSMUSG00000096768	-1,51	0,00	Erdr1
ENSMUSG00000024365	-1,43	0,00	Cyp21a1
ENSMUSG00000097930	-1,40	0,00	C330002G04Rik
ENSMUSG00000034674	-1,35	0,00	Tdg
ENSMUSG00000076609	-1,09	0,01	Igkc
ENSMUSG00000050097	-1,06	0,04	Ces2b
ENSMUSG00000100075	-1,05	0,04	1700018L02Rik
ENSMUSG00000025004	-1,01	0,04	Cyp2c40
ENSMUSG00000038880	-1,01	0,02	Mrps34
ENSMUSG00000027983	-0,98	0,00	Cyp2u1
ENSMUSG00000106838	-0,97	0,01	1810017P11Rik
ENSMUSG00000024430	-0,96	0,02	Cabyr
ENSMUSG00000015451	-0,96	0,00	C4a
ENSMUSG00000031637	-0,95	0,00	Lrp2bp
ENSMUSG00000095098	-0,94	0,03	Ccdc85b
ENSMUSG00000029725	-0,91	0,02	Ppp1r35
ENSMUSG00000015337	-0,89	0,01	Endog
ENSMUSG00000030431	-0,87	0,01	Tmem238
ENSMUSG00000016356	-0,87	0,04	Col20a1
ENSMUSG00000020308	-0,87	0,01	Tpgs1
ENSMUSG00000092274	-0,86	0,03	Neat1
ENSMUSG00000074657	-0,86	0,04	Kif5a
ENSMUSG00000041731	-0,86	0,00	Pgm5
ENSMUSG00000078570	-0,86	0,00	1110065P20Rik
ENSMUSG00000033751	-0,84	0,02	Gadd45gip1
ENSMUSG00000053175	-0,82	0,00	Bcl3
ENSMUSG00000037583	-0,82	0,04	Nr0b2
ENSMUSG00000070282	-0,81	0,00	3000002C10Rik
ENSMUSG00000004814	-0,79	0,03	Ccl24
ENSMUSG00000035711	-0,79	0,05	Dok3
ENSMUSG00000069601	-0,78	0,00	Ank3
ENSMUSG00000040264	-0,77	0,04	Gbp2b
ENSMUSG00000069919	-0,76	0,00	Hba-a1
ENSMUSG00000032077	-0,76	0,03	Bud13
ENSMUSG00000024925	-0,74	0,01	Rnaseh2c
ENSMUSG00000043251	-0,73	0,01	Exoc3l
ENSMUSG00000053613	-0,73	0,03	Notumos
ENSMUSG00000003378	-0,72	0,02	Grik5
ENSMUSG00000086544	-0,72	0,03	Chn1os3
ENSMUSG00000022010	-0,71	0,03	Tsc22d1

ENSMUSG00000074794	-0,71	0,04	Arrdc3
ENSMUSG00000008035	-0,70	0,04	Mid1ip1
ENSMUSG00000022129	-0,70	0,04	Dct
ENSMUSG00000021495	-0,69	0,02	Fam193b
ENSMUSG00000042293	-0,69	0,05	Gm5617
ENSMUSG00000091337	0,38	0,04	Eid1
ENSMUSG00000030247	0,38	0,01	Kcnj8
ENSMUSG00000028173	0,39	0,01	Wls
ENSMUSG00000056025	0,39	0,01	Clca3a1
ENSMUSG00000029765	0,39	0,05	Plxna4
ENSMUSG00000026678	0,39	0,02	Rgs5
ENSMUSG00000029385	0,40	0,01	Ccng2
ENSMUSG00000019806	0,40	0,01	Aig1
ENSMUSG00000035273	0,40	0,00	Hpse
ENSMUSG00000026728	0,40	0,04	Vim
ENSMUSG00000029571	0,40	0,01	Tmem106b
ENSMUSG00000052534	0,41	0,00	Pbx1
ENSMUSG00000026768	0,41	0,02	Itga8
ENSMUSG00000022146	0,42	0,04	Osmr
ENSMUSG00000034926	0,42	0,00	Dhcr24
ENSMUSG00000020467	0,43	0,02	Efemp1
ENSMUSG00000028211	0,43	0,01	Trp53inp1
ENSMUSG00000004631	0,44	0,04	Sgce
ENSMUSG00000025887	0,44	0,05	Casp12
ENSMUSG00000021335	0,44	0,02	Slc17a1
ENSMUSG00000031561	0,44	0,05	Tenm3
ENSMUSG00000027848	0,45	0,02	Olfml3
ENSMUSG00000023915	0,45	0,01	Tnfrsf21
ENSMUSG00000030249	0,45	0,01	Abcc9
ENSMUSG00000086332	0,45	0,01	4930480G23Rik
ENSMUSG00000025969	0,46	0,05	Nrp2
ENSMUSG00000029309	0,46	0,02	Sparcl1
ENSMUSG00000031278	0,47	0,02	Acsl4
ENSMUSG00000019929	0,47	0,00	Dcn
ENSMUSG00000030823	0,47	0,03	9130019O22Rik
ENSMUSG00000029231	0,48	0,01	Pdgfra
ENSMUSG00000014329	0,48	0,02	Bicc1
ENSMUSG00000021943	0,49	0,04	Gdf10
ENSMUSG00000021665	0,50	0,02	Hexb
ENSMUSG00000019850	0,50	0,01	Tnfaip3
ENSMUSG00000034573	0,50	0,02	Ptpn13
ENSMUSG00000026303	0,50	0,04	Mlph
ENSMUSG00000082292	0,50	0,04	Gm12250
ENSMUSG00000032245	0,51	0,00	Cln6
ENSMUSG00000041272	0,52	0,01	Tox
ENSMUSG00000021573	0,52	0,01	Tppp
ENSMUSG00000029167	0,52	0,01	Ppargc1a
ENSMUSG00000060397	0,53	0,03	Zfp128

ENSMUSG00000054942	0,54	0,01	Miga1
ENSMUSG00000027962	0,56	0,00	Vcam1
ENSMUSG00000033107	0,56	0,01	Rnf125
ENSMUSG00000011034	0,58	0,01	Slc5a1
ENSMUSG00000041773	0,59	0,01	Enc1
ENSMUSG00000029417	0,63	0,05	Cxcl9
ENSMUSG00000027864	0,63	0,00	Ptgfrn

Supplemental Table 6: Genes differentially expressed in muscle of Dex-treated *E47-/-* mice.
Results from RNA-Seq in skeletal muscle indicating the fold change (FC) in gene expression as log2 (log2FC). The top 50 up and downregulated genes (FC1.3; p-value<0.05) are listed. Data represents n=2 (WT) & 3 (E47-/-).

Ensembl gene	log2 FC	p-value	MGI (Mouse Genome Interactive) symbol
ENSMUSG00000030359	-4,91	0,01	Pzp
ENSMUSG00000029368	-4,54	0,02	Alb
ENSMUSG00000020609	-4,50	0,04	Apob
ENSMUSG00000028011	-4,27	0,04	Tdo2
ENSMUSG00000072849	-4,26	0,04	Serpina1e
ENSMUSG00000027359	-4,23	0,04	Slc27a2
ENSMUSG00000059481	-3,93	0,05	Plg
ENSMUSG00000030895	-3,92	0,01	Hpx
ENSMUSG00000022899	-3,82	0,00	Slc15a2
ENSMUSG00000006522	-3,41	0,01	Itih3
ENSMUSG00000026715	-3,39	0,00	Serpinc1
ENSMUSG00000027249	-3,05	0,00	F2
ENSMUSG00000032081	-2,56	0,02	Apoc3
ENSMUSG00000038257	-2,39	0,00	Glra3
ENSMUSG00000021922	-2,01	0,01	Itih4
ENSMUSG00000076612	-1,79	0,02	Ighg2c
ENSMUSG00000021453	-1,56	0,03	Gadd45g
ENSMUSG00000053719	-1,50	0,00	Klk1b26
ENSMUSG00000021135	-1,48	0,04	Slc10a1
ENSMUSG00000034674	-1,45	0,00	Tdg
ENSMUSG00000063320	-1,26	0,00	1190007I07Rik
ENSMUSG00000035189	-1,24	0,02	Ano4
ENSMUSG00000084803	-1,20	0,01	5830444B04Rik
ENSMUSG00000032726	-1,12	0,03	Bmp8a
ENSMUSG00000026622	-1,11	0,03	Nek2
ENSMUSG00000031394	-1,10	0,02	Opn1mw
ENSMUSG00000076441	-1,07	0,04	Ass1
ENSMUSG00000025887	-1,03	0,00	Casp12
ENSMUSG00000036902	-1,03	0,02	Neto2
ENSMUSG00000042045	-1,02	0,02	Sln
ENSMUSG00000056708	-0,99	0,00	Ier5
ENSMUSG00000021815	-0,94	0,00	Mss51
ENSMUSG00000097819	-0,92	0,04	Gm26813
ENSMUSG00000019988	-0,90	0,00	Nedd1

ENSMUSG00000027313	-0,90	0,01	Chac1
ENSMUSG00000098050	-0,83	0,00	Gm5345
ENSMUSG00000020737	-0,80	0,00	Jpt1
ENSMUSG00000070056	-0,80	0,00	Mfhas1
ENSMUSG00000075330	-0,78	0,03	A930003A15Rik
ENSMUSG00000043415	-0,77	0,04	Otud1
ENSMUSG00000060639	-0,77	0,01	Hist1h4i
ENSMUSG00000022144	-0,77	0,03	Gdnf
ENSMUSG00000075232	-0,76	0,05	Amd1
ENSMUSG00000097624	-0,70	0,02	Gm5091
ENSMUSG00000011179	-0,69	0,04	Odc1
ENSMUSG00000048489	-0,66	0,05	8430408G22Rik
ENSMUSG00000102573	-0,66	0,02	Gm7265
ENSMUSG00000024134	-0,65	0,01	Six2
ENSMUSG00000047037	-0,64	0,03	Nipa1
ENSMUSG00000032898	0,38	0,01	Fbxo21
ENSMUSG00000034708	0,38	0,03	Grn
ENSMUSG00000039831	0,39	0,01	Arhgap29
ENSMUSG00000026463	0,39	0,01	Atp2b4
ENSMUSG00000008540	0,39	0,04	Mgst1
ENSMUSG00000033096	0,39	0,02	Apmap
ENSMUSG00000032724	0,40	0,03	Abtb2
ENSMUSG00000031503	0,40	0,01	Col4a2
ENSMUSG00000040170	0,40	0,02	Fmo2
ENSMUSG00000041828	0,40	0,05	Abca8a
ENSMUSG00000060002	0,40	0,01	Chpt1
ENSMUSG00000027952	0,40	0,04	Pmvk
ENSMUSG00000032679	0,40	0,04	Cd59a
ENSMUSG00000034780	0,41	0,04	B3galt1
ENSMUSG00000002550	0,41	0,03	Uck1
ENSMUSG00000066026	0,42	0,02	Dhrs3
ENSMUSG00000031523	0,42	0,01	Dlc1
ENSMUSG00000071657	0,42	0,05	Bscl2
ENSMUSG00000065954	0,43	0,04	Tacc1
ENSMUSG00000022194	0,43	0,04	Pabpn1
ENSMUSG00000035863	0,43	0,04	Palm
ENSMUSG00000040687	0,44	0,05	Madd
ENSMUSG00000040147	0,44	0,02	Maob
ENSMUSG00000001802	0,44	0,04	Lrp3
ENSMUSG00000026796	0,44	0,01	Fam129b
ENSMUSG00000026879	0,44	0,02	Gsn
ENSMUSG00000027332	0,45	0,01	Ivd
ENSMUSG00000020432	0,45	0,00	Tcn2
ENSMUSG00000038065	0,45	0,03	Mturn
ENSMUSG00000025213	0,45	0,04	Kazald1
ENSMUSG00000031938	0,45	0,04	4931406C07Rik
ENSMUSG00000020473	0,45	0,01	Aebp1
ENSMUSG00000022261	0,45	0,05	Sdc2

ENSMUSG00000085348	0,46	0,03	Myhas
ENSMUSG00000028944	0,46	0,03	Prkag2
ENSMUSG00000021033	0,46	0,01	Gstz1
ENSMUSG00000000957	0,46	0,05	Mmp14
ENSMUSG00000026723	0,46	0,04	Trdmt1
ENSMUSG00000028369	0,47	0,03	Svep1
ENSMUSG00000033174	0,47	0,01	Mgll
ENSMUSG00000006373	0,47	0,04	Pgrmc1
ENSMUSG00000028494	0,47	0,03	Plin2
ENSMUSG00000021792	0,47	0,00	Fam213a
ENSMUSG00000029455	0,47	0,01	Aldh2
ENSMUSG00000056427	0,47	0,00	Slit3
ENSMUSG00000034353	0,47	0,04	Ramp1
ENSMUSG00000018427	0,48	0,00	Ypel2
ENSMUSG00000029009	0,48	0,03	Mthfr
ENSMUSG00000004098	0,48	0,01	Col5a3
ENSMUSG00000030737	0,48	0,00	Slco2b1

Supplemental Table 7: Genes differentially expressed in adipose tissue of Dex-treated *E47-/-* mice.
Results from RNA-Seq in white adipose tissue indicating the fold change (FC) in gene expression as log2 (log2FC). The top 50 up and downregulated genes (FC1.3; p-value<0.05) are listed. Data represents n=2.

Ensembl gene	log2 FC	p-value	MGI (Mouse Genome Interactive) symbol
ENSMUSG00000090015	-4,02	0,00	Gm15446
ENSMUSG00000076609	-3,91	0,00	Igkc
ENSMUSG00000057074	-3,07	0,00	Ces1g
ENSMUSG00000034674	-2,28	0,00	Tdg
ENSMUSG00000032315	-2,12	0,00	Cyp1a1
ENSMUSG00000045613	-2,00	0,03	Chrm2
ENSMUSG00000018486	-1,71	0,03	Wnt9b
ENSMUSG00000062329	-1,58	0,02	Cytl1
ENSMUSG00000020848	-1,54	0,00	Doc2b
ENSMUSG00000086446	-1,46	0,02	Prkag2os1
ENSMUSG00000030669	-1,45	0,00	Calca
ENSMUSG00000049404	-1,40	0,00	Rarres1
ENSMUSG00000105746	-1,36	0,03	Gm43595
ENSMUSG00000030162	-1,35	0,00	Olr1
ENSMUSG00000057606	-1,34	0,01	Colq
ENSMUSG00000047168	-1,32	0,04	Gm6684
ENSMUSG00000070465	-1,30	0,05	Gm9696
ENSMUSG00000029304	-1,27	0,02	Spp1
ENSMUSG00000028778	-1,26	0,00	Hcrtr1
ENSMUSG00000067235	-1,25	0,02	H2-Q10
ENSMUSG00000065987	-1,20	0,00	Cd209b
ENSMUSG00000050368	-1,19	0,02	Hoxd10
ENSMUSG00000039037	-1,18	0,00	St6galnac5

ENSMUSG00000028211	-1,14	0,00	Trp53inp1
ENSMUSG00000045392	-1,12	0,00	Olfr1033
ENSMUSG00000078915	-1,11	0,04	Hsp25-ps1
ENSMUSG00000028687	-1,09	0,00	Mutyh
ENSMUSG00000031981	-1,09	0,01	Capn9
ENSMUSG00000007480	-1,07	0,05	Mc5r
ENSMUSG00000081564	-1,07	0,02	Gm13717
ENSMUSG00000027674	-1,03	0,02	Pex5l
ENSMUSG00000034936	-1,00	0,00	Arl4d
ENSMUSG00000079559	-0,98	0,00	Colca2
ENSMUSG00000020108	-0,97	0,00	Ddit4
ENSMUSG00000071036	-0,94	0,05	Gm10309
ENSMUSG00000038068	-0,92	0,00	Rnf144b
ENSMUSG00000092274	-0,91	0,00	Neat1
ENSMUSG00000048376	-0,91	0,00	F2r
ENSMUSG00000021356	-0,89	0,00	Irf4
ENSMUSG00000063060	-0,88	0,00	Sox7
ENSMUSG00000005686	-0,88	0,01	Ampd3
ENSMUSG00000006221	-0,87	0,01	Hspb7
ENSMUSG00000062609	-0,86	0,00	Kcnj15
ENSMUSG00000005373	-0,86	0,00	Mlxipl
ENSMUSG00000026358	-0,82	0,00	Rgs1
ENSMUSG00000004951	-0,82	0,01	Hspb1
ENSMUSG00000026890	-0,82	0,00	Lhx6
ENSMUSG00000005950	-0,79	0,00	P2rx5
ENSMUSG00000040035	-0,78	0,01	Disp2
ENSMUSG00000019929	0,38	0,02	Dcn
ENSMUSG00000027227	0,39	0,01	Sord
ENSMUSG00000035413	0,39	0,03	Tmem98
ENSMUSG00000033306	0,39	0,02	Lpp
ENSMUSG00000053398	0,39	0,05	Phgdh
ENSMUSG00000026365	0,39	0,03	Cfh
ENSMUSG00000047528	0,40	0,04	Als2cr12
ENSMUSG00000035133	0,40	0,03	Arhgap5
ENSMUSG00000005973	0,41	0,03	Rcn1
ENSMUSG00000001663	0,41	0,02	Gstt1
ENSMUSG00000019768	0,42	0,02	Esr1
ENSMUSG00000073565	0,42	0,04	Prr16
ENSMUSG00000040037	0,42	0,01	Negr1
ENSMUSG00000020102	0,43	0,03	Slc16a7
ENSMUSG00000032549	0,44	0,02	Rab6b
ENSMUSG00000089783	0,45	0,04	Gm454
ENSMUSG00000026674	0,45	0,00	Ddr2
ENSMUSG00000037731	0,46	0,05	Themis2
ENSMUSG00000023224	0,47	0,03	Serping1
ENSMUSG00000022150	0,47	0,00	Dab2
ENSMUSG00000031375	0,48	0,03	Bgn
ENSMUSG00000020241	0,48	0,05	Col6a2

ENSMUSG00000033107	0,48	0,04	Rnf125
ENSMUSG00000002980	0,49	0,03	Bcam
ENSMUSG00000029417	0,49	0,03	Cxcl9
ENSMUSG00000025742	0,49	0,02	Prps2
ENSMUSG00000061119	0,50	0,05	Prcp
ENSMUSG00000094786	0,50	0,04	Gm14403
ENSMUSG00000024909	0,50	0,01	Efemp2
ENSMUSG00000021097	0,50	0,01	Clmn
ENSMUSG00000089774	0,50	0,00	Slc5a3
ENSMUSG00000052698	0,51	0,03	Tln2
ENSMUSG00000019899	0,52	0,03	Lama2
ENSMUSG00000025492	0,52	0,03	Ifitm3
ENSMUSG00000029059	0,53	0,01	Fam213b
ENSMUSG00000017466	0,53	0,02	Timp2
ENSMUSG00000032038	0,53	0,05	St3gal4
ENSMUSG00000028270	0,53	0,01	Gbp2
ENSMUSG00000031093	0,53	0,03	Dock11
ENSMUSG00000029869	0,53	0,04	Ephb6
ENSMUSG00000026389	0,54	0,01	Steap3
ENSMUSG00000031451	0,54	0,03	Gas6
ENSMUSG00000021416	0,54	0,01	Eci3
ENSMUSG00000001473	0,55	0,01	Tubb6
ENSMUSG00000051748	0,55	0,02	Wfdc21
ENSMUSG00000031367	0,55	0,02	Ap1s2
ENSMUSG00000000753	0,55	0,04	Serpinf1
ENSMUSG00000021185	0,56	0,01	Dglucy
ENSMUSG00000031342	0,57	0,03	Gpm6b
ENSMUSG00000032232	0,57	0,01	Cgnl1

Supplemental Table 8: Genes differentially expressed in livers of Dex-injected *E47*$^{\Delta LKO}$ mice.
Results from RNA-Seq in liver indicating the fold change (FC) in gene expression as log2 (log2FC). The top 50 up and downregulated genes (FC1.3; p-value<0.05 and selected genes discussed above) are listed. Data represents n=3 per genotype.

Ensembl gene	log2 FC	p-value	MGI (Mouse Genome Interactive) symbol
ENSMUSG00000103560	-2,66	0,00	Gm38070
ENSMUSG00000043013	-1,81	0,00	Onecut1
ENSMUSG00000047797	-1,62	0,01	Gjb1
ENSMUSG00000038599	-1,56	0,00	Capn8
ENSMUSG00000050663	-1,36	0,00	Trhde
ENSMUSG00000055866	-1,34	0,00	Per2
ENSMUSG00000067144	-1,19	0,00	Slc22a7
ENSMUSG00000092274	-1,14	0,00	Neat1
ENSMUSG00000078687	-1,14	0,01	Mup8
ENSMUSG00000094114	-1,06	0,00	Gm21967
ENSMUSG00000035686	-1,03	0,02	Thrsp
ENSMUSG00000068877	-0,99	0,00	Selenbp2
ENSMUSG00000060560	-0,94	0,04	Ces4a

ENSMUSG00000027313	-0,91	0,02	Chac1
ENSMUSG00000035451	-0,84	0,02	Foxa1
ENSMUSG00000021573	-0,84	0,00	Tppp
ENSMUSG00000090015	-0,84	0,03	Gm15446
ENSMUSG00000031441	-0,83	0,00	Atp11a
ENSMUSG00000041827	-0,82	0,01	Oasl1
ENSMUSG00000028838	-0,82	0,04	Extl1
ENSMUSG00000031530	-0,81	0,02	Dusp4
ENSMUSG00000034220	-0,81	0,01	Gpc1
ENSMUSG00000047394	-0,81	0,01	Odf3b
ENSMUSG00000031822	-0,80	0,03	Gse1
ENSMUSG00000079494	-0,80	0,00	Nat8f5
ENSMUSG00000020205	-0,78	0,01	Phlda1
ENSMUSG00000042834	-0,78	0,01	Nrep
ENSMUSG00000102095	-0,77	0,00	C730036E19Rik
ENSMUSG00000054793	-0,77	0,04	Cadm4
ENSMUSG00000036006	-0,76	0,03	Fam65b
ENSMUSG00000041417	-0,76	0,00	Pik3r1
ENSMUSG00000034640	-0,75	0,00	Tiparp
ENSMUSG00000097750	-0,74	0,03	Gm4673
ENSMUSG00000030124	-0,74	0,03	Lag3
ENSMUSG00000086231	-0,74	0,01	Rapgef4os3
ENSMUSG00000079484	-0,73	0,02	Phyhd1
ENSMUSG00000034645	-0,73	0,04	Zyg11a
ENSMUSG00000038894	-0,72	0,03	Irs2
ENSMUSG00000073940	-0,72	0,02	Hbb-bt
ENSMUSG00000073940	-0,72	0,02	Hbb-bt
ENSMUSG00000073940	-0,72	0,02	Hbb-bt
ENSMUSG00000032860	-0,72	0,02	P2ry2
ENSMUSG00000079243	-0,72	0,04	Xirp1
ENSMUSG00000063171	-0,71	0,01	Rps4l
ENSMUSG00000053175	-0,71	0,01	Bcl3
ENSMUSG00000031661	-0,70	0,03	Nkd1
ENSMUSG00000034584	-0,70	0,00	Exph5
ENSMUSG00000019947	-0,69	0,03	Arid5b
ENSMUSG00000040127	-0,69	0,00	Sdr9c7
ENSMUSG00000032080	-0,45	0,05	Apoa4
ENSMUSG00000078650	-0,23	0,26	G6pc
ENSMUSG00000093930	-0,14	0,72	Hmgcs1
ENSMUSG00000020429	-0,11	0,69	Igfbp1
ENSMUSG00000021670	-0,07	0,78	Hmgcr
ENSMUSG00000042010	-0,04	0,87	Acacb
ENSMUSG00000058454	-0,03	0,86	Dhcr7
ENSMUSG00000041798	-0,01	0,98	Gck
ENSMUSG00000034926	0,13	0,17	Dhcr24
ENSMUSG00000027513	0,18	0,23	Pck1
ENSMUSG00000024222	0,39	0,02	Fkbp5
ENSMUSG00000045854	0,39	0,05	Lyrm2

ENSMUSG00000037172	0,40	0,03	E330009J07Rik
ENSMUSG00000024863	0,40	0,01	Mbl2
ENSMUSG00000022629	0,40	0,00	Kif21a
ENSMUSG00000006445	0,40	0,02	Epha2
ENSMUSG00000027999	0,40	0,03	Pla2g12a
ENSMUSG00000020865	0,43	0,00	Abcc3
ENSMUSG00000074170	0,43	0,05	Plekhf1
ENSMUSG00000040557	0,43	0,04	Wbscr27
ENSMUSG00000031765	0,43	0,03	Mt1
ENSMUSG00000027508	0,43	0,02	Pag1
ENSMUSG00000022091	0,43	0,04	Sorbs3
ENSMUSG00000032349	0,44	0,02	Elovl5
ENSMUSG00000039745	0,44	0,01	Htatip2
ENSMUSG00000058135	0,44	0,01	Gstm1
ENSMUSG00000070690	0,45	0,00	5830473C10Rik
ENSMUSG00000028195	0,45	0,04	Cyr61
ENSMUSG00000022637	0,46	0,02	Cblb
ENSMUSG00000019806	0,46	0,04	Aig1
ENSMUSG00000020451	0,46	0,04	Limk2
ENSMUSG00000024254	0,47	0,02	Abcg8
ENSMUSG00000020023	0,47	0,00	Tmcc3
ENSMUSG00000038578	0,47	0,05	Susd1
ENSMUSG00000025915	0,48	0,01	Sgk3
ENSMUSG00000050188	0,49	0,03	Lsm10
ENSMUSG00000024962	0,49	0,03	Vegfb
ENSMUSG00000050947	0,49	0,03	Amigo1
ENSMUSG00000030237	0,49	0,01	Slco1a4
ENSMUSG00000023963	0,49	0,01	Cyp39a1
ENSMUSG00000040505	0,50	0,03	Abcg5
ENSMUSG00000042429	0,53	0,05	Adora1
ENSMUSG00000026839	0,53	0,02	Upp2
ENSMUSG00000000385	0,54	0,02	Tmprss2
ENSMUSG00000041238	0,54	0,02	Rbbp8
ENSMUSG00000056978	0,57	0,03	Hamp2
ENSMUSG00000072949	0,57	0,00	Acot1
ENSMUSG00000053411	0,58	0,05	Cbx7
ENSMUSG00000003134	0,58	0,00	Tbc1d8
ENSMUSG00000005268	0,59	0,00	Prlr
ENSMUSG00000060807	0,59	0,00	Serpina6
ENSMUSG00000030852	0,60	0,00	Tacc2
ENSMUSG00000002944	0,60	0,02	Cd36
ENSMUSG00000060470	0,61	0,04	Adgrg3
ENSMUSG00000026956	0,64	0,02	Uap1l1
ENSMUSG00000037325	0,64	0,02	Bbs7
ENSMUSG00000022089	0,64	0,00	Bin3
ENSMUSG00000034774	0,64	0,05	Dsg1c
ENSMUSG00000027487	0,65	0,00	Cdk5rap1
ENSMUSG00000019232	0,65	0,01	Etnppl

Supplemental Table 9: ChIP-MS peptide counts in wildtype and *E47* mutant liver.
Peptide read counts for each biological replicate determined by the MaxLFQ algorithm. Selected proteins discussed above are shown. Data represents n=3 per genotype.

	WT _IgG			WT _GR			E47-/- _IgG			E47-/-_GR		
Replicates	**1**	**2**	**3**	**1**	**2**	**3**	**1**	**2**	**3**	**1**	**2**	**3**
Nr3c1 (GR)	1	0	2	38	37	31	1	1	1	39	40	38
Cebpa	0	0	0	3	2	2	1	1	1	2	3	2
Cebpb	0	0	1	7	6	5	0	0	1	7	7	7
Rxra	0	0	0	17	15	5	1	0	1	17	16	17
Hnf4a	1	3	2	8	6	5	3	3	2	9	8	9
Ncoa1	0	0	0	2	3	0	0	0	0	3	3	2
Ncoa2	0	0	0	5	4	0	0	0	0	8	4	5
Ncoa3	0	0	0	5	5	0	0	0	0	6	5	4
Foxo1	0	0	0	2	2	0	0	0	0	2	0	1
Med16	0	0	0	2	2	2	0	0	0	2	1	2
Med23	0	0	0	2	3	0	0	0	0	3	1	1
Med24	0	1	0	6	5	1	0	0	0	7	6	6

Supplemental Table 10a: Relative luciferase values of reporter screen.
Luciferase value for each reporter sequence was compared to vehicle and empty vector. Average of triplicates are shown.

Plate	Well	GR + EtOH	GR + Dex	GR + Cort	Gene symbol	Gene description
1	H05	0,12	0,05	0,06	NO_ANNOTATION	Homo sapiens beta-2-microglobulin
1	D02	0,07	0,08	0,05	CAST1	
1	F02	0,24	0,09	0,09	OBSCN	obscurin
2	D10	0,06	0,09	0,09	SEPX1	
1	A11	0,17	0,10	0,07	WNT5A	Wnt 5A
1	H03	0,14	0,12	0,16	MEST	mesoderm specific transcript homolog
1	F04	0,15	0,13	0,13	HDAC7A	
2	A01	0,40	0,15	0,16	WNT5A	Wnt 5A
1	G06	0,60	0,15	0,19	FLJ44861	
1	F11	0,14	0,18	0,18	CD160	CD160 molecule
1	F08	0,53	0,19	0,19	NO_ANNOTATION	
1	F06	0,29	0,19	0,18	FMOD	fibromodulin
1	G03	0,35	0,22	0,33	MEST	mesoderm specific transcript homolog
2	D07	0,08	0,23	0,20	PSMA6	proteasome subunit, alpha type, 6
1	D05	0,30	0,24	0,32	NO_ANNOTATION	PTPRN2
2	C10	0,83	0,25	0,23	NO_ANNOTATION	
2	A02	0,26	0,25	0,26	HSP90AB1	heat shock protein 90kDa alpha class B1
1	A09	0,28	0,25	0,18	RAB11A	RAB11A, member RAS oncogene family
1	D08	0,19	0,26	0,25	NCOA1	nuclear receptor coactivator 1
2	E04	0,16	0,27	0,21	ZFP36L1	ZFP36L1-prom

1	D03	0,52	0,39	0,27	MYO18A	
2	D05	0,53	0,41	0,40	COMT	catechol-O-methyltransferase
1	E03	2,32	0,42	0,42	IFNE1	interferon epsilon 1
1	E10	0,08	0,46	0,58	NO_ANNOTATION	
2	E02	1,00	0,47	0,48	AMPD3	AMPD3-altprom2
1	D07	1,06	0,49	0,43	IL9R	interleukin 9 receptor
2	E06	1,13	0,55	0,53	CCL2	CCL2-prom
1	B06	0,19	0,55	0,45	COMT	catechol-O-methyltransferase
1	H04	0,20	0,56	0,28	SERPINA1	serpin peptidase inhibitor, clade A 1
1	A03	1,21	0,59	0,49	TXN	thioredoxin
2	D06	2,29	0,59	0,68	SMURF2	SMAD specific E3 ubiquitin protein ligase 2
1	G11	0,35	0,59	0,48	SRPK2	SFRS protein kinase 2
1	A10	0,43	0,60	0,47	CHIC2	cysteine-rich hydrophobic domain 2
2	G04	2,04	0,65	0,58	MEST	mesoderm specific transcript homolog
2	F03	0,19	0,66	0,75	TSC22d3	CHR7_P0902-R2
1	D06	1,30	0,66	0,34	RBM protein 33	
1	E04	0,82	0,67	0,45	NO_ANNOTATION	
1	A08	0,81	0,69	0,62	IER2	immediate early response 2
1	H02	0,66	0,70	0,69	UGCG	UDP-glucose ceramide glucosyltransferase
1	A02	0,77	0,72	0,40	BRD2	bromodomain containing 2
2	A03	0,20	0,77	0,83	GLUL	glutamate-ammonia ligase
2	C07	3,03	0,89	0,95	NO_ANNOTATION	

2	A11	4,19	0,90	1,00	SERPINA1	serpin peptidase inhibitor, clade A 1
2	G01	1,29	0,91	0,98	TXN	thioredoxin
2	C04	0,58	0,92	1,15	RNF10	ring finger protein 10
1	H07	2,66	0,95	0,91	RP11-85L21.3	
2	C08	4,77	1,03	1,24	AC084398	Damage-regulated autophagy modulator
1	F01	1,89	1,04	1,35	FAM55A	
1	F03	0,59	1,04	1,13	PMM2	phosphomannomutase 2
1	G02	1,02	1,06	1,16	PHGDH	phosphoglycerate dehydrogenase
2	C05	2,51	1,09	1,09	NO_ANNOTATION	
2	E11	2,57	1,09	1,28	FAM117B	ALS2CR13_b
2	G05	1,36	1,14	1,00	IGFBP1	insulin-like growth factor binding protein 1
1	A05	0,87	1,15	1,08	IDH1	isocitrate dehydrogenase 1 (NADP+)
1	B04	1,09	1,21	1,35	MEST	mesoderm specific transcript homolog
2	C03	4,28	1,22	1,36	ENC1	ectodermal-neural cortex
1	A04	1,05	1,23	0,39	HSP90AB1	heat shock protein 90kDa alpha 1
1	F07	1,55	1,24	1,07	GIMAP8	GTPase, IMAP family member 8
2	A05	1,33	1,26	1,14	ATP6AP1	ATPase, lysosomal accessory protein 1
2	B05	1,83	1,27	1,03	SERPINA1	serpin peptidase inhibitor, clade A 1
2	A06	1,18	1,28	1,10	MTCH2	mitochondrial carrier homolog 2
1	E11	0,93	1,28	0,99	NO_ANNOTATION	
2	E09	3,09	1,29	1,11	EDN1	EDN1-prom
1	B02	2,20	1,31	1,31	TPST2	tyrosylprotein sulfotransferase 2

2	C11	2,86	1,33	1,45	RABGGTB	
1	G09	0,19	1,38	1,07	SERINC3	serine incorporator 3
1	A01	1,15	1,39	1,09	RNF11	ring finger protein 11
2	G08	7,27	1,39	1,63	CKS1B	CDC28 protein kinase regulatory subunit 1B
2	F08	1,20	1,48	1,31	HSP90AB1	heat shock protein 90kDa alpha B1
2	D08	0,85	1,56	1,12	B2M	beta-2-microglobulin
1	H09	1,55	1,57	1,65	IDH1	isocitrate dehydrogenase 1 (NADP+)
2	F09	9,31	1,70	2,17	PLA2G2E	phospholipase A2, group IIE
1	H10	1,63	1,74	1,58	TTN	titin
2	D09	0,16	1,75	0,76	B2M	beta-2-microglobulin
2	A04	1,31	1,75	1,47	MKNK2	MAP kinase interacting ser/thr kinase 2
1	H01	2,12	1,83	1,92	CPS1	carbamoyl-phosphate synthetase 1
2	D02	1,94	1,87	1,81	NO_ANNOTATION	
1	F10	0,78	1,97	2,24	NO_ANNOTATION	
1	C05	0,34	2,05	2,65	CYP3A43	cytochrome P450, family 3 A43
2	B03	2,99	2,13	1,99	GH1	growth hormone 1
2	A09	4,79	2,19	2,31	KRT6E	keratin 6C
2	D11	0,98	2,31	2,32	SLC19A2	SLC19A2-prom
2	A08	2,57	2,39	2,72	NO_ANNOTATION	NBEAL2 intron
1	A06	1,31	2,70	1,67	MKNK2	MAP kinase interacting ser/thr kinase 2
1	B08	5,45	2,78	2,40	WNT5A	Wnt 5A
2	E05	2,21	2,81	3,57	MT2A	MT2A-prom

1	E01	6,04	2,97	2,40	FLJ45803	AP002448.3
1	F05	10,85	3,29	3,40	LAMA3	laminin, alpha 3
1	A07	3,73	3,39	2,91	TPST2	tyrosylprotein sulfotransferase 2
1	E02	7,17	3,45	3,19	RGL1	ral guanine nucleotide dissociation stimulator-like 1
2	B06	7,07	3,58	5,82	HSP90AB1	heat shock protein 90kDa alpha B 1
2	E10	2,09	3,59	4,51	PER1_b	PER1_b
1	H06	3,95	3,60	4,12	PFKL	phosphofructokinase, liver
1	G08	7,29	3,85	4,13	FNTA	farnesyltransferase, CAAX box, alpha
2	F10	2,09	4,16	4,22	CHIC2	cysteine-rich hydrophobic domain 2
2	G06	13,24	4,50	5,02	MEST	mesoderm specific transcript homolog
2	D01	5,71	4,63	4,17	DPEP1	dipeptidase 1 (renal)
1	E09	2,65	4,74	1,26	ATP2B3	ATPase, Ca++ transporting, plasma membrane 3
1	G10	3,54	4,87	4,21	GBF1	golgi-specific brefeldin A resistance factor 1
1	G01	1,88	5,29	5,12	YIPF5	Yip1 domain family, member 5
1	E06	0,48	5,50	3,52	NO_ANNOTATION	Unc119b exon
1	B10	12,39	5,51	5,23	AS3MT	arsenic (+3 oxidation state) methyltransferase
2	F11	9,21	5,57	5,47	CAT	catalase
1	B03	1,38	5,81	5,46	CPS1	carbamoyl-phosphate synthetase 1
2	A10	4,77	5,94	5,33	ADH1C	alcohol dehydrogenase 1C gamma
1	D10	11,70	6,05	5,02	CYBASC3	cytochrome b, ascorbate dependent 3
2	F02	9,03	6,08	5,67	HBS1L	HBS1L
2	B04	1,59	6,10	5,38	RNASE2	ribonuclease, RNase A family, 2

2	F04	12,73	6,39	5,23	LCN2	LCN2
1	B11	3,41	6,51	4,99	RAB11A	RAB11A, member RAS oncogene family
2	G03	9,85	6,62	4,99	IGFBP1	insulin-like growth factor binding protein 1
2	B08	0,57	6,67	6,17	NO_ANNOTATION	
2	E03	43,27	6,69	7,76	AMPD3-prom	AMPD3-prom
2	G09	18,57	6,96	9,30	MEST	mesoderm specific transcript homolog
2	G07	8,27	7,52	6,59	RAB11A	RAB11A, member RAS oncogene family
2	E08	14,74	7,98	8,14	IDH1-prom	IDH1-prom
2	B09	5,21	8,45	7,66	Rgr	
1	C10	12,98	8,46	6,25	MECP2	methyl CpG binding protein 2
2	D04	10,38	9,15	8,45	IGFBP1	insulin-like growth factor binding protein 1
2	C09	2,02	9,23	10,93	PREPL	prolyl endopeptidase-like
1	D11	17,51	9,55	9,22	NO_ANNOTATION	Bmp8a locus
2	E01	1,25	10,09	8,80	SRGN-prom	SRGN-prom
2	A07	10,30	10,76	9,27	C10orf108	
1	E08	21,35	11,83	11,06	LCN6	lipocalin 6
2	B01	17,34	12,01	11,77	HPS4	Hermansky-Pudlak syndrome 4
2	F06	2,77	12,21	14,53	GLUL	GLUL
2	G02	12,44	12,28	8,13	ADM	adrenomedullin
1	E05	6,10	12,52	14,13	MARK3	MAP/microtubule affinity-reg. kinase 3
1	D09	22,55	12,62	7,29	PPP2R2A	protein phosphatase 2 B, alpha isoform
1	D01	13,10	12,62	13,27	ENAM	enamelin

1	G05	23,74	12,67	10,64	NO_ANNOTATION	
2	B07	20,12	13,19	13,56	HERPUD1	homocys-ind., ER stress-ind., ubiquitin-like 1
2	B11	24,05	13,61	13,27	SCD	
1	H11	11,90	14,12	11,06	RNF11	ring finger protein 11
1	H08	12,03	15,01	16,28	C1R	complement component 1, r
1	G04	16,69	17,92	20,90	BIRC6	baculoviral IAP repeat-containing 6
1	B01	1,79	18,57	13,55	GNMT	glycine N-methyltransferase
1	C07	19,69	19,43	21,35	NO_ANNOTATION	DPEP1 first intron
1	B09	10,57	19,86	20,14	BRD2	bromodomain containing 2
2	C01	7,89	19,98	18,71	DIXDC1	DIX domain containing 1
2	F07	11,74	20,79	14,44	ANP32E	ANP32E
1	C09	22,12	20,79	19,00	SMYD4	SET and MYND domain containing 4
1	F09	24,92	21,90	23,02	PPP2R2C	protein phosphatase 2, B, gamma
1	B07	16,50	22,38	18,09	CKS1B0	CDC28 protein kinase regulatory subunit 1B
2	C06	1,97	22,85	18,41	NO_ANNOTATION	
2	B02	22,30	24,21	32,43	CKS1B	CDC28 protein kinase regulatory subunit 1B
1	C11	48,67	26,85	29,66	NO_ANNOTATION	BAHCC1 intron/exon
2	C02	38,65	28,67	26,47	WNT5A	Wnt 5A
2	F01	2,19	28,80	27,44	SNTA1	SNTA1
1	B05	22,62	28,97	25,63	MKNK2	MAP kinase interacting ser/thr kinase 2
2	F05	59,42	29,48	30,34	PHLDA1	PHLDA1
1	D04	2,45	31,44	37,36	NKPD1	NTPase, KAP family P-loop domain containing 1

1	G07	13,98	31,85	34,31	Stox2	
2	E07	15,16	39,49	31,16	SDPR-prom	SDPR-prom
2	D03	1,97	40,45	28,85	SLC38A4	solute carrier family 38, member 4
1	C08	40,72	49,42	49,30	MICAL1	microtubule ass. monoxygenase, calponin & LIM domain 1
1	C02	10,99	55,78	49,45	SMYD4	SET and MYND domain containing 4
1	C06	50,92	108,12	81,84	ITSN1	intersectin 1 (SH3 domain protein)
1	C04	36,94	122,93	116,44	C8orf46	
2	B10	44,95	160,40	208,27	NO_ANNOTATION	upstream of C20orf62
1	C01	194,03	221,04	168,45	IER2	immediate early response 2
1	C03	68,90	310,18	266,15	BAIAP2	BAI1-associated protein 2

(+-2fold)
>2fold down
>2fold up
no change
E47 sites close to GREs

Supplemental Table 10b: Reporter sequences with E47 motifs close to GREs.

Plate	Well	E47 motif	GRE motif
2	**B03**	626 + agaaacaggtggggtc	791 + tgggcacaatgtgtcctga
2	**A09**	729 + tgatccaggtgtgatc	385 + caggcccattgtgttctgc
2	**A08**	127 + ggaaccaggtgtactc	127 + 652 + aggacactctgtcctt
1	**A06**	955 + gcacccaggtgcactc 1412 - tggcacagctgttcct	39 + aagctcccctgtgttctat
1	**B08**	268 - gcgcccaggtgccccc	
1	**A07**	460 + aattacaggtgagcag 1131 + aatcacaggtgtgagc	
2	**B06**	927 + aagagcaggtggccaa	
2	**E10**	706 + tacctcaggtgatccg	168 - ggaacatcatgttctc
1	**H06**	447 - aggagcaggtgcccag	
2	**D01**	494 + ggcagcaggtggccgg 748 + gaggccaggtgtgtgc	430 - caggaaccctgtgttctct
1	**E09**	719 - acacacaggtggccgg 1053 - agcaggtgtttcg	231 - ggggctctctgtgttctgg
1	**E06**	801 + ggcatcaggtgctgct	739 + aggacagtgtgtcctg
1	**B10**	266 + ttaaccaggtgtggtg	
2	**A10**	1364 + gtttacaggtgcacag	
1	**B11**	236 - catttcaggtgctatc	
2	**G07**	236 - catttcaggtgctatc	375 + aaagatgttgt
2	**E08**	423 - gattacaggtgcacac	
2	**D04**	816 - tttaacaggtggcaac	
1	**D11**	147 - gacctcaggtgatcca	470 - tcagcacagtgtgttctgg
2	**A07**	519 + tcaaacaggtgcatgg	205 - agcacacactgttctg
2	**F06**	534 + tacctcaggtgatctg	234 - tgcacactttgtccta 785 - ggaacacattgttctc
1	**E05**	451 459 + aggctcaggtgtgcag	737 + caagtactctgtgttctct
2	**B07**	155 - cacccaggtgtcagt	
2	**B11**	453 - gacctcaggtgattcg	

1	**H11**	213 + ctcaacaggtgtgtga 286 - cagtccaggtgataga	
1	**H08**	653 - gaccacaggtggtggt 839 + accagcaggtggcacc	
1	**G04**	792 + atagtcaggtggtcaa	933 + ttggaacaatgtgtcctct
1	**B01**	983 - aatagcaggtgagcgc	
1	**C07**	395 - 450 - 505 - 560 - 615 - 869 -	930 + caggaaccctgtgttctct
2	**F07**	1239 + cattacaggtgcccac	
1	**C09**	1033 - caattcaggtgtcact	599 + aggacagaatgtcctc
1	**F09**	425 - agtctcaggtgatgac	58 + agaacactctgtgctt
2	**B02**	1335 + ggtttcaggtgttctg	
1	**C11**	746 - aagggcaggtgtggga	582 - ccggctcactgtgtccttc
2	**F01**	177 + gacctcaggtgatcca 219 + gaatacaggtgtgagc	
1	**B05**	121 + aatgccaggtgctggg	273 + tccagcccctcttga
1	**G07**	339 - 410 + 638 - 859 -	794 + caggctctctctgttcttt
2	**E07**	207 + gagaacaggtgtgcca	
1	**C08**	210 + agacacaggtgccgga 581 + gcgaccaggtggtgca	844 - agtacacaatgttctc
1	**C06**	420 + accgccaggtgcttct 991 - aatatcaggtgcaaat	191 - ggcactggatgttctt 684 + agaacagtttgttctc
2	**B10**	626 + cttaccaggtgccagg	26 + agaacaaagtgtccta 454 + ggtacagtatgtcctc
1	**C01**	586 - tttaccaggtgtgtct 1052 - ggcagcaggtgcactc	
1	**C03**	943 + tctctcaggtgtgacg	716 + ctggtacgttgtgttctta 81 - cgcacaatttgttctg

List of publications

[1] **Hemmer MC**, Greulich F, Wierer M, Schachtrup K, Downes M, Hübner N, Evans R, Uhlenhaut NH. ***E47 modulates hepatic glucocorticoid action*** (under consideration)

[2] Mir AA*, Dyar KA*, Greulich F, Quagliarini F, Jouffe C, Hubert MJ, **Hemmer MC**, Uhlenhaut NH. ***In vivo* ChIP-Seq of nuclear receptors: a rough guide to transform frozen tissues into high confidence genome-wide binding profiles** (under consideration) *These authors contributed equally to the work

[3] Greulich F*, **Hemmer MC***, Rollins DA, Rogatsky I, Uhlenhaut NH. ***There goes the neighborhood: Assembly of transcriptional complexes during the regulation of metabolism and inflammation by the glucocorticoid receptor.*** Steroids. 2016 Oct; 114:7-15 *These authors contributed equally to the work

Conference attendances and poster presentations

[1] The E Box in Glucocorticoid Receptor-Controlled Metabolism in the Liver, *Cold Spring Harbor: Mechanisms of Metabolic Signaling & Disease* (New York, USA, 2017)

[2] E boxes affect regulation of hepatic metabolism by GR, *3rd Heidelberg International Symposium on Diabetic Complications* (Heidelberg, Germany, 2016)

[3] Analysis of Cis-Regulatory Mechanisms of Glucocorticoid Receptor-Mediated Transcription, *FEBS advanced lecture course: Nuclear Receptors Signaling in Physiology and Disease* (Spetses, Greece, 2015)

Eidesstattliche Erklärung

Ich erkläre an Eides statt, dass ich die bei der Fakultät für Medizin zur Promotionsprüfung vorgelegte Arbeit mit dem Titel:

„Modulation of hepatic glucocorticoid action by the bHLH factor E47"

am Institut für Diabetes und Adipositas (Helmholtz Zentrum München) unter der Anleitung und Betreuung durch Prof. Dr. Matthias Tschöp ohne sonstige Hilfsmittel erstellt und bei der Abfassung nur die gemäß § 6 Abs. 6 und 7 Satz 2 angegebenen Hilfsmittel benutzt habe.

Ich habe keine Organisation eingeschaltet, die gegen Entgelt Betreuerinnen und Betreuer für die Anfertigung von Dissertationen sucht, oder die mir obliegenden Pflichten hinsichtlich der Prüfungsleistungen für mich ganz oder teilweise erledigt.

Ich habe die Dissertation in dieser oder ähnlicher Form in keinem anderen Prüfungsverfahren als Prüfungsleistung vorgelegt.

Die vollständige Dissertation wurde noch nicht veröffentlicht.

Ich habe den angestrebten Doktorgrad noch nicht erworben und bin nicht in einem früheren Promotionsverfahren für den angestrebten Doktorgrad endgültig gescheitert.

Die öffentlich zugängliche Promotionsordnung der TUM ist mir bekannt, insbesondere habe ich die Bedeutung von § 28 (Nichtigkeit der Promotion) und § 29 (Entzug des Doktorgrades) zur Kenntnis genommen. Ich bin mir der Konsequenzen einer falschen Eidesstattlichen Erklärung bewusst.

Mit der Aufnahme meiner personenbezogenen Daten in die Alumni-Datei bei der TUM bin ich einverstanden.

München, den Marie Charlotte Hemmer